Doctoral Dissertations   Graduate School

Fall 2012

A novel microfluidic enrichment technique for carbonylated proteins

Bryant C. Hollins
Louisiana Tech University

Recommended Citation

A NOVEL MICROFLUIDIC ENRICHMENT TECHNIQUE

FOR CARBONYLATED PROTEINS

by

Bryant C. Hollins, B.S.

A Dissertation Presented in Partial Fulfillment
of the Requirements of the Degree
Doctor of Philosophy

COLLEGE OF ENGINEERING AND SCIENCE
LOUISIANA TECH UNIVERSITY

November 2012

UMI Number: 3536678

UMI®

Dissertation Publishing

ProQuest®

LOUISIANA TECH UNIVERSITY

THE GRADUATE SCHOOL
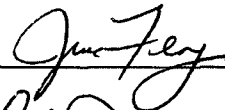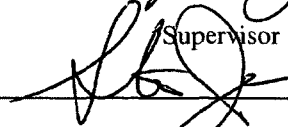
We hereby recommend that the dissertation prepared under our supervision by

Bryant C. Hollins, B.S.

entitled **A Novel Microfluidic Enrichment Technique for Carbonylated Proteins**

be accepted in partial fulfillment of the requirements for the Degree of

Doctor of Philosophy in Biomedical Engineering

Supervisor of Dissertation Research

Head of Department

Biomedical Engineering
Department

Recommendation concurred in:
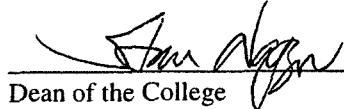
Advisory Committee

Approved:
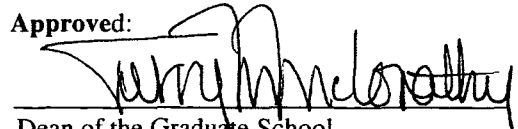
Director of Graduate Studies

Dean of the College

Approved:

Dean of the Graduate School

ABSTRACT

Proteins are the building blocks of cells in living organisms, and are composed of amino acids. The expression of proteins is regulated by the processes of transcription and translation. Proteins undergo post-translational modifications in order to dictate their role physiologically within a cell.

Not all post-translational modifications are beneficial for the protein or the cell. One type of post-translational modification, called carbonylation, irreversibly places a carbonyl group onto an amino acid residue, most commonly proline, lysine, arginine, and threonine. This modification can have severe consequences physiologically, including loss of solubility, loss of function, and protein aggregation.

Carbonylated proteins have commonly been used as a marker of oxidative stress. Oxidative stress has been suggested to play a role in many hum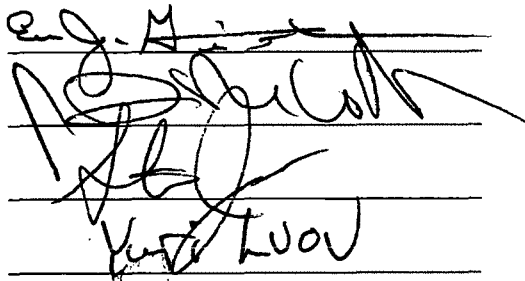an disease states, such as Alzheimer's Disease, Amyotrophic Lateral Sclerosis, Parkinson's Disease, inflammatory diseases, and others. Evidence shows oxidative stress to be a contributing factor in the progression of aging. Therefore, markers of oxidative stress, such as carbonylated proteins, can provide key information for the development of valuable therapeutics for these conditions. However, they are found in low abundance in samples and require enrichment prior to proteomic-based studies.

Currently, affinity chromatography is the chosen method for enriching carbonylated proteins in a sample. However, the technique has significant drawbacks,

including a large sample requirement, a large time requirement, the need for derivatization, and a high dilution of the sample post elution. This dissertation introduces a microfluidic enrichment technique for carbonylated proteins. The technique involves the surface modification of a polymer microchip for selective capture of carbonylated proteins. The surface chemistry is verified using different analytical techniques. Specificity of the target molecule's capture is demonstrated using a native protein. The capture conditions are optimized experimentally by studying four unique variables. Lastly, theoretical modeling is performed to determine the conditions that would lead to the technique's failure. It is seen that the technique can selectively capture target proteins from a flowing solution, even in the presence of an unoxidized protein. Protein capture is most dependent upon flow rate and crosslinker concentration. The flow rates required to break the bonds formed between an oxidized protein and the crosslinker exceeds feasible levels within a microfluidic channel. The microfluidic enrichment technique provides a promising alternative to the current "gold standard" of avidin affinity chromatography. The device has promise as a possible protein biomarker discovery tool in the search for therapeutic targets in human disease states where oxidative stress has been implicated.

APPROVAL FOR SCHOLARLY DISSEMINATION

The author grants to the Prescott Memorial Library of Louisiana Tech University the right to reproduce, by appropriate methods, upon request, any or all portions of this Dissertation. It is understood that "proper request" consists of the agreement, on the part of the requesting party, that said reproduction is for his personal use and that subsequent reproduction will not occur without written approval of the author of this Dissertation. Further, any portions of the Dissertation used in books, papers, and other works must be appropriately referenced to this Dissertation.

Finally, the author of this Dissertation reserves the right to publish freely, in the literature, at any time, any or all portions of this Dissertation.

Author _____

Date _____ 10/29/12 _____

DEDICATION

To my wife, Amanda; my son, Brayden; and his sibling, I dedicate this dissertation.

TABLE OF CONTENTS

LIST OF TABLES

LIST OF FIGURES

ACKNOWLEDGMENTS

First, I want to thank my Lord and Savior Jesus Christ, Who has granted me the intellectual ability to be able to persevere and complete the work described in this dissertation. I thank Dr. June Feng, my research advisor, for taking me as a student in her research lab and having faith in my ability to develop into an independent researcher. The discussions and guidance given by her made the work completed in this dissertation possible. I thank Dr. Mark Decoster for always having time to answer any questions I had and for the discussions in the hallways that always seemed to provide a clearer direction to pursue in my work. I thank Dr. Eric Guilbeau for his constant support in my development as a scientist and his continued support of my academic endeavors. I thank Dr. Steven Jones for his assistance whenever I had questions concerning modeling and for always offering his expertise without hesitation. I thank Dr. Alan Chiu for having the small items that I needed to complete a project, whether it was a penny, a stapler, or a hole punch. I thank Dr. Teresa Murray for the valuable discussions we have had since she arrived at Louisiana Tech University and for allowing me to use her computer for the enhancement of some images for my first publication. I thank Dr. Patrick O'Neal for his continued interest in my development as a young researcher, for his expertise on optics, and for allowing me to use some of his equipment for the testing of our optical systems within the lab. I also thank Mrs. Arlene Hill for always guiding me in the right direction whenever I had administrative issues that needed to be addressed. I thank my lab mates,

Hui Xia, Siyang Wang, Gang Chen, and Cheng "Vickie" Zhang, for being sounding boards for my research frustrations and helping me to look at problems from a different angle. Without the assistance of all of these people, the work described in this dissertation would not have been possible.

Lastly, I acknowledge my family for their understanding when I was not able to have extended stays with them. I thank them for their continued support in everything that I do. It is important for them to know that this dissertation would not have been possible without their encouragement and positive attitude toward my education. To all who aided in the completion of this work, I thank you.

CHAPTER 1

INTRODUCTION

1.1   Proteins

Proteins are key components of cells (Vogel, 2011). They serve numerous physiological functions, including regulatory activities, enzymatic activity, and structural purposes. They are considered an important part of the diet; if there are too few proteins in their nutritional intake, humans can become very ill. Proteins can also serve as toxic agents. A few examples of these would be Botulinum toxin A and ricin, some of the most potent known toxins.

Proteins are also called polypeptides because their structure resembles a polymer chain of peptides. Peptides are small chains of amino acids connected by a peptide bond. These molecules are typically less than 10 kDa in molecular weight. The building blocks of peptides are amino acids, small organic molecules that form the backbone of proteins (Lusk, 1910). Protein synthesis occurs inside the cell, and their expression is regulated by DNA and RNA in processes called transcription and translation. Following the translation process, proteins are further modified through processes called post-translational modifications that are often used as signaling mechanisms for what the protein's function will be, along with where in the cell the protein will be permanently located.

1

1.1.1   Amino Acids Are the Building Blocks of Proteins

There are over 300 naturally occurring amino acids; however, proteins are usually

composed of 20 α-amino acids (Uddin et al., 2012). The amino acids share a common

structure; they have an anime group (-NH₂) linked to an α-carbon atom, which is attached

to a carboxylic acid group (-COOH). The α-carbon contains a hydrogen atom and an R

group, known as the side chain. The basic structure of all amino acids is shown in Figure

1-1. The side chain determines most of the chemical features of the amino acids, and

thus is used as the basis for categorizing them. They are divided into four groups, based

on the sidechain, 1) non-polar, neutral amino acids, 2) polar, neutral amino acids, 3)

negatively-charged amino acids, and 4) positively-charged amino acids. The non-polar

amino acids are glycine, valine, alanine, leucine, isoleucine, methionine, phenylalanine,

tryptophan, and proline. The polar amino acids are serine, threonine, cysteine, tyrosine,

asparagine, and glutamine. The negatively-charged amino acids are aspartic acid and

glutamic acid. The positively-charged amino acids are lysine, arginine, and histidine.
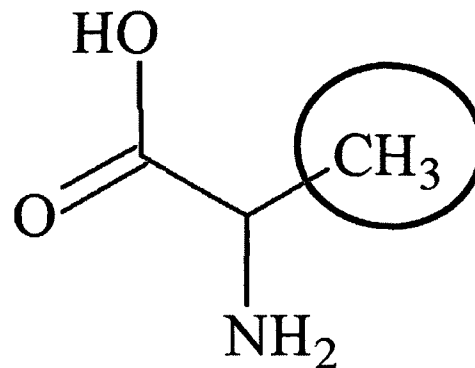
Figure 1-1: The typical structure of an amino acid. The figure above shows alanine.
The circled group is the sidechain, commonly referred to as an R group

To form a peptide, amino acids are linked together through a peptide bond. A

peptide bond occurs at the C-terminus of one amino acid and the N-terminus of the next

amino acid. The reaction results in the release of a water molecule. An example of a

peptide bond is shown in Figure 1-2. Multiple amino acids can be joined together

through peptide bonds to form peptides and proteins. The structure, abbreviations, and

chemical properties of amino acids are included in Appendix A.
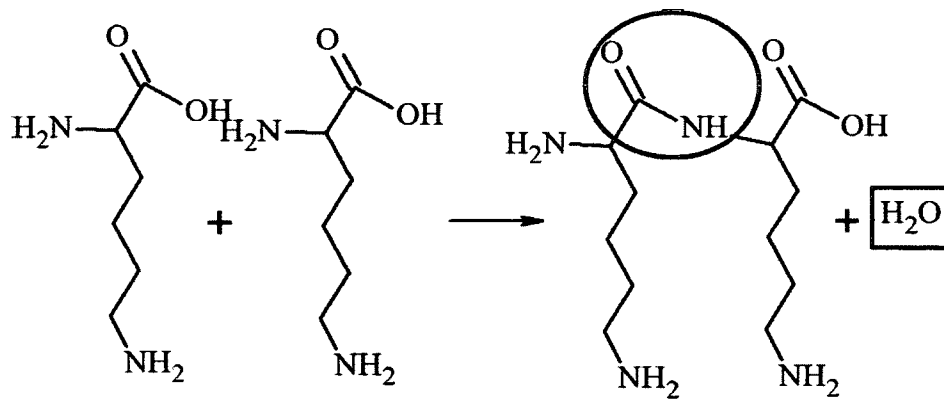
Figure 1-2: The formation of a peptide between two lysines

1.1.2   Transcription and Translation

Protein synthesis is regulated through gene expression by both deoxyribonucleic

acid (DNA) and ribonucleic acid (RNA) in processes called transcription and translation,

respectively (Vogel, 2011). Transcription is the process by which a complementary

strand of RNA is created from DNA. This process takes place within the nucleus of the

cell. RNA polymerase reads the base pairing of the DNA gene, and places the

complementary base pair on the RNA molecule. The nucleotides in DNA are adenosine

(A), guanosine (G), thymine (T), and cytosine (C). Adenosine and thymine are

complementary bases (A-T), and guanosine and cytosine are complementary bases (C-G).

RNA uses the same base pairing, except that the nucleotide thymine is replaced with

uracil (U), which is the RNA complementary base pair for adenosine. Transcription is

the first step in gene expression. It is a multi-step process, resulting in the formation of RNA genes.

Most of these RNA are non-coding and serve other purposes inside the cell, but one type of RNA, messenger RNA (mRNA), is used for the coding of proteins. After mRNA is transcribed, it is transported out of the nucleus and into the cytosol. There, the mRNA goes to a ribosome, where the process of translation begins. During the process of translation, the sequence of the mRNA gene is read and the corresponding encoded peptide is synthesized.

The nucleic acid, mRNA codes for amino acids through a sequence of nucleotide triplets, or codons (Frederick and Ibba, 2010). There are 61 codons that specify the 20 amino acids for protein synthesis. With few exceptions, this mechanism for protein coding is universal through all species. The coding always begins at a START codon (AUG), which codes for methionine. The coding continues in sequences of three nucleotide base pairs until a STOP codon is encountered (UAA, UAG, or UGA). For example, the mRNA sequence AAGCCACGC would encode for the three amino acids lysine, proline, and arginine (Lys-Pro-Arg), all connected with peptide bonds. Figure 1-3 shows the three base sequences required for coding the amino acids.

First Position	Second Position								Third Position
	U		C		A				
	code	Amino acid	code	Amino acid	code	Amino acid	code	Amino acid	
U	UUU	Phe	UCU	Ser	UAU	Tyr	UGU	Cys	U
	UUC	Phe	UCC	Ser	UAC	Tyr	UGC	Cys	C
	UUA	Leu	UCA	Ser	UAA	STOP	UGA	STOP	A
	UUG	Leu	UCG	Ser	UAG	STOP	UGG	Trp	G
C	CUU	Leu	CCU	Pro	CAU	His	CGU	Arg	U
	CUC	Leu	CCC	Pro	CAC	His	CGC	Arg	C
	CUA	Leu	CCA	Pro	CAA	Gln	CGA	Arg	A
	CUG	Leu	CCG	Pro	CAG	Gln	CGG	Arg	G
A	AUU	Ile	ACU	Thr	AAU	Asn	AGU	Ser	U
	AUC	Ile	ACC	Thr	AAC	Asn	AGC	Ser	C
	AUA	Ile	ACA	Thr	AAA	Lys	AGA	Arg	A
		Met	ACG	Thr	AAG	Lys	AGG	Arg	G
	GUU	Val	GCU	Ala	GAU	Asp	GGU	Gly	U
	GUC	Val	GCC	Ala	GAC	Asp	GGC	Gly	C
	GUA	Val	GCA	Ala	GAA	Glu	GGA	Gly	A
	GUG	Val	GCG	Ala	GAG	Glu	GGG	Gly	G

Figure 1-3: mRNA codons for transcribing proteins

1.1.3   Post-translational Modifications

Following translation, proteins are moved from the ribosomes to the endoplasmic reticulum, where further modification through post-translational modifications occurs. These modifications serve various functions. Some of these functions include identifying proteins for proteolysis (Shigi, 2012), regulating transcriptional activity (Duquet et al., 2006), and regulating gene expression (Yang et al., 2010). These examples demonstrate the biological relevance of protein post-translational modifications. Figure 1-4 shows an image of a cell, with the key areas of protein processing highlighted. These areas include the nucleus (transcription), the ribosome (translation), and the endoplasmic reticulum (post-translational modifications).

Ribosomes Nucleus Mitochondrion

Cytoskeleton

Golgi
apparatus

Rough
endoplasmic
reticulum

Smooth
endoplasmic
reticulum

Centrioles

Peroxisome Plasma membrane
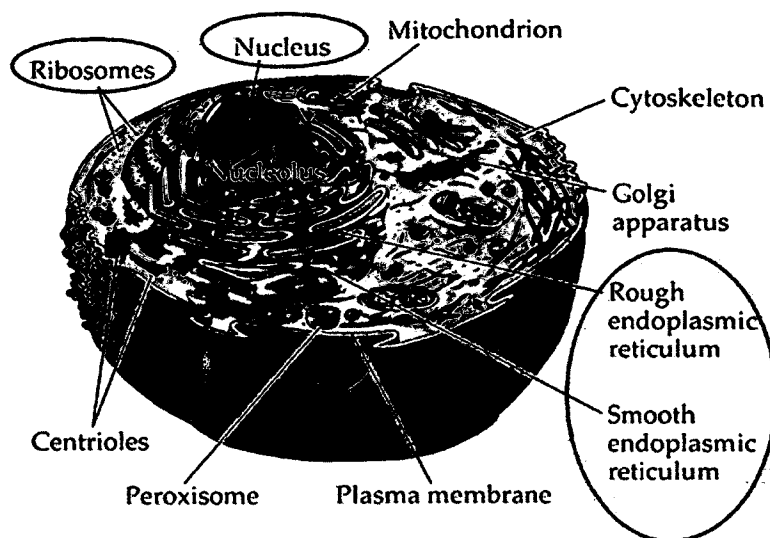
Figure 1-4: The image of a cell, with the key locations for protein processing highlighted

Other forms of post-translational modifications are induced with a cell is exposed to external stresses. Two sources of stressors are reactive oxygen species (ROS) and reactive nitrogen species (RNS). Some examples of ROS include singlet oxygen, hydrogen peroxide, and hydroxyl ions. A major source of RNS is NO. These species both play critical roles in cell signaling (Klatt and Lamas, 2000), but when unregulated, result in oxidative and nitrosative stress, respectively. These stresses can cause extensive damage to biologically relevant macromolecules, including membrane lipids, proteins, DNA, and lipoproteins.

1.2   Central Hypothesis

One of the key markers of oxidative stress within a cellular system is the production of carbonylated proteins. Carbonylation levels are generally associated with *in vivo* oxidative stress conditions (Madian et al., 2011). Carbonylated proteins are involved in a large number of human pathologies (Dalle-Donne et al., 2003); therefore,

these proteins could serve as biomarkers for these diseases. They also have the potential to become novel therapeutic targets for the treatment of these conditions. However, we do not have enough knowledge to determine the therapeutic or diagnostic capabilities of these proteins. One of the factors contributing to our limited understanding of these proteins is their low abundance in samples. In order for research to be conducted on this sub-proteome, the carbonylated proteins in the sample must be enriched.

Currently, the preferred methodology for carbonylated protein enrichment is affinity chromatography, specifically avidin affinity chromatography. Carbonylated proteins are derivatized with biotin hydrazide, which has an affinity for carbonylated proteins. Avidin affinity chromatography takes advantage of the strong affinity between avidin and biotin for positive enrichment of a target. However, this technique has significant drawbacks, including a large sample requirement, excessive sample waste, and the need for a derivatization step. The process of affinity chromatography is also time-intensive. Therefore, the work in this dissertation was organized to develop a more efficient way to enrich carbonylated proteins so that their potential as disease biomarkers could be assessed. The central hypothesis is that a microfluidic enrichment technique for carbonylated proteins, utilizing oxalyldihydrazide as a novel crosslinker, will require less sample, produce a smaller elution volume, and be less time-intensive than the current enrichment technique of avidin column chromatography.

The technique developed in this dissertation is microfluidic-based. Microfluidic techniques require smaller volumes than conventional analytical techniques. The reduced sample requirement would allow for easier translation into clinical settings. In addition,

clinical samples, such as serum and biopsies, are considered very precious, and as such, it is critical that these samples are not squandered using high-waste analytical methods.

1.3 Dissertation Aims

The three specific aims for this dissertation were as follows:

(i) Develop and test a microfluidic enrichment technique for the selective and specific capture of carbonylated proteins. A novel surface modification technique, utilizing oxalyldihydrazide, was created for the selective capture of carbonylated proteins. Selective protein capture was tested using a model protein, cytochrome c, oxidized *in vitro*. The specificity of the capture mechanism was tested using a mixture of our oxidized protein and a native form (unoxidized) protein, bovine serum albumin (BSA).

(ii) Optimize the microfluidic enrichment technique with respect to four variables to reduce sample, waste, and time requirements. The four variables were the interior post density of the microchip, the concentration of the crosslinker, oxalyldihydrazide, the flow rate at which proteins were injected, and the amount of time that oxalyldihydrazide was allowed to incubate inside the microchannel prior to being washed out of the channel.

(iii) Determine the conditions at which the microfluidic enrichment technique would fail. Because of the novelty of the surface modification technique, the binding energies of oxalyldihydrazide with poly (methyl methacrylate) (PMMA) and amino acid residues were calculated. The results were compared with fluid dynamics calculations for determining the conditions in which the microfluidic enrichment technique would fail.

1.4   Dissertation Outline

This dissertation consists of six chapters. Chapter 2 provides background information about the established knowledge in the field. Topics covered include oxidation and oxidative stress, protein oxidation, disease states where protein oxidation has been implicated, a more detailed look at carbonylated proteins, history and applications of microfluidics and MEMS technology, a discussion about the historic uses of oxalyldihydrazide, and some basics about the theoretical techniques used for model. The chapter closes with a conceptual example of oxidative stress. Chapter 3 presents the development of the microfluidic carbonylated protein enrichment technique that stands at the heart of this dissertation. The optimization of the technique is discussed in Chapter 4. Chapter 5 focuses on the theoretical determination of the conditions that would cause the enrichment technique to fail. In Chapter 6, general conclusions are presented, including future directions for the research and suggestions for improving the method.

CHAPTER 2

LITERATURE REVIEW

2.1 Oxidation and Oxidative Stress

Oxidation is a naturally occurring process in cell development that is used in many cellular processes (Zhao and Jensen, 2009). The major source of free radicals in an organism is the mitochondria (Zhou et al., 2010; Finkel and Holbrook, 2000; and Balahan et al., 2005), although other organelles within the cell, such as peroxisomes, also contain oxidizing agents. Figure 2-1 shows the location of free radical stores and sources inside a cell. During inflammation, these free radicals are released to oxidize foreign macromolecules. Oxidation marks these foreign molecules for degradation by the immune system. After these free radicals have completed their jobs, they are inactivated by the anti-oxidant system, composed primarily of enzymes (Reed et al., 2008).

Ribosomes Nucleus Mitochondrion

Cytoskeleton

Nucleolus

Golgi apparatus

Rough endoplasmic reticulum

Smooth endoplasmic reticulum

Centrioles

Peroxisome   Plasma membrane
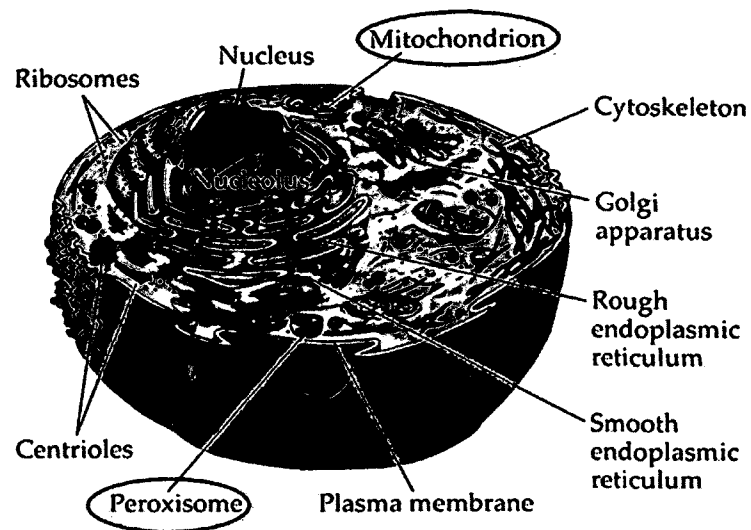
Figure 2-1: Location of the primary free radical stores and sources (peroxisome and mitochrondrion) within the cell

If free radicals are not quickly neutralized by anti-oxidants, they begin to oxidize

macromolecules (lipids, DNA, and proteins) that are neither damaged nor foreign. This

damage to native tissue is called oxidative damage, with the cumulative effect labeled as

oxidative stress. Oxidative stress occurs over time (Chang et al., 2000), as an organism is

exposed to its internal stores of oxidizing agents and those in its external environment.

Some physiological effects of oxidation include molecular switch action, enzyme

inactivation, and triggering of the apoptotic cascade (Alberghina and Colangelo, 2006;

Krause and Muller, 2010). These consequences become more pronounced as the

organism ages, as anti-oxidant efficiency decreases (Apelt et al., 2004). To further

diminish the anti-oxidant system's efficiency, certain anti-oxidant enzymes become

oxidized and lose their function. An example such enzyme is superoxide dismutase

(SOD), whose function is to convert superoxide ($O_2^{\bullet}$) to hydrogen peroxide (H_2O_2)

(Czapski et al., 2002). Hydrogen peroxide is broken down by catalase into water (H_2O)

and oxygen (O_2) (Maehly and Chance, 1954). Oxidative stress has been implicated in

age-related processes and neurodegenerative diseases, such as Alzheimer's Disease
(Nunomura et al., 2006).

2.2 Protein Oxidation

Oxidation is used by the immune system to fight foreign agents, such as in the
case of bacterial infection. However, when native tissues begin to be oxidized, the results
are detrimental to the cell. Some consequences of protein oxidation include protein
misfolding, loss of function, loss of solubility, and protein aggregation (Sultana et al.,
2010). There are 35 different ways that a protein can be oxidized, with many residues
having multiple oxidation products possible (Madian and Regnier, 2010). For a detailed
look at possible oxidation products, see Appendix.

2.3 Disease States Where Protein Oxidation has been Implicated

2.3.1 Alzheimer's Disease

Hallmarks of Alzheimer's Disease (AD) include cognitive impairment and
dementia. An official diagnosis of AD is not possible prior to autopsy, where
neurofibrillary tangles (NFTs) are observed. Increased levels of protein dysfunction and
de-regulation have been seen in cases of AD (Alberghina and Colangelo, 2006; Eckert et
al., 2010). Oxidative stress is hypothesized to be a contributing factor to the protein
dysregulation seen in AD. High levels of protein carbonylation, a key marker of
oxidative stress, have been observed in AD (Dalle-Donne, Rossi, et al., 2003). Recent
findings suggest a deterioration of the antioxidant system within the brain as a driving
factor toward the increased oxidative stress levels seen in the temporal cortex of aged
mice rats (Wang et al., 2010). It is believed that the neuropathology develops many years

before any clinical symptoms manifest (Sultana et al., 2010). However, the link between protein oxidation and the physiological manifestations of AD still remains unclear.

2.3.2   Amyotrophic Lateral Sclerosis

A link has been suggested between oxidative stress and other neurodegenerative diseases, such as amyotrophic lateral sclerosis (ALS) (Dalle-Donne et al., 2003). ALS is a neurodegenerative disease that results in muscle wasting, paralysis, and death, often within a two to three year period post-diagnosis. It has been suggested oxidative stress plays a key role ALS, and as such, should be treated as a potential therapeutic target (Barber and Shaw, 2010). Another study suggests the dysregulation of two key antioxidants, glutathione and the enzyme superoxide dismutase-1 (SOD1), results in the increased levels of oxidative stress seen in this condition (Schulz et al., 2000; Fischer et al., 2012; and Robberecht, 2000). However, the exact pathogenesis of ALS is poorly understood (Robberecht, 2000), requiring much more work prior to actively pursuing oxidative mechanisms as a therapeutic target in ALS.

2.3.3   Inflammation

As stated earlier, one of the effects of inflammation is the release of oxidizing free radicals. Organisms use this mechanism as a defense against foreign macromolecules. However, inflammation plays a key role in several human diseases (Dalle-Donne et al., 2003). Some of these conditions include atherosclerosis and autoimmune diseases. A study observed that the impairment of vascular reactivity in atherosclerosis was a direct result of the reaction between NO and superoxide (O_2^-) to form the powerful oxidant peroxynitrite ($ONOO^-$) (White et al., 1994). Peroxynitrite served as a potent mediator for oxidation of lipoproteins, as well as a substrate for (NO), which reduced the capability of

the smooth muscle to respond to changes in blood flow. The production of ROS in the

skin causes protein damage in allergic and inflammatory skin diseases (Okayama, 2005).

A free radical pathway has also been suggested in systemic lupus erythematosus, and

further studies have implied a unifying theme of oxidative stress, including protein

oxidation, in the pathogenesis of these inflammatory autoimmune diseases (Kovacic and

Jacintho, 2003).

2.3.4   Aging

Denham Harman proposed the free radical theory of aging in 1954 (Harman,

1956). He proposed that irradiation induces cancer, mutations, and aging. One of the

mechanisms of this irradiation effect was the liberation of free radicals, including OH⁻.

The theory was later extended in 1972, adding the suggestion that superoxide was the

primary free radical from which most others stemmed (Harman, 2006). Mitochondria

aging effects were added to the theory in 1983. The effects of tissue exposure to air were

examined in 1993. Through extensive work over the past 50 years, the free radical theory

of aging has been established as a valid and useful theory for explaining the aging

process in organisms (Harman, 2009).

2.4   Carbonylated Proteins

Carbonylation, the most widely accepted form of protein oxidation, has been used

as a marker for oxidative damage to proteins *in vivo* (Colak, 2008). Carbonylation is an

irreversible post-translational modification (PTM) that attaches an aldehyde functional

group to an amino acid residue (Madian and Regnier, 2010; Suzuki et al., 2010). The

most common residue targets for carbonylation are lysine, proline, threonine, and

arginine (Suzuki et al., 2010). While other forms of protein oxidation exist,

carbonylation is the most common, and thus best characterized. Carbonylated proteins are often formed *in vivo* through metal-catalyzed oxidation reactions, one of the primary means of enzymatic deactivation within the body (Amici et al., 1989). Typically, when proteins are carbonylated, the proteins become more susceptible to proteolytic destruction (Davis et al., 1987). Therefore, protein carbonylation can serve as a powerful tool in cellular signaling (Wong et al., 2010), but the relationship between carbonylated protein marking and destruction are poorly understood.

2.4.1   Detection of Carbonylated Proteins in a Sample

There are techniques for detecting the existence of carbonyls in a protein sample. The first technique was proposed by Levine et al. (1990) and uses a spectrophotometric assay called the DNPH assay. This assay derivatizes carbonyls with 2,4-dinitrophenylhydrazine (DNPH) to form a hydrazone bond. Another technique for detecting carbonyls is immunochemistry-based (Barreiro et al., 2005). Carbonyls are derivatized with dinitrophenyl (DNP), and run through a gel. The gel is transferred to a membrane, and the membrane is probed using the anti-DNP antibody. This method can be used to visualize the presence of carbonylated proteins within a sample. Total carbonyls can also be measured by enzyme-linked immunosorbent assay (ELISA) (Buss et al., 1997), slot blotting (Robinson et al., 1999), or immunohistochemistry (Smith et al., 1998). While DNPH methods of detecting carbonyls are the most prominent, other techniques exist. One of these techniques uses sodium borotritide. This technique can be used either in solution (Lenz et al., 1989) or as a reaction step prior to gel electrophoresis (Yan and Sohal, 1998).

2.4.2   Identification of Carbonylated Proteins

Proteomics is the study of protein expression in an organism. Proteomics is closely

related to genomics. Because protein expression is tightly regulated by DNA and RNA

processes, a change in the genome could result in a change in protein expression. The

total collection of all proteins within the cell is called the proteome. Each cell, while

possessing the complete proteome, uses different factors and environment cues for

determining protein expression (Schulenborg et al., 2006). Therefore, the identification

of proteins, specifically carbonylated proteins, is important. The field has been greatly

aided by the cooperation of the scientific community in the creation of online theoretical

databases, such as SwissPROT and MASCOT. Using mass spectroscopy, structural and

sequential information can be gathered. This information can even determine small mass

shifts (on the order of Daltons) of individual amino acid residues. This sensitivity allows

for in-depth analysis of site-specific post-translation modifications. Through the use of

proteomics, a lot has been learned about protein expression in disease states (Schulenborg

et al., 2006; Marcus et al., 2004).

2.4.3   Measurements of Carbonylated Proteins

When using the DNPH method for the determination of carbonyls in a sample, a

hydrazone bond is formed between the carbonylated proteins and the hydrazine. The

bond formation is advantageous for measurements because it has a distinctive peak at

370 nm when analyzed using a spectrophotometer. Beer's Law, given in Eq. 2-1 below,

is used for determining the carbonyl relative concentration:

$$A = \varepsilon bc.$$ Eq. 2-1

In Eq. 2-1, A is the absorbance, ε is the molar extinction coefficient, b is the pathlength, and c is the concentration. Typically, the pathlength and the molar extinction coefficient are known. The absorbance is found experimentally, using spectrophotometry. Using the known terms, concentration of the carbonyl content can be found. The concentration is expressed in the units (nmol carbonyl)/ (mg protein). Carbonyl content for individual proteins can be determined using a conventional one-dimensional (Keller et al., 1993; Yan et al., 1998) or two-dimensional (Nakamura and Goto, 1996) sodium dodecyl sulfate (SDS) gel electrophoresis. This step would be followed by a Western blot analysis. While this approach is more robust in terms of selectivity and specificity than other carbonyl assays, it produces only semi-quantitative results (Shacter, 2000).

2.4.4   Metal-catalyzed Oxidation

One of the primary theories for protein oxidation *in vivo* is metal-catalyzed oxidation (MCO). MCO is a site-specific reaction that results in the reduction of Fe (III) to Fe (II), producing hydrogen peroxide (H_2O_2) in the process (Amici et al., 1989). The residues most susceptible to MCO reactions are lysine, arginine, threonine, and proline. Stadtman and Oliver (1991) suggested that MCO reactions are the primary mechanism of increased protein carbonylation in numerous disease states.

2.4.5   Enrichment Requirements and Technology Gap

A limitation on carbonylation studies and a restriction on its use clinically is the low abundance of these proteins in a sample. In order to extract useful data, these proteins must be enriched and purified. None of the three enrichment methods

commonly used, affinity chromatography, strong cation exchange (SCX), and 2D-polyacrimide gel electrophoresis (2D-PAGE), are ideal.

In affinity chromatography, most commonly, avidin column chromatography (Mirzaei and Regnier, 2005; Yoo and Regnier, 2004), carbonyls are derivatized with biotin hydrazide and flushed through the column. The high affinity between biotin and avidin allow for the labeled proteins to be captured. Elution occurs by rinsing the column with excess biotin. Disadvantages of traditional affinity column chromatography include the amount of sample needed for the protocol, the amount of reagents needed, and the time requirements, the high dilution of the eluted targets, and the need for a derivatization step. Recent work has been done to miniaturize the avidin column onto a disposable PMMA microfluidic chip (Xia et al., 2012). The study demonstrated a 10^6-fold reduction in the amount of sample needed from the commercially available technology. The use of a microfluidic platform also reduced the time needed for the sample analysis. However, a derivatization step with biotin hydrazide, a time intensive step, is still required.

Strong cation exchange (SCX) takes advantage of Girard's P Reagent (GPR). GPR contains a hydrazide group for derivatization with carbonyls, as well as a quaternary amine that can be selected using SCX at pH 6.0. This approach is often used in combination with reverse-phase chromatography coupled with tandem mass spectroscopy (RPC-MS/MS). While an advantage of this technique is that excess reagent does not have to be removed after derivatization, the approach requires a trypsin digestion of the GPR-derivatized proteins, adding overall analysis time to the technique (Madian and Regnier, 2010).

In 2D-PAGE, proteins are moved to their isoelectric point (pI) in a pH gradient strip. Then, they migrate down the gel, separating by molecular weight (Schulenborg et al., 2006). Once separation is completed, selected bands can be excised and analyzed using MS. Limitations to this technique include the time needed for analysis and the inability to determine if a band is composed of more than one protein while on the gel.

2.5   Microfluidics and MEMS

2.5.1   History

Microfluidics refers to the use of fluidic devices on the spatial scale of 1 – 100 μm (Ghosal, 2012). The field of microfluidics is still considered immature. Most of the progress in the field has occurred within the last decade. It is difficult to find examples of the first "microfluidic" device, but if the spatial definition is recognized, the first ink-jet printers, patented in 1951, would qualify as microfluidic devices. The first commercially available "lab on a chip" was sold by ALIGENT in 1999. Despite its brief history, the field has rapidly emerged to the forefront of scientific exploration. This emergence is seen through the number of patents issued related to microfluidics; in the nineties, there were only a few. Today, the number of patents exceeds 350 annually. Microfluidics is promising for collaborative science because it incorporates principles from physics, chemistry, engineering, and mathematics. For certain applications, including a few discussed in this dissertation, biological considerations must be applied as well (Grayson et al., 2004).

2.5.2   Manufacturing Techniques

The simplest microfluidic devices are manufactured relatively inexpensively and require little expertise. A microfluidic device can be constructed using two glass

microscope slides, a drill press, double-sided tape, and a cutting device, such as a knife.

On one glass slide, place a strip of double-sided tape. Using the knife, the design of the

channel can be cut into the tape. Two holes are drilled into the remaining microscope

slide for an entrance and exit reservoir. The microfluidic device is sealed by pressing the

two glass slides together. For smaller-scale features, a laser could be used to cut the

chip's design.

For wet and dry etching of a pattern onto the surface of a microchip, a technique

called soft lithography, or photolithography, is first employed (Kim et al., 2008). The

process is shown schematically in Figure 2-2. Photolithography is the process by which

the mold master is formed, which is then used for the formation of the stamp for creating

microfluidic channels. This contrasts with the way in which the mold master is created

for hot embossing. For hot embossing, the mold master is formed through the process of

micromilling. Typically, the starting substrate is silicon, with a thin layer of silicon

dioxide on top. A photoresist can be applied to the substrate. There are two types of

photoresists, negative and positive. The classification is dependent upon how the

substance reacts to UV radiation. Following the application of the photoresist, the

substrate is exposed to UV irradiation. Post UV-exposure, the photoresist is developed.

It is during development that the type of photoresist chosen becomes important. When a

positive photoresist is exposed to UV radiation, its crosslinks are weakened. UV-exposed

photoresist is removed during development. Negative crosslinkers, on the other hand, are

strengthened by exposure to UV radiation. Therefore, the areas not exposed are removed

during development. The substrate is then etched using wet or dry etching techniques.

Lastly, the photoresist is stripped from the substrate, and the master can be used for the construction of microfluidic devices.

Starting substrate (Si)

NEGATIVE PHOTORESIST

1. Apply photoresist

3. Develop photoresist | 4. Etch substrate | 5. Strip photoresist

2. Expose photoresist

POSITIVE PHOTORESIST
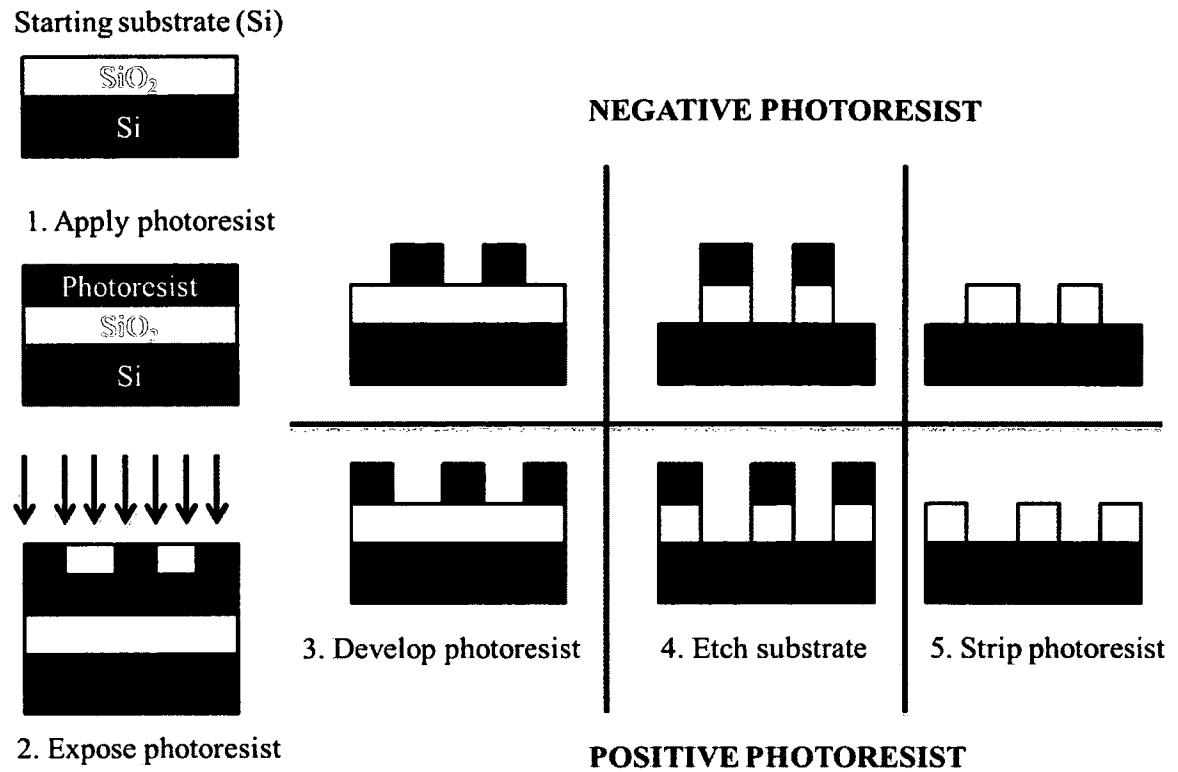
Figure 2-2: Flowchart for the use of photolithography to create a microfluidic device

Silicon is one of the most popular base substrates used in microfluidic devices. Silicon is suitable for a variety of applications, due to desirable mechanical properties, including high melting temperature and a high strength-to-weight ratio (Ayon et al., 2001). However, the substrate requires etching prior to being used as a microfluidic device. There are three methods for achieving this, mechanical etching, dry etching, and wet etching. Mechanical etching is easier, but cannot generate smooth surfaces. Dry etching is effective, but has a low etch rate. Wet etching is the most common form of etching for silica-based microfluidic devices (Iliescu et al., 2007). Solutions based upon

hydrogen fluoride (HF) are used for wet etching. Even though wet etching has a high etch rate, one of the trade-offs is less control over the profile due to an isotropic etching. Because the substrate is immersed in solution, the etching occurs equally in all directions.

Whereas wet etching involves the immersion of a substrate, such as silicon, to etch the desired pattern, dry etching involves the bombardment of the substrate surface with high energy molecules (Kameoka et al., 2001; Chun et al., 2006). The high energy molecules etch the substrate pattern by colliding with the surface of the substrate. Another term for dry etching is reactive ion etching (RIE). Dry etching can give higher profile control than wet etching, due to anisotropic etching. In this case, the photoresist provides additional protection, as the high-energy molecules can only contact the substrate where there is no photoresist. The difference results in smoother surfaces for dry etching vs. more rounded features in wet etching. However, the tradeoff for additional control over the microfluidic profile is the lower etching rate.

Hot embossing is seen as an alternative to the fabrication techniques primarily used for silicon or glass-based MEMS (wet and dry etching, discussed above) (Becker and Heim, 2000). This technique is a low cost microfabrication technique applied to polymer substrates, typically PMMA or polycarbonate (PC). Figure 2-3 shows how hot embossing is used for the construction of a microfluidic device. Figure 2-4 shows a schematic of a typical hot-embossing system. The two platens in the system (upper and lower) are attached to thermocouples, allowing for their temperatures to be controlled independently. The metal mold master is placed in contact with the polymer substrate and held there to emboss the negative of the master onto the substrate. The process is completed within a vacuum chamber. The high temperatures and contact force used in

hot embossing make the technique undesirable for use with other microfluidic substrates

based on silica.

Starting metal mold

1. Mill metal mold to create a master

2. Emboss structure onto polymer surface

Heat and contact force

3. Remove polymer substrate and allow to cool
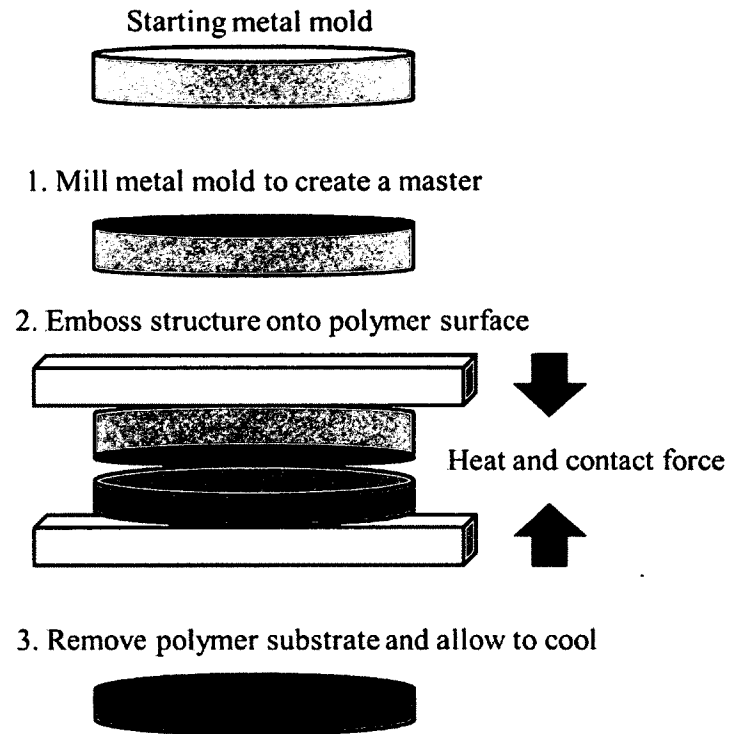
Figure 2-3: Process for the use of hot embossing for the creation of a microfluidic device
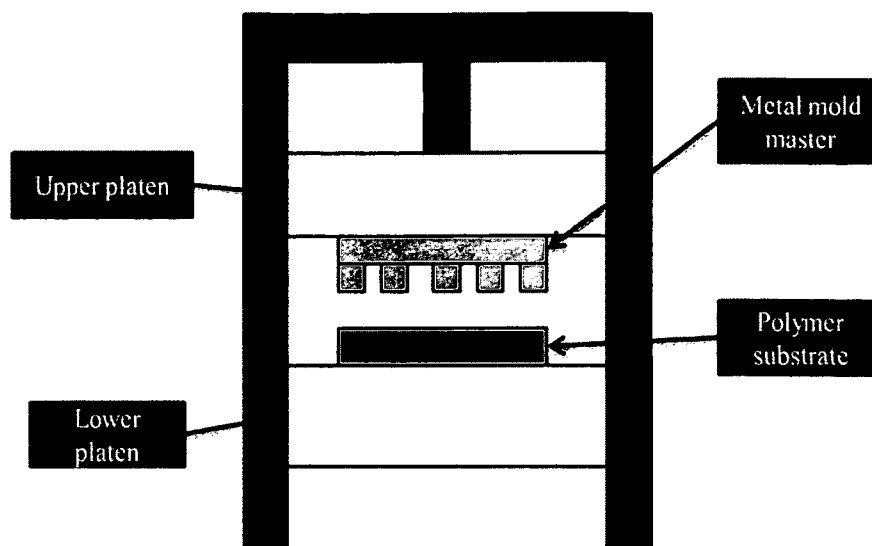
Figure 2-4: Schematic of a typical hot embossing system

Polymer-based microchannels are advantageous to life sciences applications.

Some of the advantages polymers have over glass-based substrates include having a wide

range of material properties, allowing for the substrate to be optimized to the application.

In addition, polymers have a high volume fabrication for low material costs (a necessity

for disposability) and the microfabrication is simplified because of the replication

methods. In some of the earlier descriptions of work using hot-embossing, polymer

based microfluidics were used for chromatographic columns (Arnold et al., 1998), DNA

concentrators (Christel et al., 1998), DNA separations (Simpson et al., 1998), and

capillary electrophoresis (Llopis et al., 2007). PMMA and PC are the main two polymers

used for hot embossing. Table 2-1 shows the conditions for using hot embossing on these

two substrates. PMMA has some advantages over PC, in particular, its lower glass

transition temperature (T_g) and the lack of toxic chemicals leeching off the substrate.

Therefore, PMMA is the substrate used for the experiments described within this

dissertation. Due to the limitations of micromilling being a mechanical etching

technique, all microfluidic devices formed by this method will have an inherent roughness to them. Table 2-2 shows a side-by-side comparison of the etching techniques used in microfluidic device construction.

Table 2-1: Hot embossing conditions for PMMA and PC.

Material	T_g (°C)	Embossing Temperature (°C)	Embossing Force (kN)	Hold Time (s)
PMMA	106	120-130	20-30	30-60
PC	150	160-175	20-30	30-60

Table 2-2: Comparison of different techniques for the manufacture of microfluidic devices.

Etching Technique	Control	Etching Speed	Feature details	Photolithography required	Substrate
Wet etching	Low	Medium	Less detail	Yes	Silica
Dry etching	Medium	Slow	More detail	Yes	Silica
Hot embossing	High	Fast	Most detail	No	Polymer

2.5.3   Applications

Miniaturization and automation are gaining popularity in biomedical research labs, primarily because of the reduced analysis times and reduced human participation (and consequently, error). An example of an analytical technique that has undergone miniaturization is electrophoresis. Originally, this technique was completed in a gel on a benchtop. An advance to this approach was the introduction of capillary electrophoresis

(CE), which can be coupled to a laser light source for laser-induced fluorescence studies (CE-LIF) (Feng and Arriaga, 2008; Feng et al., 2008). This technique combines the resolving power of gel electrophoresis with the sensitivity of fluorescence. When combined with the automated control of the experiment, this technique has advantages over traditional gel electrophoresis (Osiri et al., 2008; Shadpour et al., 2007). Now, 2D-micro-CE-LIF (2D-μCE-LIF) is possible and has been reported in the literature (Osiri et al., 2008; Shadpour and Soper, 2006; Wang et al., 2012). This technique offers a few advantages over CE-LIF. Some of these advantages include smaller size, faster migration times, smaller samples, and higher resolving power (Osiri et al., 2008; Shadpour and Soper, 2006; Wang et al., 2012). The technique can also be coupled directly to mass spectroscopy.

Because of their small volume, reagent requirements, and high-throughput capacity, microfluidic devices are excellent for drug screening. Numerous studies have been conducted on drug effectiveness inside the chamber of a microfluidic device. One study used a microfluidic device to detect bacteria within a sample (Boedicker et al., 2008). The researchers also analyzed the bacteria's susceptibility to different antibiotics inside the microchannel. Using this methodology, the authors were able to identify the antibody sensitivity of methicillin-resistant *Staphylococcus aureus* (MRSA) using multiple antibiotics in a single experiment. Another study created a high throughput method to quantify the motility of a parasite (Smout et al., 2010). This study is concerned with the pre-emptive detection of livestock parasites prior to human infection. The importance of this technique was that it conducted real-time drug screening. This screening allowed for the quick identification of drug resistance development in the

parasite. Microfluidics provides a great platform for pharmaceutical research and drug development, including the simple coupling with micro-titre technology for more efficient drug discovery techniques (Tolan et al., 2008; Kang et al., 2008).

2.5.4   Microfluidic Cell Capture and Enrichment

In the past decade, microfluidic devices have been used to reduce the reagent requirements in cell culture. In one of the studies, a technique was developed to control the microenvironment in cell culture (Young and Beebe, 2010). This study was one of the first to look at cell biology principles within a microfluidic device. The technique has the promise to revolutionize the way cell biology is conducted in the future.

However, at the intersection of cell research and microfluidic technology, most attention is paid to the capability of microfluidics to provide a great platform for cell capture. In particular, positive enrichment of cancer cells has been one of the primary goals of using microfluidics in cell biology. This enrichment has been accomplished using different techniques. One of the techniques was the use of aptamers for selective capture of prostate-specific membrane antigens (PSMA) (Dharmasiri et al., 2009). Anti-PSMA aptamers were immobilized onto the surface of a PMMA microchip, and sample was loaded into the chip. The analysis was completed in a high-throughput manner, with 1 mL of solution being analyzed in less than 30 minutes. The PSMA could be released from the channel completely intact, allowing for easier analysis post-chip.

Another technique for capturing cells inside a microchip involved the immobilization of antibodies onto the surface of a microfluidic chip (Nagrath et al., 2007; Adams et al., 2008). These studies analyzed the capture of rare circulating tumor cells (CTCs) from a sample. The authors used anti-EpCAM antibodies for the detection of

CTCs associated with prostate and breast cancer, respectively (Nagrath et al., 2007, Adams et al., 2008).

Another technique used electromagnetism as the mechanism for cell enrichment on a microchip. One research group used self-assembled magnetic beads for the selective capture of cancer cells (Saliba et al., 2010). The researchers were able to type the cancer cells on-chip as well using the technique. All of these examples demonstrate notable advances to cancer biology studies, as well as the high adaptability of microfluidics and microelectromechanical systems (MEMS) towards almost any application.

2.5.5   Promise for Novel Diagnostic Tools

Biomedical applications of MEMS (BioMEMS) typically address diagnostic or therapeutic goals. Advances in lab-on-chip diagnostic systems and implantable therapeutic biomedical microdevices, such as implantable electrodes, have paved the way for novel treatments to improve quality of life (Cheung and Renaud, 2006). In the future, these devices will continue to make contributions to the advancement of health science. Even now, the technology exists for the development of "smart" lab on chip technology for point-of-care clinical diagnosis (Ahn et al., 2004). These devices are small, portable, and have a self-contained power source. This combination makes for simple use in the field when access to standard medical equipment is difficult or unrealistic to obtain. The addition of renewable power supplies to this technology is being pursued to make it available in places like home health and developing countries (Weigl et al., 2008). These adjustments would lead to devices that are both minimally-invasive and minimally-instrumented. A simplified diagnostic tool reduces both the need for specialized

equipment for diagnosis and extensive training for analyzing the results. Microfluidics is also being applied provide additional novel diagnostic functionality.

The use of MEMS provides a promising platform for protein analysis, especially low abundant proteins, where samples may be limited or difficult to obtain (Diercks et al., 2009). Microfluidic chips, composed of materials such as glass or silicon, are usually simple to construct using basic photolithography techniques. In the last decade, polymeric chips have become increasingly popular, due to their versatility and lower cost (Becker and Lacascio, 2002; Stachowiak et al., 2003). Particularly, high precision micromilling for metal mold master fabrication is desirable for researchers who do not have access to extensive lithography based equipment. The combination low cost and mass production allows these chips to be disposable, reducing the likelihood of cross-contamination between samples on a reused chip. Fast analysis, high throughput, and low reagent consumption are advantages of BioMEMS over conventional techniques for low-abundance samples.

2.6   Oxalyldihydrazide

2.6.1   Historic Uses

Oxalyldihydrazide is a small molecule (MW = 119.6) that has a two carbon backbone. Each carbon is double-bonded to an oxygen atom (C=O), and single bonded to a hydrazide functional group (-NHNH$_2$). Figure 2-5 shows the chemical structure of an oxalyldihydrazide molecule. More recently, it has been used in the synthesis of biologically active compounds derived from oxalyldihydrazide and complexes it forms with different metals (Singh et al., 2009; Aruna and Patil, 1998; Aggarwal and Singh, 2004). It was originally applied in a method for determining copper content within a

sample, particularly blood (Stark and Dawson, 1958; Beale and Croft, 1960; Kekki and

Siltanen, 1960). It has also been used in a colorimetric assay to determine phosphate

levels in drinking waters and soil for environmental monitoring (Salem, 1991).
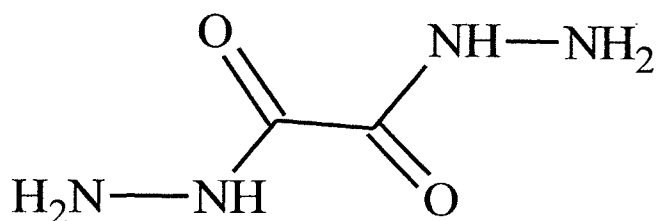
Figure 2-5: Chemical structure of an oxalyldihydrazide molecule

2.6.2 Reasons for Choosing Oxalyldihydrazide as the Enrichment Crosslinker

Even though the molecule had never been used before for microfluidic

enrichment, there are reasons to believe the molecule would work as an effective

crosslinker for this project. As demonstrated through the continued use of the DNPH

assay, carbonyl groups have a strong affinity for hydrazide. Therefore, it was necessary

to have a hydrazide functional group available for reacting with the carbonyl group of the

carbonylated proteins. Microfluidic devices, especially polymer-based chips, lend

themselves well to surface modification (Dharmasiri et al., 2010; Bai et al., 2006; Lee et

al., 2005). Therefore, proper surface modification would allow the successful

immobilization of oxalyldihydrazide onto the channel surface. Chapter 3 provides

experimental support for the process. The crosslinking is verified further in theoretical

modeling presented in Chapter 5. Figure 2-6 shows a simplistic scheme for crosslinking

oxalyldihydrazide to the PMMA substrate.
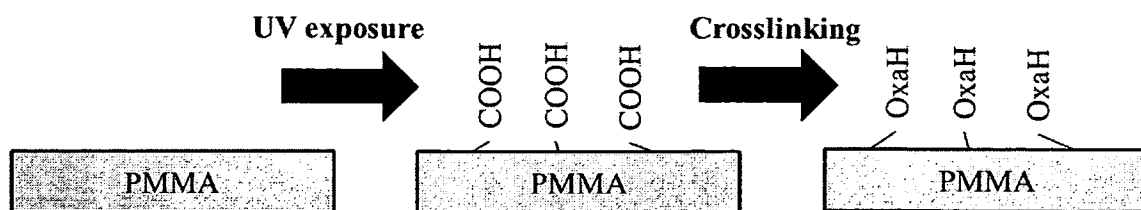
Figure 2-6: Scheme for immobilizing oxalyldihydrazide onto the surface of PMMA

2.7 Theoretical Modeling

Oxalyldihydrazide has not been used for microfluidic enrichment prior to the work presented in this dissertation. It is important to examine the aspects that can lead to failure of the enrichment technique. Failure will depend on the energy and critical velocity required to break the bond formed between oxalyldihydrazide and PMMA and oxalyldihydrazide and amino acid residues of carbonylated proteins. Therefore, density functional theory was used to simulate these reactions and calculate the binding energies, and Stokes' law was used to determine the critical velocity is calculated.

2.7.1 Density Functional Theory

Density functional theory (DFT) is based on functions that describe the ground state of a multi-electron system by using electron density (Li et al., 2012). DFT is more efficient than other theories that involve electronic structures because it reduces the number of variables required to complete the calculation. The process is not computationally costly and the results are relatively accurate compared to other methods. Therefore, DFT is seen as an acceptable method for calculating bonding strengths, reactivities, molecular properties, and structural analysis (Bealing et al., 2012). For additional details on density functional theory, refer to Kunjumon (2011).

2.7.2   Critical Velocity Calculation

If it is assumed that excessive shear stress will break the bonds between oxalyldihydrazide and the protein, then the critical velocity that would cause such breakage can be determined using Stokes' Law. Assuming that the protein, of radius r is immobilized and stationary and exposed to a fluid flow velocity, v, then Stokes Law gives the total force on the protein as:

$$F = 6\pi\eta rv, \qquad \text{Eq. 2-2}$$

given by Bell (1978). In the equation, η is the viscosity of the flowing fluid. A critical force can be determined using the binding energy determined from the DFT calculations. Because the critical force is directly proportional to the critical flow velocity, the critical flow velocity can be calculated. For additional details on Stokes' law and its application, see Bell (1978).

2.7.3   Diffusion of a Protein through a Channel

For a small molecule in a flowing field of velocity v inside a channel of length L, the distance of diffusion inside the channel can be calculated using Eq. 2-3:

$$d = \sqrt{\frac{DL}{v}}. \qquad \text{Eq. 2-3}$$

Using the protein cytochrome c as the diffusing molecule, a diffusion distance inside a microchannel of length 1.5 cm in a flowing velocity of 0.1666 cm/s can be calculated as shown in Eq. 2-4. The diffusion coefficient was taken from experimental data presented by Kontturi et al. (1992):

$$d = \sqrt{\frac{(1.65 \times 10^{-6})(1.5)}{0.1666}}, \qquad \text{Eq. 2-4}$$

$$d = 0.0038 \; cm \; or \; 38 \; \mu m. \qquad \text{Eq. 2-5}$$

2.7.4 Oxidative Stress Block Diagram

Figure 2-7 shows a flowchart of the oxidative stress process. When an organism is exposed to a foreign entity or suffers an injury, an inflammatory response occurs. This response triggers the release of ROS into the cytosol, which contributes to oxidative stress. This event is transient as ROS activity activates the anti-oxidant system. Anti-oxidants inactivate the ROS, stopping further oxidative stress. Cumulative oxidative events contribute to aging. Aging inhibits the activity of the anti-oxidant system, as the enzymes break down over a lifetime. Some enzymes are even oxidized under oxidative stress conditions, such as superoxide dismutase (SOD). So, as demonstrated in the block diagram, oxidative stress is a cumulative process that expands, even under short, transient conditions.
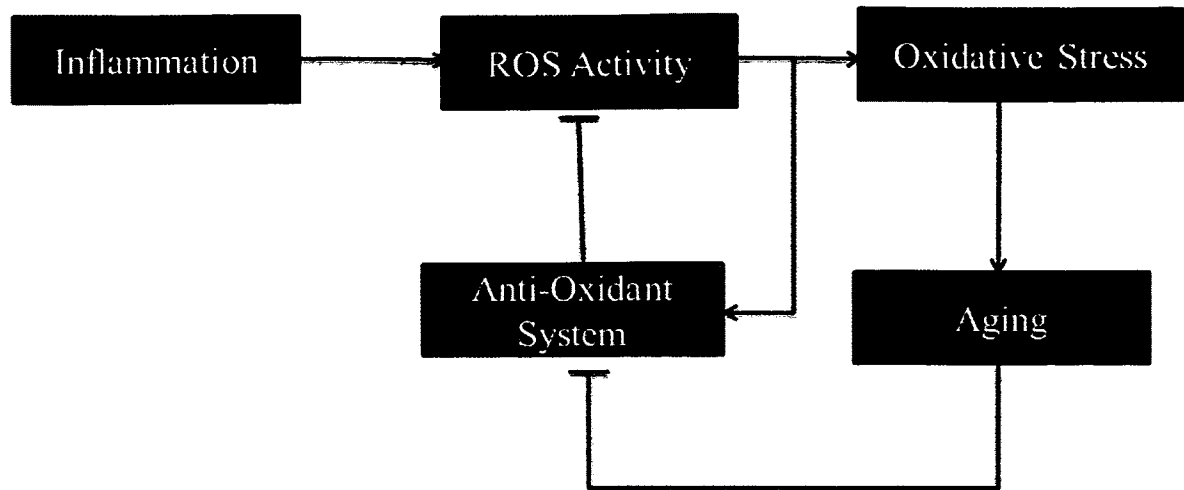
Figure 2-7: Flowchart of the oxidative stress process

2.7.5 One-compartment Model of Oxidative Stress in the Cytosol

The effects of oxidative stress will be demonstrated further by analyzing a one-compartment model of anti-oxidant activity inside the cell cytosol. The model is shown in Figure 2-8. The model is based on the activity of catalase, an enzyme that degrades hydrogen peroxide into water and oxygen. There are five assumptions for this model.

1. All catalase activity is included in the clearance

2. ROS introduction is treated like a bolus injection

3. No ROS is present in the cytosol prior to the introduction

4. $K_e = K_{cat}$ of catalase

5. All activity takes place in the cytosol, therefore organelles are not considered in this model.
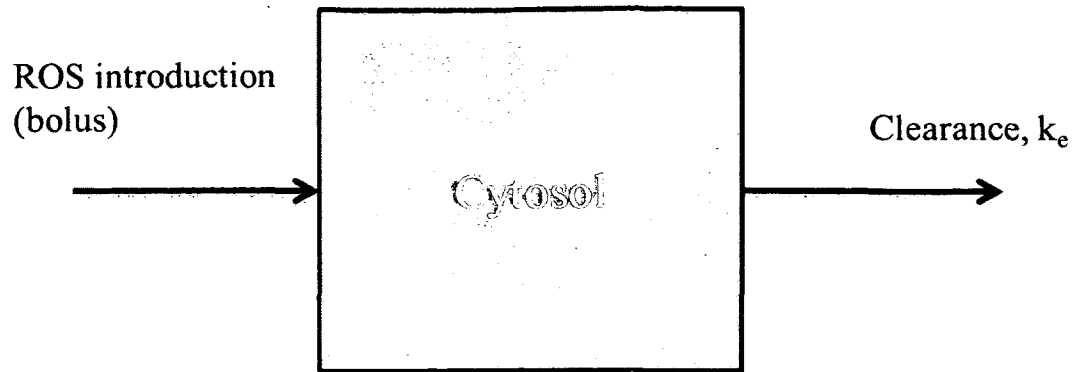
Figure 2-8: One-compartment model of the cell cytosol

There are three conditions investigated within the model.

1. Physiological conditions: 50 μM H_2O_2, 100 % catalase activity

2. Inflammation response: 100 μM H_2O_2, 100 % catalase activity

3. Aging condition: 50 μM H_2O_2, 20 % catalase activity

The governing equation is given as follows:

$$\frac{dC}{dt} = -k_e C + C_0 \delta(t),$$
<div align="right">Eq. 2-6</div>

where

$$C_0 = \frac{D}{V}.$$
<div align="right">Eq. 2-7</div>

The boundary condition, $C = 0$ at $t = 0$, will be used because there is no ROS

present in the system prior to injection, as given by Assumption 3. Applying the

boundary condition to Eq. 2-6, the equation simplifies to Eq. 2-8:

$$\frac{dC}{dt} = -k_e C.$$
<div align="right">Eq. 2-8</div>

With the initial condition $C = C_0$ at $t = 0$, the solution to the differential equation is:

$$C = C_0 e^{-k_e t},$$ Eq. 2-9

where, according to Assumption 4, $k_e = 4 \times 10^7$, and where C_0 takes different values, according to the three stated conditions. The solutions for the equations, with these constant values are as follows:

Condition 1:

$$C = 50 e^{-4 \times 10^7 t},$$ Eq. 2-10

Condition 2:

$$C = 100 e^{-4 \times 10^7 t},$$ Eq. 2-11

Condition 3:

$$C = 50 e^{-8 \times 10^6 t}.$$ Eq. 2-12

The half-life of the reactive oxygen species is important to consider when looking at an oxidative stress situation. Half-life can be calculated from Eq. 2-13:

$$t_{1/2} = \frac{\ln(2)}{k_e}.$$ Eq. 2-13

From Eq. 2-13, the half-lives for the stated conditions are:

Condition 1: 17.32 ns

Condition 2: 17.32 ns

Condition 3: 86.62 ns

These results indicate that half-life depends on the enzymatic activity of the anti-oxidant system, and not the amount of oxidants present. If the activity of the enzyme is

maintained, the oxidants will be inactivated before they can do heavy oxidative damage to native tissues.

The area under the curve (AUC) is the integral of the concentration, which is directly related to oxidative stress. It is calculated from Eq. 2-14:

$$AUC = \int C \, dt. \qquad \text{Eq. 2-14}$$

The solution of Eq. 2-14 is Eq. 2-15.

$$AUC = \frac{C_0}{k_e} = 1.443 C_0 t_{1/2}. \qquad \text{Eq. 2-15}$$

The two solutions to AUC in Eq. 2-15 are the result of a manipulation of Eq. 2-13 that relates $t_{1/2}$ to k_e. Applying Eq. 2-15 to the conditions generates the following results:

Condition 1: 1250 μM·ns,

Condition 2: 2500 μM·ns,

Condition 3: 6250 μM·ns.

The model gives valuable insight into the workings of oxidative stress, even though it is simplistic in nature. The AUC results tell us that under transient inflammation response and in aging conditions, oxidative stress increases at a greater rate. These results imply that an organism suffers oxidative stress over the course of its life through enzymatic inactivation and through immune responses.

CHAPTER 3

MICROFLUIDIC ENRICHMENT TECHNIQUE DEVELOPMENT

3.1 Introduction

In this chapter, the development of a novel microfluidic enrichment technique for carbonylated proteins will be discussed. *In vitro* oxidized cytochrome c is used as a model protein. Capture is achieved through specific manipulation of the PMMA polymer to attach oxalyldihydrazide, a crosslinker specific to carbonyls, to the surface of the microchip. *In vitro* oxidized BSA is used to verify the working of the surface modification and *in vitro* oxidized cytochrome c is used as the target molecule to demonstrate the selectivity of the chip. Finally, the study is concluded with analysis of the technique's ability to capture low abundance target proteins from a mixture containing an excess of a large blocking protein. Surface modification of PMMA is verified through unique analytical techniques. Surface elemental analysis and roughness were examined by X-ray Photoelectron Spectroscopy (XPS) and Atomic Force Microscopy (AFM), respectively. Additionally, fluorescence microscopy was used for chemical functional groups mapping to verify the presence of desired crosslinkers. This work is the first to propose the use of oxalyldihydrazide as a method of carbonylated protein enrichment. Use of a crosslinker that is specific to carbonyls eliminates the need for derivatization, extensive washing, and preconcentration steps afterwards. In addition,

this is the first report of carbonylated protein enrichment through coupling the use of a

crosslinker to a microchip. Portions of this chapter are published in Hollins et al. (2012).

3.2   Materials and Methods

3.2.1   Materials

PMMA sheets were purchased from Goodfellow. 2,4-dinitrophenylhydrazine

(DNPH), EDTA, HEPES, potassium chloride, magnesium chloride, sodium ascorbate,

iron(III) chloride, hydrochloric acid, formic acid, N-(3-dimethylaminopropyl)-N'-

ethylcarbodiimide (EDC), albumin, tetramethylrhodamineisothiocyanate (TRITC-BSA)

and bovine serum albumin were purchased from Sigma Aldrich (St. Louis, MO).

Oxalyldihydrazide was purchased from Alfa Aesar (Ward Hill, MA). N-

hydrosuccinimide (NHS) was purchased from Thermo Scientific (Rockford, IL).

Naphthalene-2,3-dicarboxaldehyde (NDA) was purchased from Invitrogen (Eugene, OR).

Cytochrome c was purchased from EMD Chemicals (Gibbstown, NJ).

3.2.2   Metal Catalyzed Oxidation

Bovine serum albumin (BSA) and cytochrome c were dissolved at 10 mg/mL and

5 mg/mL, respectively, in oxidation buffer (50 mM HEPES buffer, pH 7.4, containing

100 mM KCl and 10 mM $MgCl_2$). The proteins were oxidized *in vitro* using metal

catalyzed oxidation (Amici et al., 1989). Briefly, 30 mL of oxidation buffer containing

proteins was supplemented with neutral ascorbic acid and $FeCl_3$, to final concentrations

of 25 mM and 100 μM, respectively. The mixture was incubated overnight at 37° C in a

shaking bath. Oxidation was terminated by adding EDTA to a final concentration of

1 mM. Proteins were aliquoted and frozen at -20° C until use. Proteins were diluted to

required concentrations prior to experiments. Successful oxidation was confirmed using the spectrophotometric DNPH assay.

3.2.3   DNPH Assay of Proteins

Protein oxidation was characterized using the well-established DNPH spectrophotometric assay. A 500 μL solution of 2 M HCl containing 10 mM DNPH was prepared. 100 μL of oxidized BSA was added to the solution and allowed to sit at room temperature for one hour. After incubation, TCA was added to a final concentration of 10 % (w/v) and the solution was incubated on ice for thirty minutes to precipitate the proteins. The solution was centrifuged for 3 minutes at 11000 rpm and the supernatant was discarded. The protein pellet was washed in a solution composed of equal parts ethanol and ethyl acetate. After each wash, the solution was centrifuged at 11000 rpm for 90 seconds and the supernatant was removed. After washing, the protein pellet was redissolved in 6 M guanidine. Absorbance was read using a Nanodrop 2000 UV/Vis spectrometer at 370 nm to determine the concentration of carbonyls in the oxidized BSA model.

3.2.4   Off-chip Protein Loading

Prior to experiments inside the channel, oxidized cytochrome c was labelled with naphthalene-2,3-dicarboxaldehyde (NDA), a fluorogenic probe (Pinto et al., 2003). Briefly, NDA was dissolved in 100% methanol. 100 μL of 2 mg/mL oxidized cytochrome c was placed in a tube. 400 μL of 10 mM borate buffer (pH 9.4) was added to the tube, followed by 100 μL of 10 mM KCN dissolved in water. Lastly, 400 μL of 5 mM NDA/methanol stock was added to the tube. The tube was allowed to incubate for 30 minutes at room temperature. Following incubation, the sample was rinsed in an

Amicon Ultra-4 centrifugal filter unit (3,000 MW cutoff) to remove any unbound NDA. The rinse was done in 10 mM borate buffer for 20 minutes. The solution was spun down to about 200 μL, and the sample was supplemented with 800 μL of borate buffer to give a total volume of 1 mL.

3.2.5   Microchip Fabrication

The microchip used in these experiments is shown in Figure 3-1. The bed of the PMMA channel has microposts of 100 μm diameter. The depth of the channel is 50 μm, and the length of the channel is 12.5 mm. The capture bed is 1 mm wide, containing 150 microposts. The post-to-post spacing is 150 μm. The surface area available for protein capture is 27.6 mm^2. Because the channel is relatively wide, the posts are included to prevent the coverslip from collapsing into the channel during annealing. The reservoirs are 1.6 mm in diameter. The chip fabrication process started with the micromilling of a mold master. Specifically, the above-mentioned microstructures were milled on the surface of a 6.3 mm thick brass plate (alloy 353 engravers brass, McMaster Carr, Atlanta, GA) using a high-precision micromilling machine (Kern Mmp 2522, Kern Micro-und Feinwerktechnik Gmbh & Co. KG; Germany). A typical milling cycle started with a rough milling to prepare an approximate shape for subsequent finishing cut. The feed rates were 20 mm/min for a 50 μm drill bit.
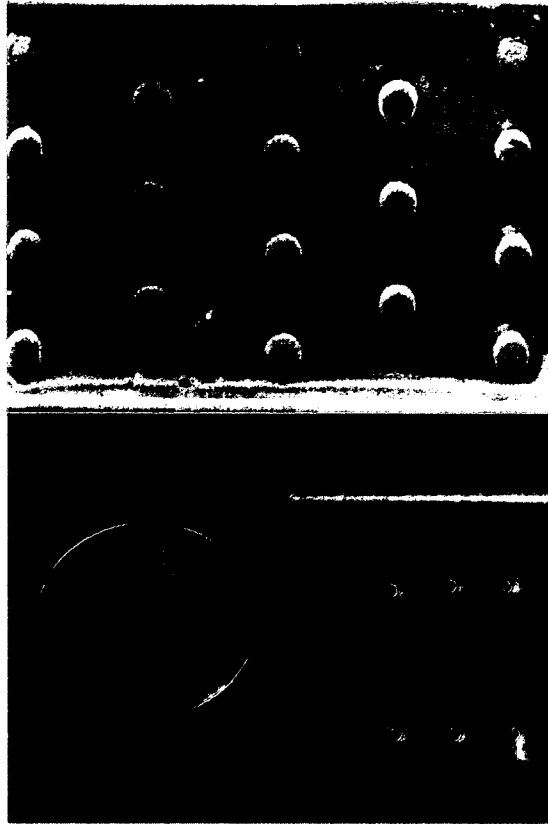
Figure 3-1: The microchip used in the studies discussed in this chapter

PMMA sheets (Plexiglas MC, GE Polymershapes, New Orleans, LA) were cut

into 65 mm diameter discs and cleaned by rinsing with 2-propanol and distilled water.

After removing residual moisture by placing them in an oven at 75 °C overnight, the

milled microstructures were pressed into the chips using a commercial hydraulic press

(PHI Precision Press model TS-21-H-C, City of Industry, CA). A home-built vacuum

chamber was installed into the hot embossing press to keep ultra-low air pressure

(< 10 kPa) for complete filling of the mold master. The embossing was performed at a

force of 5 kN for 5 minutes at 155 °C. After embossing, injection and collection

reservoirs were created by using a drill press and a 1/16" black oxide drill bit. For the

final assembly, a thin PMMA cover plate of 250 μm thickness (Goodfellow, Oakdale,

PA) was thermo-bonded to the face of the micropost array chip. For this purpose, the

microfluidic chip and the cover plates were clamped between two 3" x 3" glass plates

(McMaster) and placed inside a convection oven at 97 °C for 30 minutes. PEEK tubing

(800 μm diameter) was attached to enclosed microchips using EPOXY. Chips were

stored until ready for use for experiments. Prior to experiments, the chips were

connected to a syringe pump using a LUER connector. The instrumental setup is shown

in Figure 3-2.
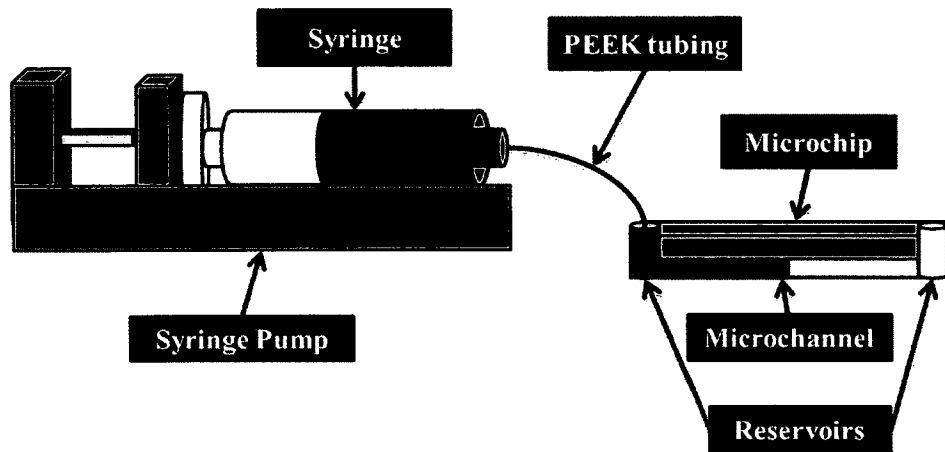
Figure 3-2: Instrumental setup used for loading the microfluidic device

3.2.6   PMMA Surface Modification

The PMMA surface was modified according to the first two steps shown in Figure

3-3 to produce a PMMA chip containing a crosslinker with hydrazide functions that

immobilize carbonylated proteins onto carbonyl and ketone moieties. Exposure to UV

radiation functionalized the PMMA chips with a carboxylic acid group, after which this

group was modified by the crosslinker oxalyldihydrazide to provide a hydrazine group.

These groups could then react with the carbonyl group of the proteins of interest to form

hydrazone linkages. The proteins of interest (BSA and cytochrome c) could then be removed from the modified PMMA with formic acid and heat.
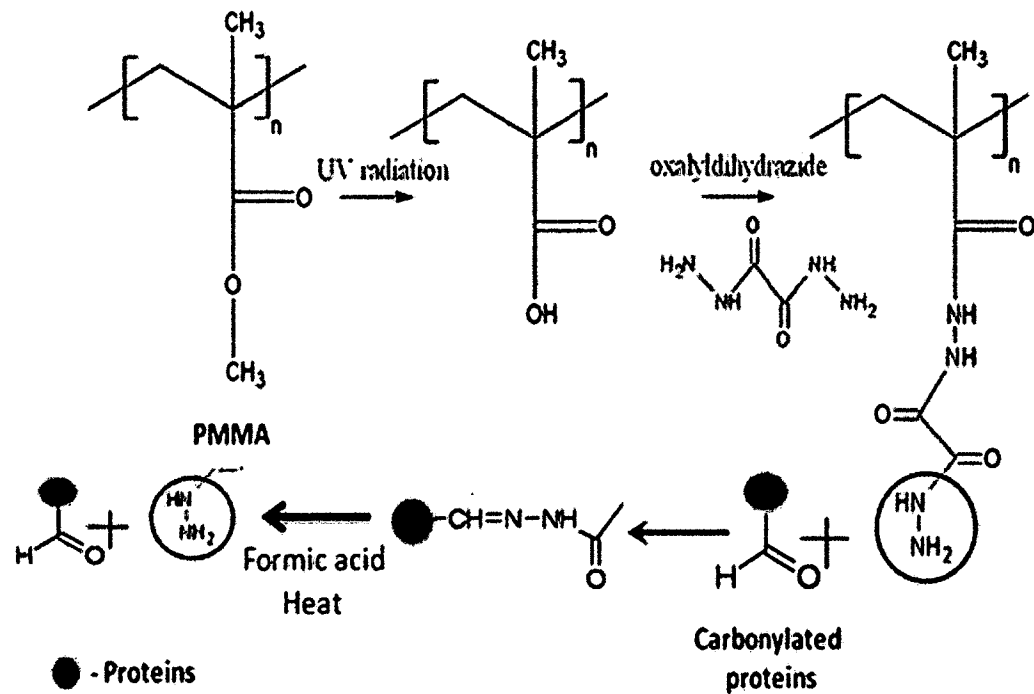
Figure 3-3: Chemical scheme employed for the enrichment of carbonylated proteins within a microchip.

Prior to surface modification, the microchips were cleaned using Micro-90 in water and rinsed with 10 % isopropanol and water. Excess fluid was removed under a flowing stream of nitrogen and dried in an oven at 70 °C to evaporate any water trapped in the microstructures. 250 μm PMMA cover slips were cut to enclose the microstructures. Both the microchips and cover slips were then exposed to ultraviolet light (254 nm, 15 mW/cm^2) for one hour. After UV exposure, the chips and cover slips were pressed together for annealing. Afterwards, PEEK tubing was attached to the injection reservoir of the chips. A syringe pump was used to pump 100 μL of MES

buffer containing 200 mM EDC and 50 mM NHS through the channel at a flow rate of

10 μL/min and the solution was allowed to incubate for 30 minutes. After the incubation,

100 μL of 50 mM oxalyldihydrazide dissolved in MES buffer was flushed through the

channel at a flow rate of 10 μL/min and allowed to incubate overnight. The channels

were loaded with proteins the following morning. Solutions of NHS, EDC, and

oxalyldihydrazide were prepared fresh daily. For experiments conducted on PMMA

sheets, the same procedure was used for surface modification. Figure 3-4 shows an

overall flow chart of the surface modification procedure.

Start with micromilled PMMA chip		Crosslink PMMA with oxalyldihydrazide	→	Block non-specific binding sites with BSA
↓		↑		↓
Clean PMMA and dry overnight in oven		Attach PMMA to PEEK tubing		Load proteins into chip and incubate for two hours
↓		↑		↓
Expose PMMA to UV light	→	Thermal bond PMMA		■
Verified using analytical techniques (AFM, XPS)		■		Verified using both analytical/fluorescence techniques
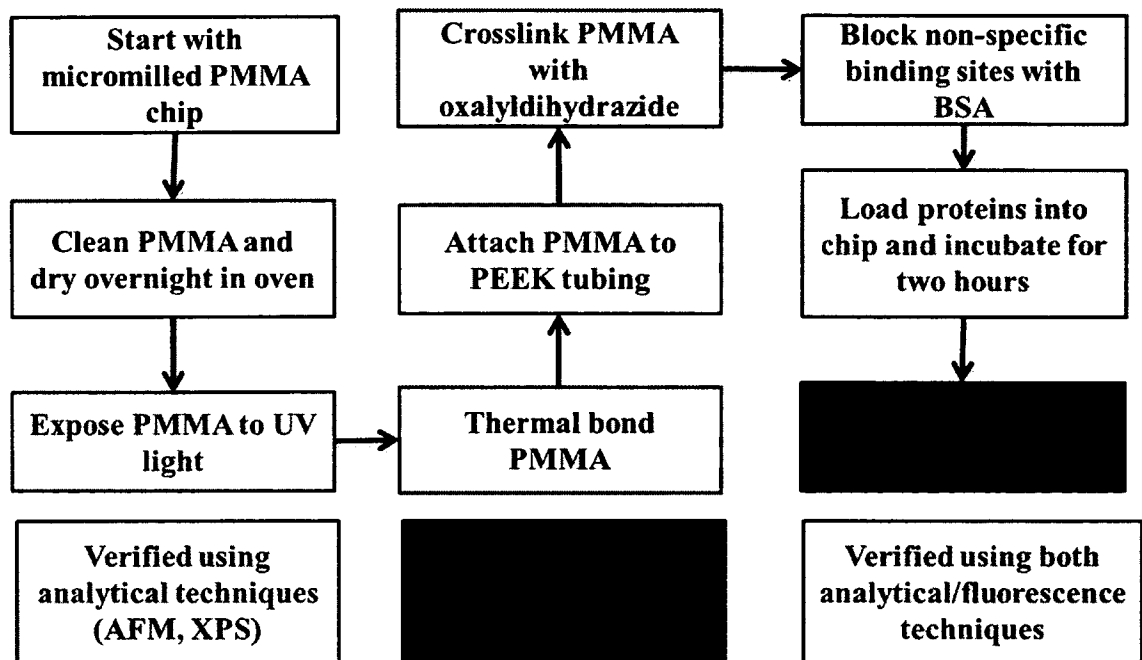
Figure 3-4: Flowchart for the enrichment procedure on a microfluidic device

3.2.7   Validation of Surface Chemistry

Surface modification was validated at each step of the procedure using a PMMA

sheet. Successful UV exposure was demonstrated using water contact angle

measurements. All modification steps were analyzed using X-ray Photoelectron

Spectroscopy (XPS) and Atomic Force Spectroscopy (AFM). For XPS and AFM studies, PMMA sheets were treated with UV radiation, and then incubated in 1 mL of EDC/NHS, oxalyldihydrazide, and proteins. After incubation, each sheet, it was rinsed in dH_2O and dried under a flowing stream of nitrogen and stored until analysis.

For XPS analysis, all modified and pristine PMMA surfaces were measured by a Karatos AXIS ultra-X-ray photoelectron spectrometer using a monochromatic Al Kα X-ray source (240 W) and charge neutralization. The sample analyses were performed with a 90° takeoff angle and spectral peaks were analyzed using the Kratos software.

AFM studies were performed with a commercial instrument (Nanosurf easyScan 2 equipped with a TFT-LCD display). It was operated by a silicon SPM-sensor (NanoWorld, Neuchâtel, Switzerland) in contact mode with 0.2 N/m spring constant and 13 kHz response frequency. The ammonium-coated detector is 2 μm thick, 450 μm long, and 50 μm wide. All images were recorded in air at room temperature, at a scan speed of 1.4 Hz. The background slope was resolved using the program provided by the manufacturer. No further filtering was performed.

Oxalyldihydrazide immobilization within the chip was demonstrated using a fluorescent analogue, Alexa 488 hydrazide. Alexa 488 hydrazide was loaded as described above, and fluorescence was detected using an Olympus IX-51 Fluorescence Microscope with an attached CCD camera. Images were taken using a 10x objective and 500 ms exposure time. Filter settings for FITC was used for image capture.

3.2.8   Protein Capture

Prior to loading the target protein into the channel, the channel was blocked by loading 75 μL of 2 mg/mL BSA at a rate of 5 μL/min. The BSA solution remained in the

channel for 1 hour and then was pushed out using air. Following the blocking,

0.2 mg/mL of NDA-labeled oxidized cytochrome c was loaded into the channel for

100 minutes at a rate of 5 µL/min using a syringe pump. Solution was collected at the

collection reservoir every minute for analysis. After the channel was loaded, the chip

was incubated in the dark for two hours. Protein capture was visualized using

fluorescence microscopy. For the selective capture study, cytochrome c and TRITC-

BSA were mixed, with concentrations of 0.2 mg/mL and 0.8 mg/mL, respectively, in the

same solution and pushed through the channel at 5 µL/min following BSA blocking.

Solution was collected as described above and analyzed every minute on the

Nanodrop 3300 fluorescence spectrophotometer.

3.2.9 Protein Elution

Proteins were eluted using 10 % formic acid. The channel was filled with formic

acid. Formic acid was loaded at a rate of 10 µL/min. The channel was incubated in an

oven at 60 °C for 30 minutes. Borate buffer was also heated to 60 °C. After incubation,

the channel was rinsed with borate buffer at a rate of 5 µL/min to collect the proteins.

The rinsing occurred on a hot plate held at a constant 60 °C. The eluted solution was

analyzed every minute.

3.3 Results and Discussion

3.3.1 Protein Characterization

Oxidized BSA absorbance was measured with the well-established DNPH

spectrophotometric assay (Levine et al. 1990). Measuring the absorbance at 370 nm

yielded a carbonyl concentration of 18 nmol/mg protein. Figure 3-5 shows the results of

the DNPH assay. The results obtained from this study verified the placement of carbonyl

48

groups on our model protein for further studies. For experiments within the chip, protein

samples were diluted prior to loading to prevent chip saturation. For XPS and AFM

studies, protein concentrations of 10 mg/mL were used. Concentrations were determined

spectrophotometrically using a Nanodrop 3300 Fluorescence Reader. For cytochrome c,

a large native peak around 400 nm is present, completely covering the carbonyl

absorbance at 370 nm. Therefore, carbonyl content was not quantified for cytochrome c

following the metal-catalyzed oxidation process.
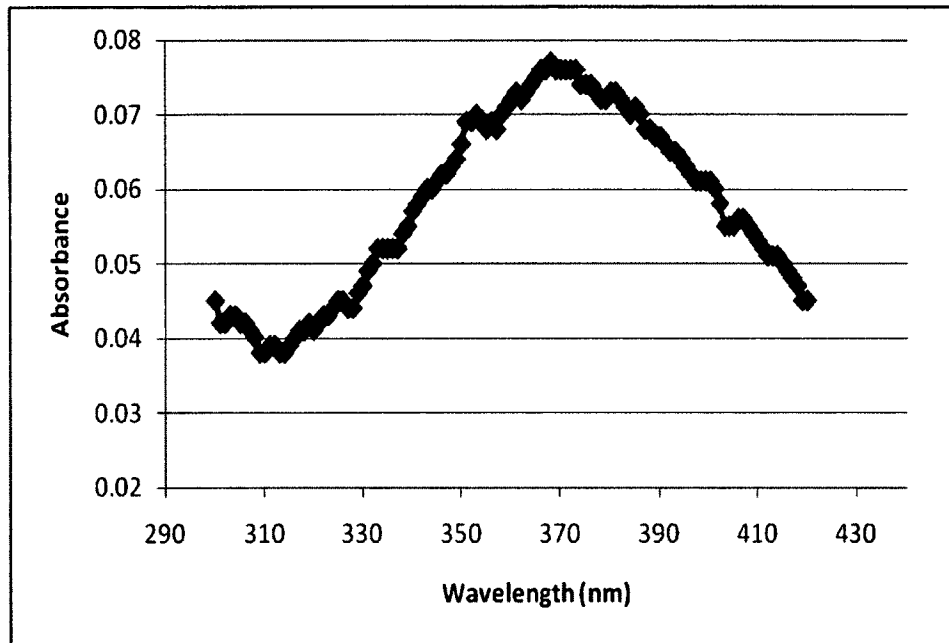
Figure 3-5: Results of the DNPH assay for the determination of carbonyl content in
oxidized BSA

3.3.2   Water Contact Angle Measurement

Several techniques were used to verify the surface chemistry. First, UV

modification was confirmed using water contact angle measurements. Carboxyl groups

on the surface of PMMA make the surface more hydrophilic. After exposing a PMMA

sheet to UV treatment for twenty minutes, a contact angle of 46.0 ± 5.7° (n = 3) was

observed. This angle was compared to a contact angle of 72.2 ± 7.8° (n = 3) for pristine, unmodified PMMA. The decrease was not as low as reported values in the literature of 30° for a similar exposure time (Wei et al., 2005), so UV exposure time was increased to one hour for subsequent experiments. The literature results demonstrate a plateau at around 40 minutes, so a one hour exposure time was used to generate the expected results. A one hour exposure time was chosen to compensate for any differences between the setups of the two UV systems used in this study and the one used in the literature study. The difference in the system setup could account for the difference between surface contact angles after 20 minutes. Figure 3-6 shows the change in water contact angle on the PMMA coverslip after UV exposure.
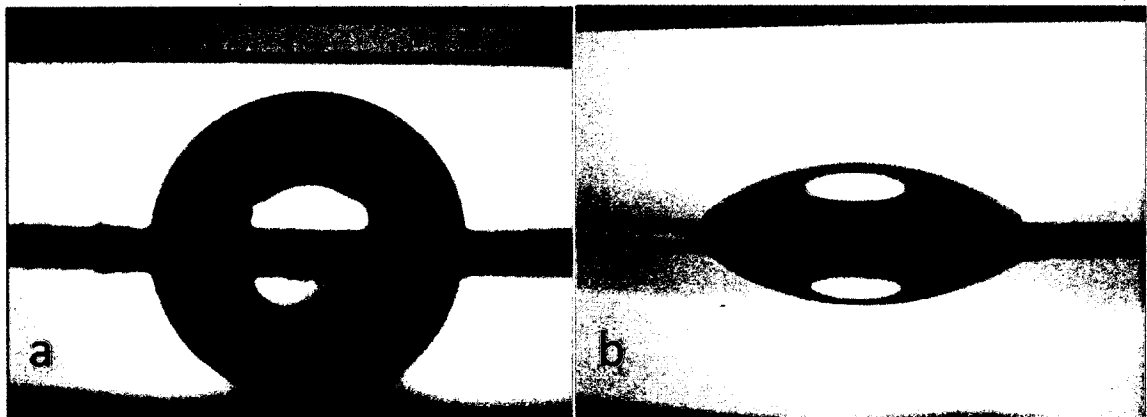
Figure 3-6: Water contact angle between pristine PMMA (a) and UV-modified PMMA (b)

3.3.3   Fluorescence Microscopy

To ensure that oxalyldihydrazide would bind to the modified PMMA, a fluorescent analogue, Alexa 488 hydrazide, was used in chip. This analogue was used because it has the same functional group as the chosen crosslinker. Alexa 488 hydrazide was loaded into the closed microchip in the same fashion as described for

oxalyldihydrazide (detailed in the Methods section). The fluorescence observed in the

channel after a buffer rinse indicated Alexa 488 hydrazide was immobilized on the

surface of the microchannel. As a control, Alexa 488 hydrazide was incubated in a

similar fashion inside a pristine (unmodified) PMMA microchip. After a buffer rinse, no

fluorescence was observed within the microchannel from the unmodified PMMA. The

observation is shown in Figure 3-7.
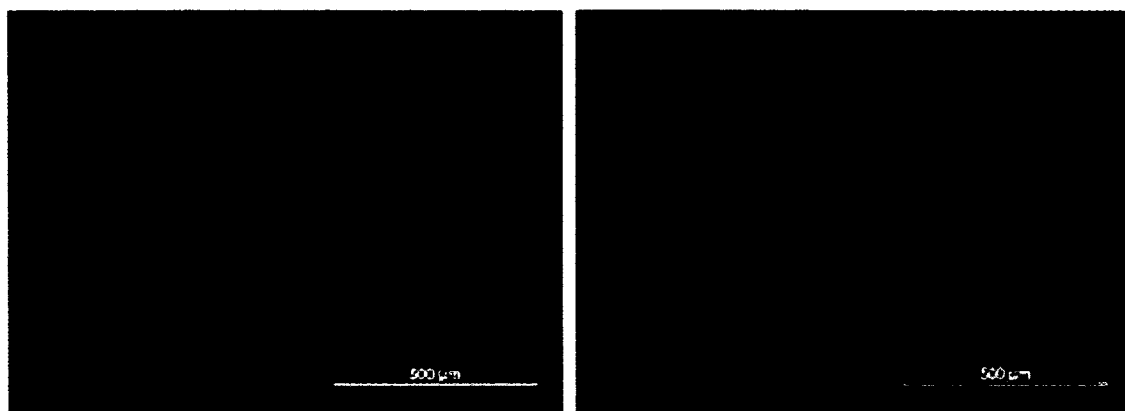
Figure 3-7: Fluorescence microscopy images of an unmodified channel (a) and a UV-modified channel (b) after an Alexa 488 hydrazide incubation and rinse

3.3.4   XPS Analysis

XPS studies were conducted on PMMA sheets to verify the chemistry used in the

surface modification procedure. The samples were prepared modularly, so each new

modification built upon the last, as indicated in Figure 3-3. The results of the XPS study

are shown in Table 3-1. After UV modification, oxygen percentage increased,

demonstrating the loss of a carbon atom as the methyl group was replaced with a

hydrogen. The value obtained in this step (O% = 26.74) matched reported values in the

literature (O% = 26.28) after one hour UV exposure time (Wei et al., 2005). After

oxalyldihydrazide incubation, an increase in nitrogen was observed, corresponding to the

attachment of the hydrazide functionalities. Oxidized BSA was used to demonstrate

protein immobilization on the modified surface of PMMA. Protein incubation shows a

great increase in nitrogen composition. Because the coverslip was rinsed prior to

completing the next step, the nitrogen increase seen here was attributed to BSA

immobilization. BSA is a large protein that contains numerous nitrogen atoms in its

lysine side chains and through its peptide bonds, so the increase in nitrogen content is not

surprising. The presence of nitrogen after UV exposure can be attributed to leakage of

nitrogen present in the air into the sample container. Native BSA was used as well to

investigate the results of non-specific binding on the coverslip.

Table 3-1: XPS data for the different surface modifications

Sample	C (at. %)	O (at. %)	N (at. %)	C/O
Native PMMA	78.78	21.22	0	3.71
UV-modified PMMA	70.52	26.74	2.74	2.64
Oxalyldihydrazide crosslinked PMMA	71.80	18.94	4.24	3.79
Oxidized-BSA immobilized PMMA	69.97	19.93	10.11	3.51
Native-BSA immobilized PMMA	70.50	17.72	11.78	3.98

3.3.5   AFM Analysis

PMMA sheets were prepared as indicated in Section 3.2.6. AFM studies were

done to calculate the surface roughness of PMMA following each step of the process.

Because additional molecules were being placed on the surface of PMMA, the roughness was expected to increase. The results are shown in Table 3-2. The increase in roughness after UV treatment and oxalyldihydrazide immobilization was small, consistent with the small size of the molecules placed on the surface. A great increase is observed following oxidized BSA incubation. Because of the size of BSA (66 kDa), a large increase such as this could be expected. A similar increase was observed with native BSA, though not as large.

Table 3-2: AFM results for the different surface modification stages

Stage	Area Surface Roughness (RMS)
Native PMMA	4.03 nm
UV-modified PMMA	6.41 nm
Oxalyldihydrazide-crosslinked PMMA	9.87 nm
Oxidized BSA-immobilized PMMA	31.5 nm
Native BSA-immobilized PMMA (Control)	20.5 nm

These experiments were conducted on the PMMA sheets, which were used as received from Goodfellow. Within the microchip, it is important to consider the effect that the micromilling process will have on the surface roughness of the microfluidic channel. Any milling marks present on the mold master will be transferred to the microfluidic chip, since hot-embossing is a technique capable of replicating structures to the nanometer range. Over time, the characteristics of the mold master can change, and introduce inconsistencies in the microstructures. To minimize this problem, a two-fold strategy was employed. First, because of its excellent machining characteristics, brass

was used as the mold master. Secondly, the mold master milling was completed using two steps, removal of the bulk material using a large diameter (500 μm) bit, followed by use of a smaller milling bit for the finer structures of the design.

3.3.6   Protein Capture

NDA-labelled oxidized cytochrome c (0.2 mg/mL) was loaded into the channel and allowed to incubate for two hours. During the loading process, the solution that flowed through the channel was collected for spectrophotometric analysis. NDA is a fluorogenic molecule that is only fluorescent after it has reacted with a primary amine group. Because we use BSA as a blocking protein for the channel, it is necessary to remove any unbound NDA prior to loading it into the channel. This removal prevented any blocking BSA from being labelled with the NDA and altering the results obtained. The amount of oxidized cytochrome c captured in the microchip could be quantified using a Nanodrop 3300 spectrophotometer. Figure 3-8 shows the protein amounts collected each minute. The total protein mass captured during the continuous injection period of 100 minutes is 7.5 μg. The plateau seen in Figure 3-8suggest binding of the target molecule to the reactive sites on the surface of the microchannel, allowing for less binding to occur as more proteins are exposed to the chip, indicating a move toward saturation. Chip saturation occurs when all the available reactive sites for binding are consumed on the surface of the modified PMMA. Protein capture is also demonstrated qualitatively using fluorescence microscopy. The capture is shown in Figure 3-9. Capture is expected to be linear throughout the experiment, but the results indicate an area of non-linearity at the beginning of the study. A potential explanation for the non-linearity could be that the chip does not capture proteins during the initial loading phase,

when the solution is first exposed to the crosslinkers. As the chip becomes filled with fluid, capture improves because there are not two phases present against the crosslinkers.

In the fluorescence study, while not shown here, there are controls that could be used to verify the capture of the targeted proteins. One example would be to compare the channel following capture to a channel that does not have any proteins inside of it. Another control would be to not conduct multiple steps of the surface modification procedure, such as not doing a UV-modification step or crosslinking with oxalyldihydrazide, and comparing the fluorescence within the channels.
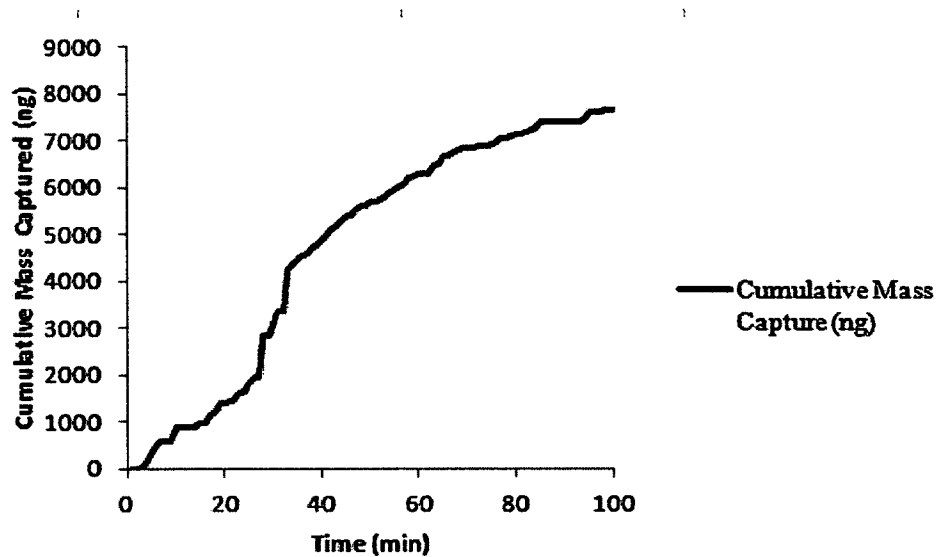
Figure 3-8: Cumulative capture of cytochrome c
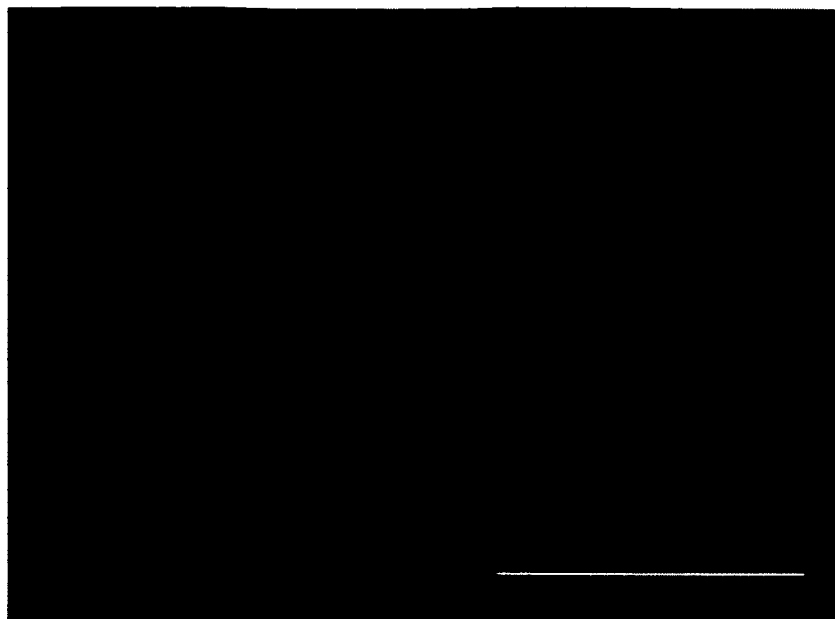
Figure 3-9: Fluorescence microscopy of cytochrome c capture following protein loading and excess fluid removal

3.3.7   Protein Elution

Formic acid and heat were used to elute the proteins. Formic acid breaks

hydrazone bonds when incubated at an elevated temperature (Roe et al., 2007). After

thirty minutes of incubation at 60 °C, the channel was rinsed with borate buffer. Since

the proteins were labelled and injected into the channel using borate buffer, this same

medium was chosen to collect the proteins during elution. The solution was collected

from the microchip and analyzed using the Nanodrop 3300. All the proteins injected into

the channel were eluted within three minutes of continuous injection of borate buffer.

The results are shown in Figure 3-10. The total amount of protein eluted was 8.5 µg.

When the amount of protein eluted is compared to the amount determined to be captured,

a cumulative elution efficiency of 113 % is obtained. The cumulative elution efficiency

was calculated as the percentage of proteins eluted from the channel and divided by the

total amount available for elution. For the data shown in Figure 3-10 as an example, after

one minute, 3.5 µg of the 7.5 µg captured is eluted, resulting in a cumulative elution

efficiency of 46 %. For each additional minute, the total of all the proteins eluted are

summed together and divided by the total protein amount available. The additional

proteins found in the elution could have been inside the injection tubing when injection

finished. Because the proteins are allowed to incubate for two hours following injection,

any proteins still in the tubing could diffuse into the chip and react with any available

surface. It is proposed that this action added the additional 1 µg of protein to the elution,

therefore yielding a cumulative elution efficiency in excess of 100 %.
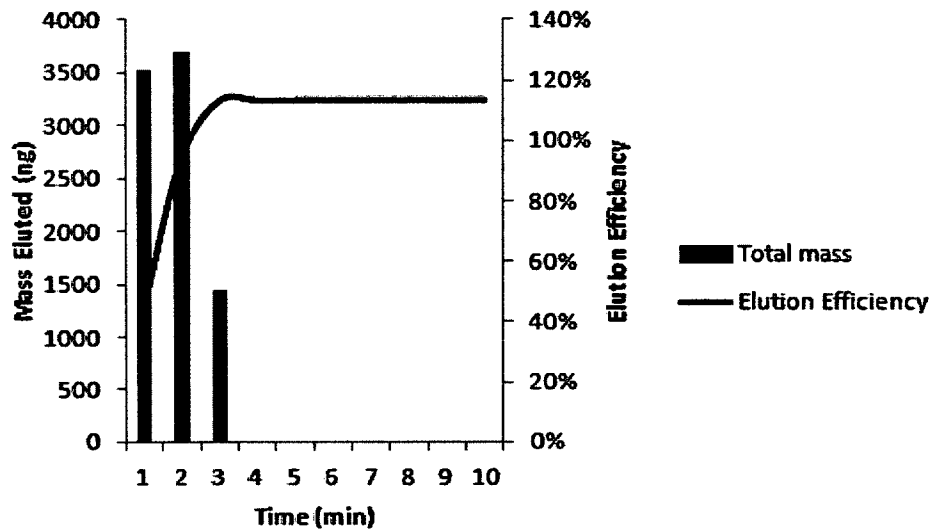
Figure 3-10: Protein elution per minute from the microfluidic device

The elution of the proteins increased the concentration of proteins available from

the original stock solution (0.2 mg/mL). The new concentration, using the 15 µL

required to elute all the proteins, is 0.53 mg/mL, an increase of 265 %.

3.3.8   Protein Mixture Results

To determine the specificity of the chip for oxidized proteins, oxidized

cytochrome c, labelled with NDA, was mixed in low abundance (1:4) with TRITC-BSA

and injected into the chip. The results of that study are shown in Figure 3-11. The chip

was able to capture 40 % of oxidized proteins over the 100 minute injection period,

whereas only 5 % of the unoxidized protein was captured. These results show that, even

in low abundance, the chip is highly specific to oxidized proteins. The 5 % capture

observed from the unoxidized protein (TRITC-BSA) could have been the result of some

proteins displacing BSA, which was used to block the chip. The results found for the

non-specific binding was confirmed by loading TRITC-BSA into a modified channel.

These results are seen in Figure 3-12. Without blocking, TRITC-BSA is captured within

the chip; after blocking, the capture is significantly lower. These results support the

reasoning that TRITC-BSA is displacing BSA within the channel and indicate the

necessity of blocking the chip prior to enrichment studies in order to increase the chip's

discrimination of oxidized and unoxidized proteins.
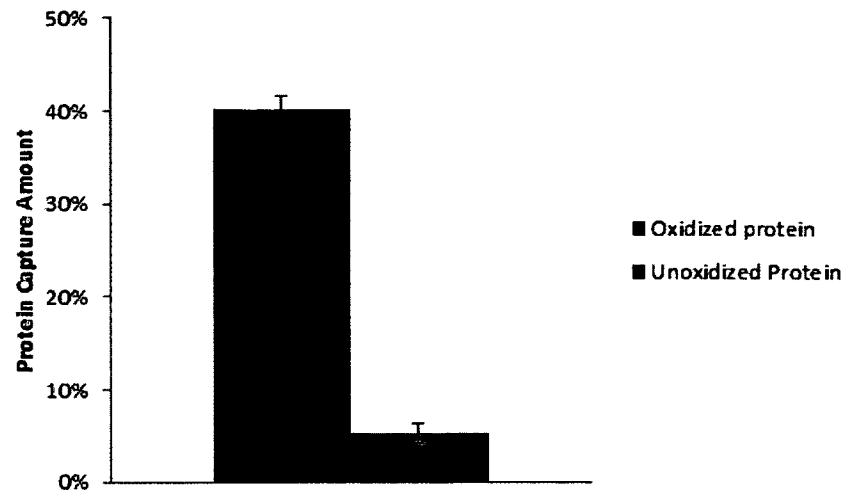
Figure 3-11: Results of the protein mixture study
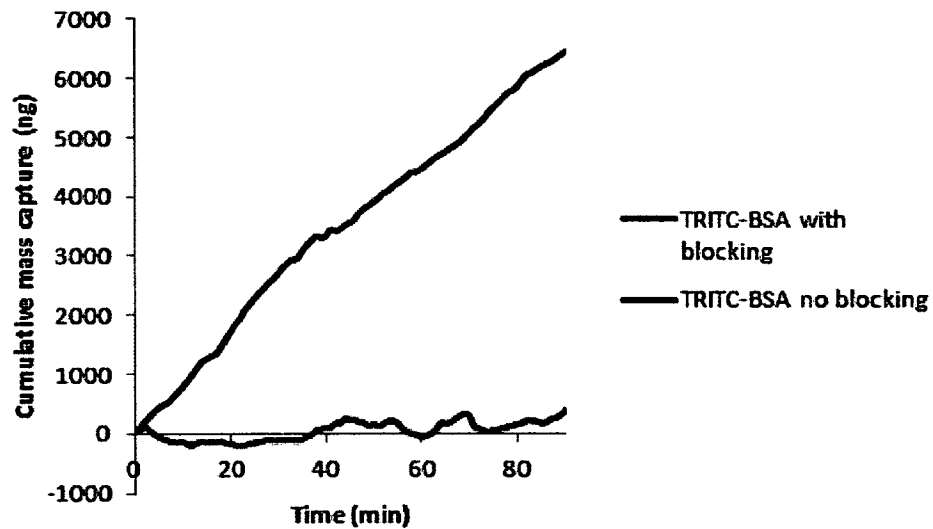
Figure 3-12: Non-specific binding with and without prior blocking of the channel with BSA

3.3.9   Discussion

The effect of fluid dynamics on the ability of the microchip to capture targets is

an area of future work. Flow rate studies can be used as a variable for optimizing protein

capture efficiency. While a faster flow rate would expose the modified surface to

additional proteins during the loading process, the effects of shear stress on the crosslinker, oxalyldihydrazide, would have to be considered. To date, no studies have been done on the strength of the bond formed between oxalyldihydrazide and the carboxyl-labelled PMMA surface or the hydrazone bond formed with the carbonyl of the protein. Excessively high flow rate could break the links that capture the target molecules, but excessively low flow rate will increase the time of the experiment. Therefore, flow rate needs to be optimized in future work.

Another area of consideration is the interior geometry of the chip. In this experiment, we used a low-density micropost interior. For future studies, the density of the microposts can be altered to determine if capture efficiency has a dependency on the interior geometry.

The method presented in this chapter has several advantages over the conventional avidin chromatography technique for carbonylated protein enrichment. One, there is no need to derivatize samples prior to enrichment for the technique. Even though the sample was derivatized with fluorogenic agents, it is not necessary if the device is being used as a preconcentrator. Chromatography requires the sample be derivatized with biotin, a process that is very time-consuming, including 12 hours for dialysis to remove unbound hydrazide. The technique presented here takes 4.5 hours from protein loading to elution. Also, in order to be effective, avidin chromatography needs at least 2.5 mg of protein, whereas this technique can enrich any amount of protein. The use of a microfluidic chip greatly reduces sample waste and protein elution occurs in a very small volume, greatly increasing the concentration of low abundance targets. Chromatography requires a high volume of elution solution, diluting even further an

already very dilute sample. Also, when the targets are released from the microchip, they are readily available for future studies, with the carbonyl available for additional labeling if necessary. In standard affinity chromatography, should the carbonyl need to be relabeled post-elution, the hydrazone bond between biotin and the carbonyl would need to be broken.

It is important to consider that the elution procedure for this technique is harsh for biomacromolecules such as proteins. Because of the increased temperature and acidic conditions for reversing the bond, the protein being captured will be denatured. In studies where the proteins are being identified, denaturing the protein will not be a concern. However, for applications in which the protein's function needs to be conserved, this technique may not be the best approach for protein enrichment.

3.4   Conclusions

In this chapter, proof of principle of a microfluidic enrichment technique for carbonylated proteins using oxalyldihydrazide as an immobilized crosslinker was presented. The preliminary results shown in this chapter demonstrate that the methodology is effective at capturing and eluting carbonylated proteins. Based on the new concentration of the proteins following elution, the microdevice has a preconcentration factor of 2.65. An area of work that remains is optimizing the capture process. Key areas for optimization include the flow rate at which proteins are injected into the channel and the effect of density on the capture efficiency of the chip. The optimization of these conditions, along with two other key variables, will be discussed in the following chapter.

CHAPTER 4

TECHNIQUE OPTIMIZATION

4.1   Introduction

In Chapter 3, a proof-of-principle microfluidic technique for enriching

carbonylated proteins was demonstrated. Capture, enrichment, and elution could be

achieved using the novel methodology. The procedure is capable of enriching proteins

on the microgram (μg) level, and the sample is eluted at a much higher concentration than

what is possible using the commercial standard. Specificity toward the target of interest

when a mixture of oxidized and unoxidized proteins was injected into the channel was

also shown. This chapter examines the effects of micropost density inside the

microchannel, concentration of the crosslinker, flow rate, and incubation time of the

crosslinker on capture within the microfluidic platform. It is shown that micropost

density has little effect on capture and that shorter incubation periods result in capture

that is marginally better than longer incubation times. In addition, slower flow rates

result in significantly better capture and protein capture follows a parabolic curve with

crosslinker concentration.

4.2   Materials and Methods

4.2.1   <u>Materials</u>

PMMA sheets were purchased from Goodfellow. EDTA, HEPES, potassium

chloride, magnesium chloride, sodium ascorbate, iron (III) chloride, and N-(3-

dimethylaminopropyl)-N-ethylcarbodiimide (EDC) and bovine serum albumin (BSA)

were purchased from Sigma Aldrich (St. Louis, MO). Oxalyldihydrazide was purchased

from Alfa Aesar (Ward Hill, MA). N-hydrosuccinimide (NHS) was purchased from

Thermo Scientific (Rockford, IL). Naphthalne-2, 3-dicarboxaldehyde (NDA) was

purchased from Invitrogen (Eugene, OR). Cytochrome c was purchased from EMD

Chemicals.

4.2.2   <u>Channel Construction</u>

The microchannels were formed using a nickel mold master and hot embossing.

The process is described in detail in the previous chapter. The two microchip designs

used in the study are shown in Figure 4-1. Both channels are 12.5 mm long and 1 mm

wide. The first channel, shown on the left, contains 150 microposts, with a post-to-post

spacing of 150 μm, measured edge to edge. This channel was used in the studies

discussed last chapter. The second channel, shown on the right, contains 465 posts, with

a post-to-post spacing of 100 μm, measured edge to edge. Following hot embossing, the

PMMA chips and PMMA sheets were washed and dried in an oven at 65 °C overnight.

Following drying, the chip and PMMA coverslips (250 μm thickness) were exposed to

UV light (254 nm, 15 mW/cm^2) for one hour to place carboxylic acid residues on the

PMMA surface. The chip and cover sheet were pressed together using 3" x 3" glass

plates and annealed at 97 °C for 30 minutes. PEEK tubing (800 μm diameter) was

attached to the reservoirs using marine EPOXY. The experimental setup is the same as

shown in Figure 3-2.
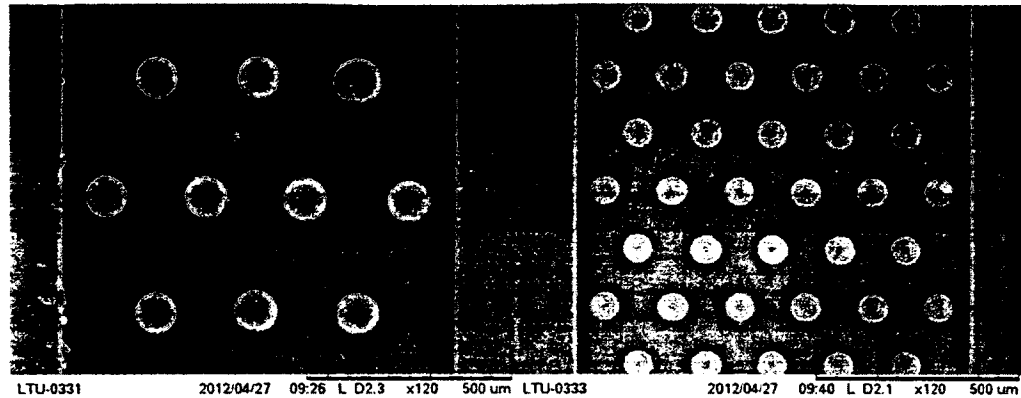
Figure 4-1: The two channel designs used in the optimization experiments. The channel on the left is the same channel used in the experiments in the last chapter. The channel on the right has a higher post density. The scale bar is 500 μm

4.2.3 Surface Modification

After the EPOXY was allowed to fully cure, 100 μL of MES buffer containing

200 mM EDC and 50 mM NHS was loaded into the channel using a syringe pump at a

rate of 10 μL/min to activate the carboxylic acid functional groups on the surface of the

PMMA microchip. The PEEK tubing was connected to the syringe pump using a LUER

connector. The solution was allowed to incubate within the channel for 30 minutes.

After incubation, 100 μL of oxalyldihydrazide, dissolved in MES buffer, was loaded into

the channel at a rate of 10 μL/min and allowed to incubate. Air was pushed through the

channel after the incubation to remove unbound hydrazide. The channel was filled with

2 mg/mL BSA to block non-specific binding at a rate of 5 μL/min. The BSA was

allowed to incubate for one hour, followed by a 100 μL rinse with 10 mM borate buffer

at a rate of 10 μL/min. Finally, air was pushed through the channel to remove the borate

buffer and the proteins were loaded into the channel. Fresh solutions of EDC/NHS and oxalyldihydrazide were prepared daily.

4.2.4   Off-chip Protein Labeling

Cytochrome c (5 mg/mL) was oxidized *in vitro* using metal catalyzed oxidation (MCO). Oxidized cytochrome c was diluted to 2 mg/mL in 100 % methanol and placed in freezer until experiments. A stock solution of 5 mM NDA dissolved in methanol was prepared and stored in refrigerator protected from light. The stock solution was used within a week. Prior to loading into the channel, proteins were labeled with the fluorescent tag NDA. 100 μL of oxidized cytochrome c was placed in a small centrifuge tube. Into the tube was added 400 μL of 10 mM borate buffer (pH 9.3), 100 μL KCN, and 400 μL of NDA, in that order, giving a total sample volume of 1 mL. The tube was allowed to incubate for 30 minutes in the dark. Following incubation, the sample was loaded into an Amicon Ultra-4 centrifugal filter unit (3000 MW cutoff) to remove unbound NDA. Two rinses occurred in 10 mM borate buffer at a speed of 4500x g for 20 minutes, followed by a final spin down to about 200 μL at the same conditions. The sample was supplemented to a total volume of 1 mL with 10 mM borate buffer. Fluorescence measurements using the Nanodrop 3300 photospectrometer were taken to verify the presence of the fluorescently-tagged proteins within the sample. The proteins were then loaded into the channel.

4.2.5   Interior Geometry Studies

Protein capture was measured using the two different interior geometries shown in Figure 4-1. Proteins were loaded into the channel at a flow rate of 5 μL/min. Proteins were loaded through the PEEK tubing and collected at the exit reservoir of the chip using

a pipettor. The flowthrough solution was collected every minute and analyzed using the Nanodrop 3300. Both channels were surface modified on the same day using the same oxalyldihydrazide, EDC/NHS, and BSA solutions.

4.2.6   Oxalyldihydrazide Concentration Studies

Oxalyldihydrazide concentration was varied to assess its impact on protein capture. The concentrations used were 5 mM, 10 mM, 25 mM, and 50 mM. The protein was loaded and collected as described above. The oxalyldihydrazide concentrations were serially diluted from the same sample of 50 mM. All channels were surface modified on the same day using the same solutions. Experiments were performed in the lower density channel shown in Figure 4-1.

4.2.7   Flow Rate Studies

Different flow rates were tested to determine protein capture. The flow rates used were 5 μL/min, 10 μL/min, and 20 μL/min. The concentration of oxalyldihydrazide was 25 mM. Experiments were completed using the lower density channel shown in Figure 4-1. All channels were surface modified the same day using the same solutions. Proteins were loaded and collected as described above.

4.2.8   Oxalyldihydrazide Incubation Studies

Incubation time for oxalyldihydrazide following chip loading was varied to determine protein capture. The incubation times chosen were 1 hour, 4 hour, and overnight (16 hours). The protein loading flow rate was 5 μL/min. All other conditions from the flow rate study were applied.

4.2.9   Statistics

For data collected from the flow rate and crosslinker incubation time experiments,

a two-tailed, equal variance Student's t-test was used for statistical analysis with a

$p < 0.05$ being considered statistically significant.

4.3   Results

4.3.1   Interior Geometry Studies

Interior geometry of the microfluidic chip was varied to investigate the effects on

protein capture. Figure 4-2 shows the results of these studies. After 40 minutes of

continuous protein flow, both channels capture about 5 μg of proteins. The capture

occurs at a steadier rate using the lower density channels, whereas the higher density

channels begin to capture later, but over time achieve equality with the lower density

channel.
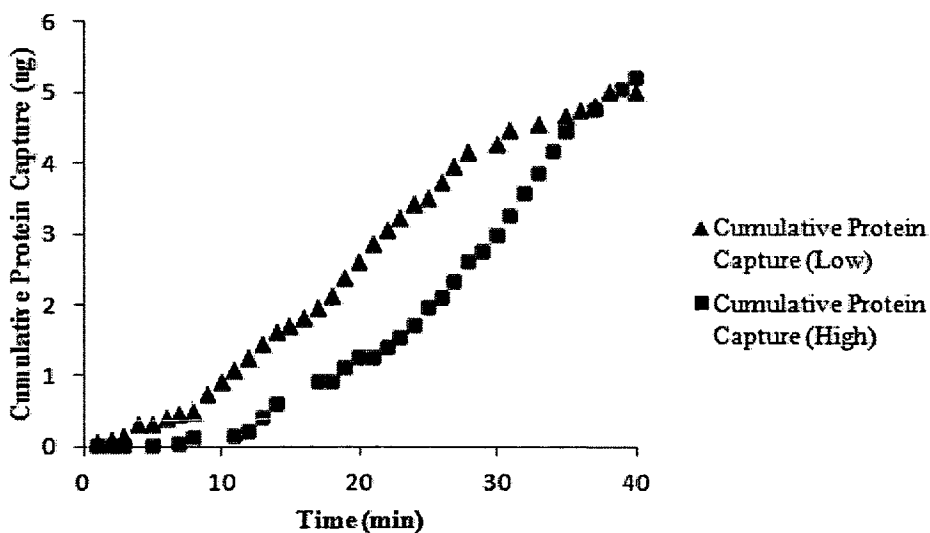
Figure 4-2: Results of the interior geometry studies

4.3.2 Oxalyldihydrazide Concentration Studies

The effects of oxalyldihydrazide concentration on protein capture were studied.

The results are shown in Figure 4-3. The highest capture is observed at an

oxalyldihydrazide concentration of 25 mM. Both 5 mM and 10 mM resulted in lower

capture, while using 50 mM resulted in the lowest capture efficiency. After 40 minutes,

both 5 mM and 50 mM are decreasing their positive slope, suggesting a move toward

saturation, whereas 10 mM and 25 mM are still increasing.
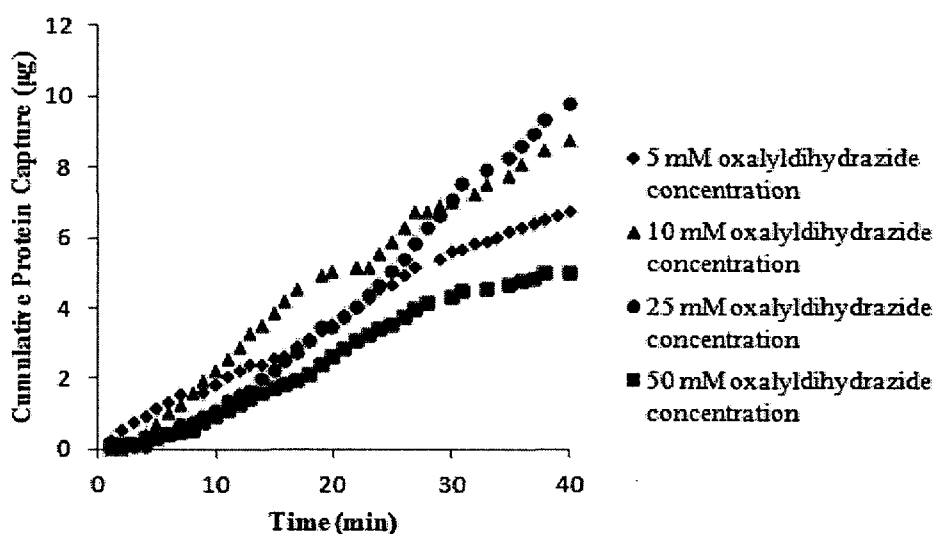
Figure 4-3: Results of the oxalyldihydrazide concentration studies

4.3.3 Flow Rate Studies

Protein capture for different flow rates is shown in Figure 4-4. Each channel had

the same mass of proteins (40 μg) injected into it. Protein capture per minute was

normalized to allow for easier comparison. The highest normalized capture occurs at

5 μL/min. Capture decreases with each faster flow rate. Capture is significantly higher

under 5 μL/min flow vs. the other two flow rates (10 and 20 μL/min: $p = 5.8 \times 10^{-7}$ and

7.67 x 10^{-5}, respectively), whereas a significant difference was not observed between the 10 and 20 µL/min flow rates.
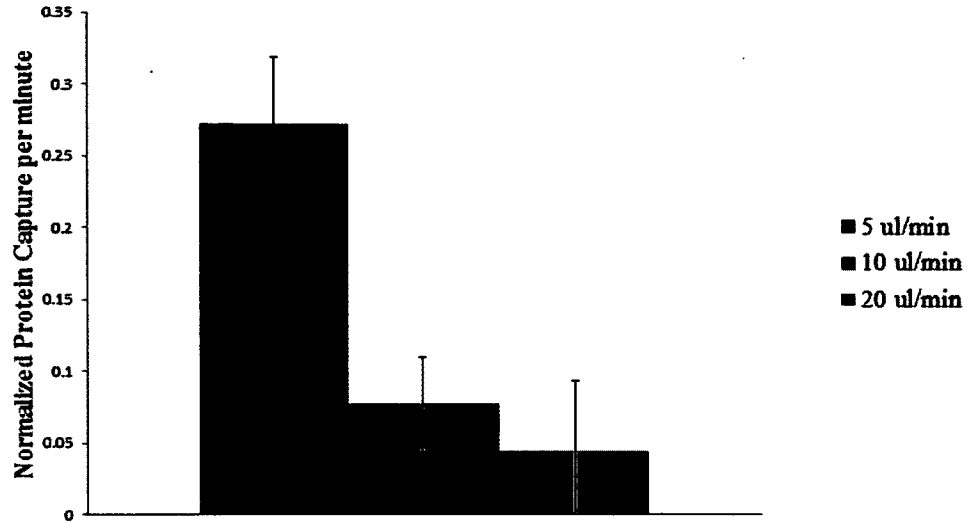
Figure 4-4: Protein capture as a function of flow rate. The bars represent the average normalized protein capture with bars representing a 95 % confidence interval (mean ± 95 % CI)

4.3.4   Oxalyldihydrazide Incubation Time Studies

Lastly, oxalyldihydrazide incubation times were varied to enhance protein capture. The results are shown in Figure 4-5. As with flow rate, protein capture per minute is normalized to allow for comparison between the groups. Capture efficiency was slightly lower for the larger oxalyldihydrazide incubation times, but the results were not statistically significant between the groups.
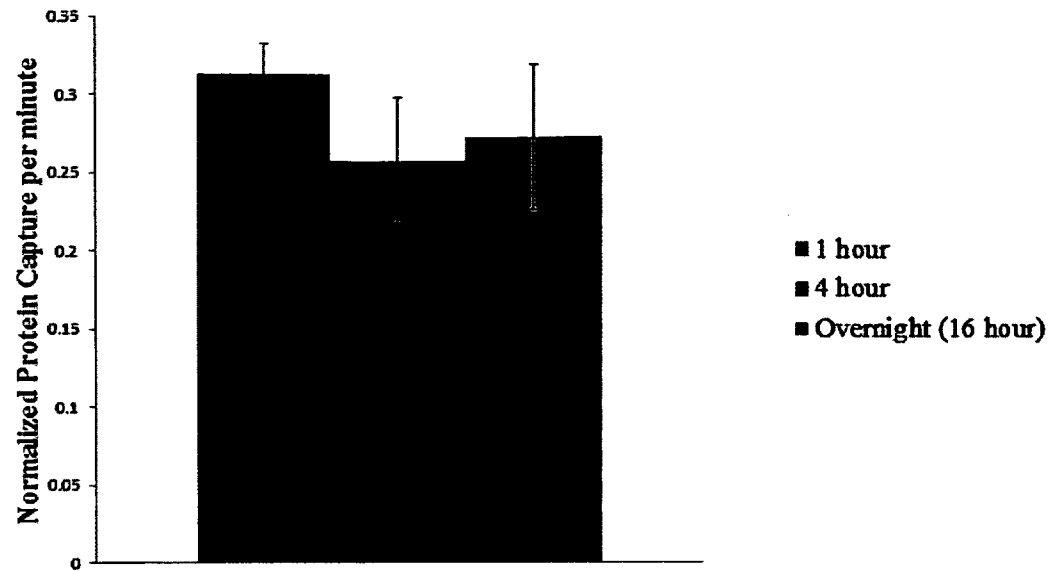
Figure 4-5: Results of the oxalyldihydrazide incubation studies

4.4   Discussion

It was expected that additional microposts would increase the surface area for

hydrazide modification and therefore, protein capture. However, it was observed that

capture was not enhanced in a higher density channel. It is suspected that the capture is

not different because of the way UV light is exposed to the chip. The chip is directly

underneath the UV light source when carboxylic acid groups are placed on the surface.

The posts are parallel to the UV light source; therefore, the sides of the posts are not

exposed to UV light. This lack of exposure prevents carboxylic acid groups from being

generated there. Therefore, the area available to capture proteins is completely dependent

upon the area of the floor of the channel and the coverslip above the channel (Figure 4-6).

The two designs do not differ much in this available area, so it is not surprising to see

such a result. Because the amount of capture was similar between the two channels, the

lower density channel was used for future experiments because it had a smaller pressure drop. A potential method for overcoming the lack of exposure for the sides of the microposts would be to use fiber optics. The sides of the posts could be modified by shining a UV fiber optic parallel to the walls of the channel and perpendicular to the microposts. This approach, while not allowing for total activation of the sides of the posts, would increase the amount of UV activation on the posts compared to the current UV exposure technique.
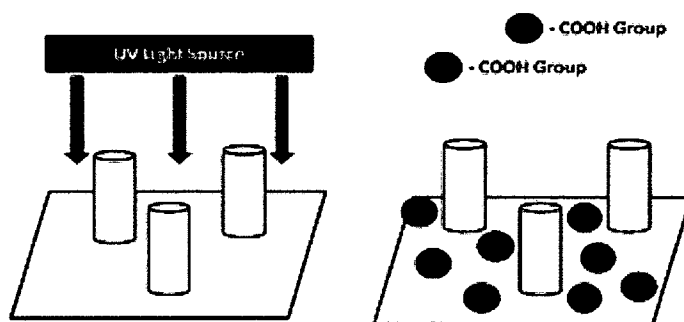
Figure 4-6: Approach of UV light to the microchip makes activation of the sides of the microposts difficult

For the proof-of-principle studies detailed in the previous chapter, an oxalyldihydrazide concentration of 50 mM was used. The concentration of oxalyldihydrazide was varied in order to determine whether reagent usage could be optimized within the enrichment protocol. The results show that an oxalyldihydrazide concentration of 25 mM was optimal for protein capture. The observation that both 5 mM and 10 mM concentrations of oxalyldihydrazide had higher capture efficiency than a 50 mM concentration was unexpected. Upon further investigation, it is seen that oxalyldihydrazide is supersaturated at a concentration of 50 mM when dissolved in MES

buffer. This is the only concentration at which it is not completely dissolved in solution. The undissolved oxalyldihydrazide may interfere with the binding capacity of the chip. This interference could occur as undissolved hydrazide settles onto carboxylic acid residues, but does not react with the functional group. These particles are pushed out during the evacuation step, leaving unreacted carboxylic acid groups which are then blocked with BSA. This process would reduce the capture ability of the chip. The parabolic capture curve seen from the oxalyldihydrazide studies support this hypothesis, shown in Figure 4-7.

$$y = -0.0077x^2 + 0.3781x + 5.331$$
$$R^2 = 0.9764$$
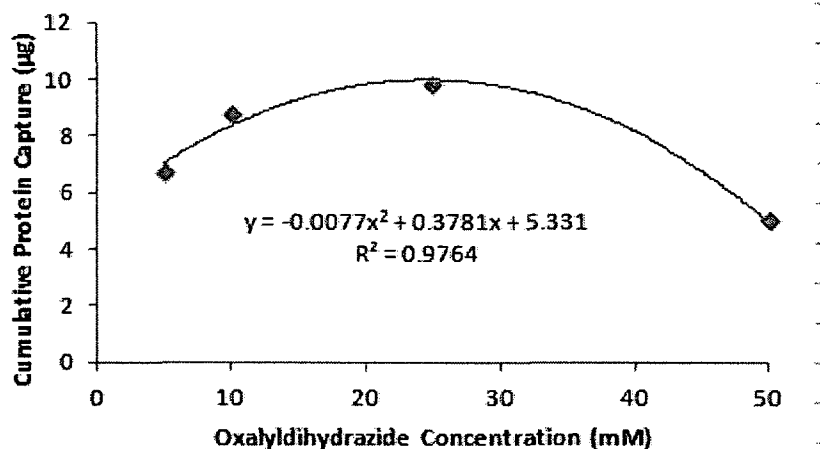
Figure 4-7: Parabolic nature of protein capture in relation to the concentration of oxalyldihydrazide

For the flow rate experiments, it was decided that the best approach would be to inject the same amount of mass into each channel. This approach would prevent a mass bias from being introduced into the experiment, where additional proteins are captured at faster flow rates because an additional amount of protein mass flows into the channel. This scenario would have been the case if each flow rate was allowed to be injected for the same amount of time. Additionally, by using normalized protein capture per minute

in the data analysis, the potential for mass bias was prevented even further. Protein capture was normalized by dividing the fluorescence value obtained from the solution collected at the collection reservoir by the fluorescence value collected from the original sample prior to loading it into the chip. Normalized protein capture differed significantly between the lower flow rate and the other flow rates used in the study. The greater capture is attributed to the targets being in contact with the sample for a longer period of time. This increase in contact time would result in a higher chance of the bond being formed, and thus, a better capture efficiency. Indeed, when cell capture studies were completed inside a microfluidic channel, a similar phenomenon was observed, as capture increased linearly with the amount of time the cells were allowed to remain in contact with the aptamers (Phillips et al., 2009). Another study looked at microfluidic negative enrichment of target cells. Their results demonstrated higher sample purity at lower flow rates, indicating that lower flow rates result in higher capture in microfluidic environments (Li et al., 2011). The difference between the 10 and 20 μL/min flow rates was not significant. However, it is believed that the difference would have been significant if the 20 μL/min flow rate had more samples. An increase in sample points would have allowed the data to be in closer agreement with the central limit theorem's minimum requirements.

An effort was made to prevent a mass bias in this study by loading the same mass of proteins through the chip. If all studies were conducted for the same amount of time, the expectation that lower flow rates would result in higher mass capture would be counter-intuitive. One would tend to expect a higher capture at faster flow rates because of the increased mass exposed to the functionalized surface.

The results also lead to the possibility of a misconception being formed concerning protein capture. Based on the results seen here, it would be expected that as the flow rate moves slower, the capture efficiency would proceed to 100 %. However, protein stability needs to be considered. Slower flow rates would result in longer experimental times. Increasing experimental time also increases the likelihood of the protein becoming more labile. Also, the detection methodology used in these studies, fluorescence, is sensitive to time as well. Therefore, the longer the experiment occurs, the less observable the fluorescence intensity becomes. As fluorescence intensity decreases, overestimation of the protein capture within the microchannel would occur.

Lastly, a study on the amount of time oxalyldihydrazide was incubated inside the channel was completed. The purpose of this study was to determine if shorter incubations had a negative effect on protein capture. In previous studies, oxalyldihydrazide was allowed to incubate overnight. This study was conducted to determine if the total time for enrichment could be reduced. It was seen that a reduction in incubation time resulted in a slight increase in capture efficiency. However, the increase is not statistically significant. In fact, the cumulative capture percentage difference between a one hour incubation and an overnight incubation is roughly 3 %, or 3 μg per 100 μg of proteins injected. When taking into account that the system's dead volume can easily contain 3 μg, this difference is statistically insignificant. However, lack of statistical significance does not imply the data is not meaningful. On the contrary, these results allow for time optimization of the enrichment protocol, as it is now known that the chip is ready for capture after only one hour of oxalyldihydrazide incubation.

4.5   Conclusions

In this chapter, a series of experiments were presented with the intention of optimizing protein capture using the microfluidic technique. Micropost density and oxalyldihydrazide incubation time only marginally affected protein capture. Oxalyldihydrazide concentration and flow rate significantly affected capture efficiency. Following the optimization studies, sample size, perfusion time, and reagent consumption were reduced. A critical consideration of the methodology is the determination of the point-of-failure. In particular, it is important to analyze the conditions at which the chip would not be effective at enriching the target carbonylated proteins. The theoretical modeling for this determination is discussed in the next chapter.

CHAPTER 5

MODELING THE POINT OF FAILURE

5.1   Introduction

In Chapter 3, a novel microfluidic enrichment technique was developed for the

capture, enrichment, and elution of carbonylated proteins. The technique had a

preconcentration factor of 265 %. In Chapter 4, progress continued on making this

technique an attractive alternative to the commercially available avidin chromatography

technique currently considered the gold standard in enrichment technology. Four

variables were studied for optimization of the process. The optimization of the process

resulted in a reduction of sample, reagent, and time requirements.

It is important to determine experimental conditions that would cause the

technique to fail. Failure is defined in this sense as conditions that would result in

reduced ability for the methodology to enrich carbonylated proteins. In this chapter,

theoretical modeling is used to analyze experimental conditions that would result in

failure. Density functional theory is used to determine the binding energies of the

oxalyldihydrazide molecule to both the UV-modified PMMA and to the amino acid

residues lysine, proline, arginine, and threonine. Cytochrome c is used as the protein

model for protein capture. The results obtained from density functional theory allow for

the calculation of a critical force. This critical force is used in Stokes' law to determine a

critical velocity for proteins. Based on these calculations, the experimental conditions

75

leading to failure are identified. It is seen from the results that failure of the microfluidic device will most likely not be a result of the bonds breaking, as the critical velocities calculated are not feasible within a microfluidic environment.

5.2   Methods

5.2.1   Chip Dimensions

The microchannels were formed using a nickel mold master and hot embossing. The process is described in Chapter 3. The microchannels used for modeling were described in Chapter 4. Refer to Figure 4-1. Both channels are 12.5 mm long and 1 mm wide. The first channel, shown on the left, contains 150 microposts, with a post-to-post spacing of 150 μm, measured edge to edge. The post diameter is 100 μm and the depth of the microchannel is 50 μm. The total area available for capture is 27.6 mm^2. The second channel, shown on the right, contains 465 posts, with a post-to-post spacing of 100 μm, measured edge to edge. The post diameter is 70 μm and the depth of the microchannel is 35 μm. The total area available for capture is 26.4 mm^2.

5.2.2   Reaction Scheme and Model Assumptions

The purpose of this study is to model the reaction shown in Figure 3-3 inside the microchannels. First, the microchip is exposed to UV radiation, carbonizing the pristine PMMA. The carbonization places carboxylic acid functional groups on the surface of the channel. Then, the carboxylic acid residues are activated using a mixture of EDC and NHS, followed by exposure to oxalyldihydrazide (Figure 2-5) to immobilize the crosslinker to the microchannel surface. Lastly, proteins are injected into the channel. These proteins are captured by the immobilized oxalyldihydrazide molecules. In this chapter, four different oxalyldihydrazide concentrations are modeled: 5 mM, 10 mM,

25 mM, and 50 mM. These concentrations are the same as were used experimentally in Chapter 4.

The model protein used is cytochrome c. Cytochrome c is a highly conserved protein among many species. The particular molecule used in this paper is equine horse heart cytochrome c. It has 104 amino acid residues. It is a membrane associated protein. *In vivo,* it is spherical in shape with a radius of 1.2 nm (Choi and Dimitriadis, 2004).

For the model presented in this paper, certain assumptions are used. These assumptions are the following:

1. All PMMA monomers are carbonized during the UV exposure step.

2. The monomers have a 1:1 reaction with oxalyldihydrazide molecules.

3. Oxalyldihydrazide molecules can only react with one UV activated PMMA monomer. That is, the molecule cannot bind so that two monomers are consumed by the two hydrazide functional groups on one oxalyldihydrazide molecule.

4. When oxalyldihydrazide is immobilized on the surface of the microchannel, it is immobilized with an even distribution across the unit cell. This assumption prevents the model from allowing an area of an unsaturated unit cell from being capable of more protein capture than any other area of the unit cell.

5. No capture occurs during loading; all capture occurs during the incubation step.

5.3   Results and Discussion

5.3.1   PMMA Unit Cell and Oxalyldihydrazide Approximation.

A PMMA unit cell approximation was used for modeling the molecular interactions within our microdevice. The PMMA unit cell is 4.196 nm wide, 2.434 nm long, and 1.05 nm deep, determined from experimental data (Sane et al., 2002). The unit cell contains 150 monomers of the PMMA polymer, arranged in 3 chains of 50 monomers each. There are a total of 2250 atoms per cell. The unit cell is shown in Figure 5-1. There are a total of 3.08×10^{12} and 3.04×10^{12} PMMA unit cells in the lower and higher density microchannel, respectively. Therefore, there are a total of 4.63×10^{14} and 4.56×10^{14} PMMA monomers inside each microchannel, respectively. Using the sidearm of the PMMA molecule as a base, the length of the oxalyldihydrazide molecule was estimated to be 2.1 nm, based on the molecule having twice as many similarly-sized atoms (Figure 2-5). The capture cells within the microchannel are 4.196 nm wide, 2.434 nm long, and 3.15 nm deep, accounting for capture of oxalyldihydrazide within 3.15 nm of the channel surface for the model. The capture cell is shown in Figure 5-2. The entire channel was divided into equal sized capture cells, with only the cells in contact with the wall surface being capable of oxalyldihydrazide and/or protein capture. There are a total of 3.02×10^{16} and 2.11×10^{16} total cells in the low density and high density channels, respectively. Figure 5-3 shows a representation of the cells, with the cells capable of capture shown in green.
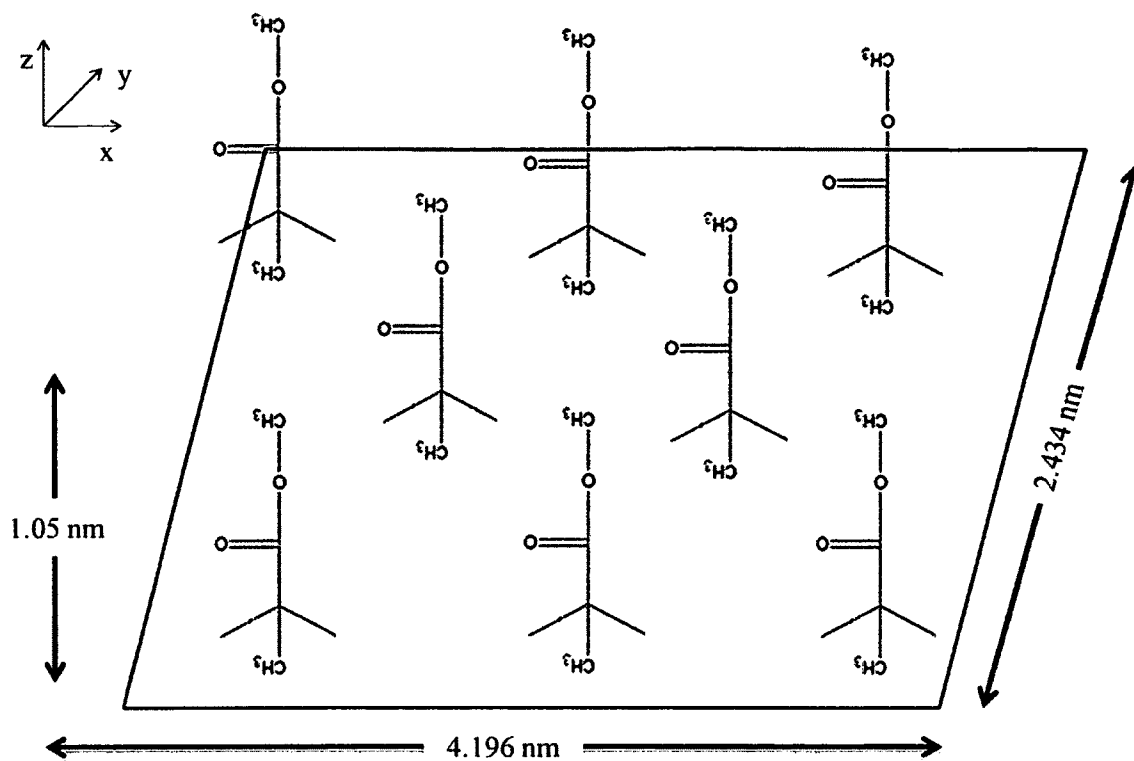
Figure 5-1: A schematic of a PMMA unit cell
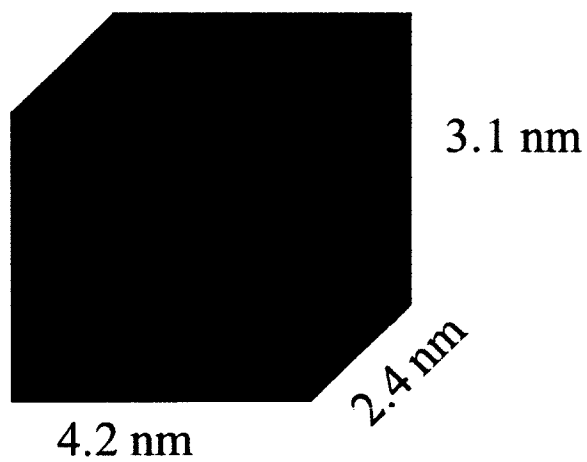
Figure 5-2: Dimensions of the capture cells used in modeling oxalyldihydrazide and cytochrome c capture
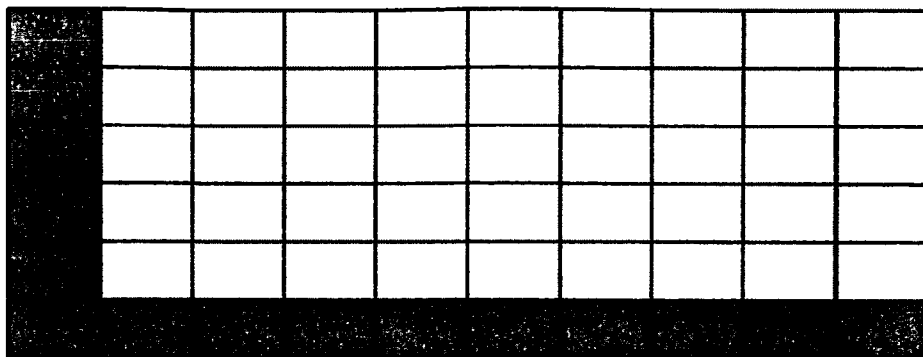
Figure 5-3: Representation of the arrangement of capture cells within the microfluidic device

Four concentrations of oxalyldihydrazide were used in the model. At these concentrations, the number of oxalyldihydrazide molecules present within a volume of a capture cell (32.1 yL) was 67, 134, 334, and 668 for the four concentrations, respectively, in the lower density channel. For the higher density channel, the number of oxalyldihydrazide molecules was 45, 90, 224, and 448, respectively. These values were compared to the available PMMA monomers for reaction (150 monomers) in each condition. The results are shown in Figure 5-4.
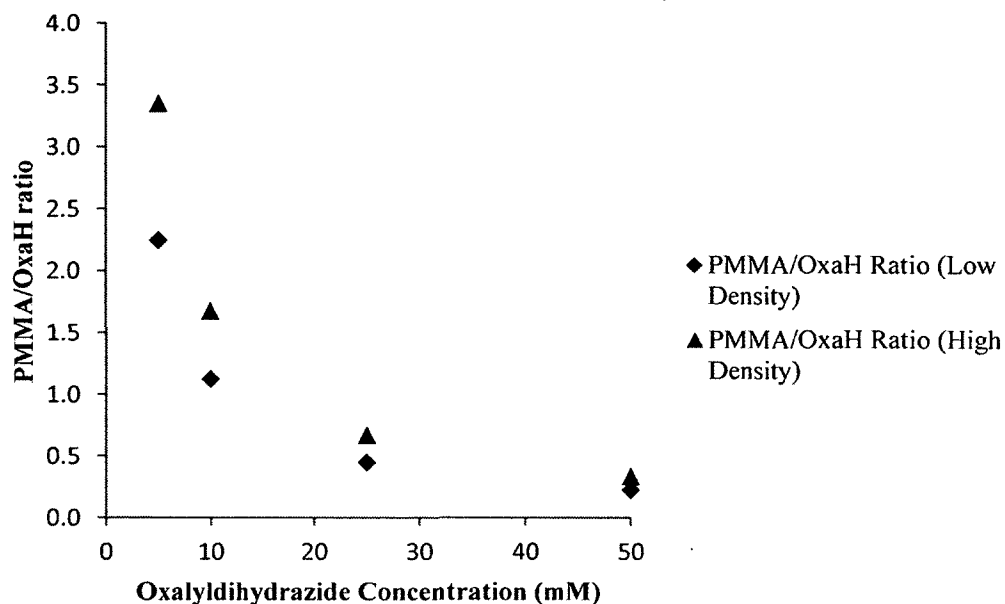
Figure 5-4: Ratio of PMMA to oxalyldihydrazide molecules at the four different concentrations of oxalyldihydrazide

By using a ratiometric approach in the analysis, it is easier to determine full saturation of the PMMA monomers. Ideally, a concentration that results in an equal number of oxalyldihydrazide to PMMA monomers would be desirable. Above that point, as seen in the 5 mM and 10 mM concentrations in both densities, there are unreacted PMMA molecules, and the efficiency of the protein capture will not be optimized. Below that point, as observed at 25 mM and 50 mM, excessive oxalyldihydrazide will compete with bound oxalyldihydrazide for the limited number of PMMA monomers. Therefore, once the ratio of PMMA molecules to oxalyldihydrazide molecules decreases below 1, reagent usage is no longer optimized.

5.3.2   Binding Energies from DFT

Using DFT, the binding energy between UV activated PMMA and oxalyldihydrazide and between oxalyldihydrazide and the four amino acid residues was

determined, according to the reaction scheme seen in Figure 3-3. The binding energy for

oxalyldihydrazide and UV activated PMMA was -4.47 kcal/mol. The binding energies

for oxalyldihydrazide reacting with proline, lysine, arginine, and threonine, respectively,

was -3.06 kcal/mol, -4.00 kcal/mol, -7.80 kcal/mol, and -5.43 kcal/mol. The binding

energies are presented in Table 5-1.

Table 5-1: Binding energies for PMMA and amino acid residues to oxalyldihydrazide

Phase	Binding Energy (kcal/mol)
UV-PMMA to oxalyldihydrazide	-4.47
Oxalyldihydrazide to proline	-3.06
Oxalyldihydrazide to lysine	-4.00
Oxalyldihydrazide to threonine	-5.43
Oxalyldihydrazide to arginine	-7.80

5.3.3   Protein Binding

In this model, oxidized equine horse heart cytochrome c was used as the target

protein of interest. Cytochrome c is a highly-conserved protein throughout many

organisms. It is a spherical protein, with a radius of 1.2 nm, giving it an area of 4.52 nm^2.

Using this value, 2.2 cytochrome c molecules can attach per unit cell of PMMA. Each

cytochrome c molecule will occupy the space of 66 PMMA monomers. At the

concentrations used in this model, per cytochrome c surface area, there will be

27 oxalyldihydrazide molecules bound at 5 mM, 57 at 10 mM, and 66 at both 25 mM and

50 mM within the lower density channel. For the higher density channel, the number of

oxalyldihydrazide molecules is 18, 39, 66, and 66 for each concentration, respectively.

The oxalyldihydrazide consumption is shown in Figure 5-5. It is assumed in this case that after the ratio of PMMA to oxalyldihydrazide molecules decreases below one, the PMMA unit cell becomes saturated, and as such, all possible PMMA binding sites are occupied with an oxalyldihydrazide molecule.
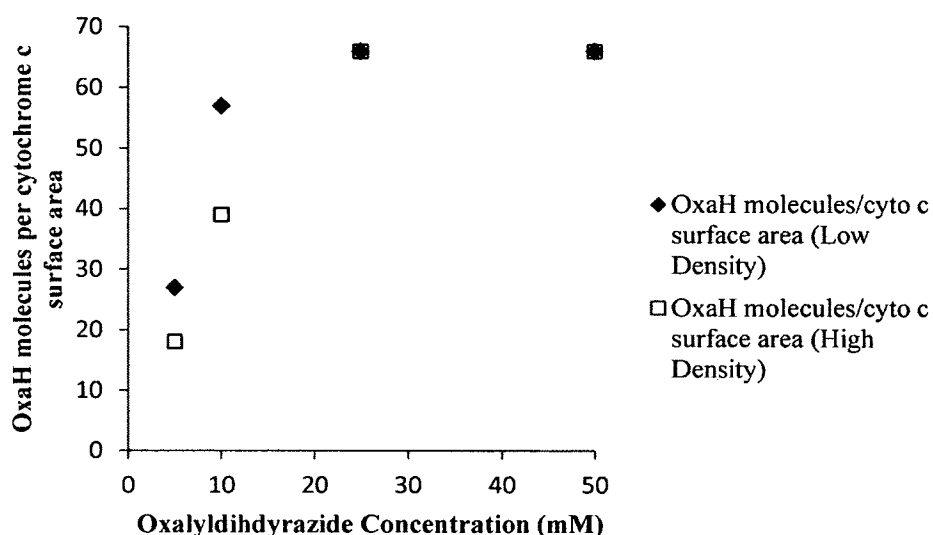
Figure 5-5: Oxalyldihydrazide molecules per cytochrome c surface area

These values were used to calculate the number of protein molecules captured within the chip. For each concentration, a molecule of cytochrome c consumes the number of oxalyldihydrazide molecules determined above. Those values were used to determine the maximum number of carbonylated proteins that could be enriched in each condition. For the lower density channel, 3.12×10^{12}, 6.23×10^{12}, 7.00×10^{12}, and 7.00×10^{12} proteins could be captured for each concentration, respectively. For the higher density channel, 2.06×10^{12}, 4.22×10^{12}, 6.91×10^{12}, and 6.91×10^{12} proteins could be captured for each concentration, respectively. The results are shown in Figure 5-6.
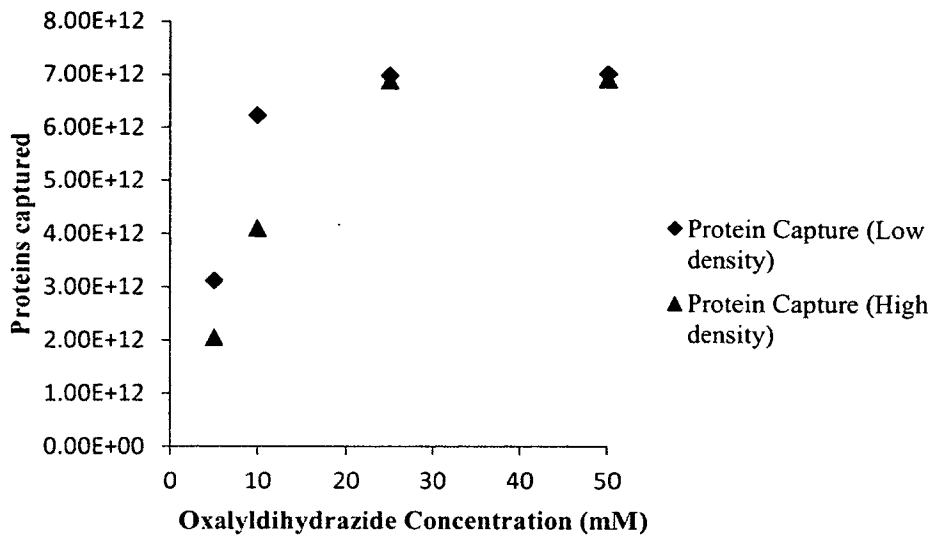
Figure 5-6: Number of proteins captured for each oxalyldihydrazide concentration

After the number of proteins captured was determined, this number was converted

to a mass. Compared to experimental values found in Chapter 4, the model

underestimated the experimentally measured values by almost two orders of magnitude.

The values found using the model and the experimental findings are shown in Table 5-2.

Table 5-2: Comparison of experimental protein capture to predicted capture by the model

	Low Density		High Density	
Concentration	Model Results (μg)	Experimental Results (μg)	Model Results (μg)	Experimental Results (μg)
5 mM	0.06	6.73	0.04	N/A
10 mM	0.12	8.79	0.08	N/A
25 mM	0.14	9.79	0.14	N/A
50 mM	0.14	5.01	0.14	5.18

The model underestimated the protein capture because it only considered the interior of the microchannel. In order to improve upon these results, the model was adjusted to also include the surface area of the reservoirs. Including the reservoirs significantly increased the total surface area available for protein capture. Because the majority of the experimental data collected in Chapter 4 is for the lower density channel, the reservoir consideration was applied to the results of the lower density channel. The protein capture for the model's adjustment is compared to the original model's results in Figure 5-9.
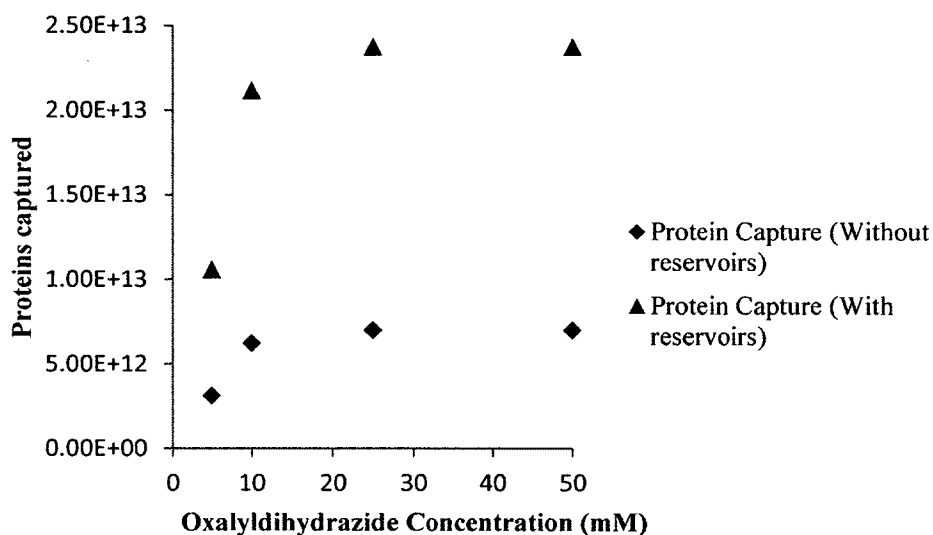
Figure 5-7: Comparison of protein capture when reservoirs are considered

These protein values were converted to a mass quantity. The model still underestimated the amount of proteins found in experimental conditions, but the consideration of the surface area contributed by the reservoirs produced a significant improvement from the original model's results. Table 5-3 shows the comparison of the protein mass using the new adjustment and the experimental results found in Chapter 4.

Table 5-3: Comparison of model results to experimental results when the reservoirs are considered

Concentration	Model Results (µg)	Experimental Results (µg)	Fold difference
5 mM	0.21	6.73	32.0
10 mM	0.42	8.79	20.9
25 mM	0.47	9.79	20.8
50 mM	0.47	5.01	10.6

It is important to consider that volume would be expected to have an impact on the protein capture. The PMMA unit cell and the capture cell used in this model have a set volume (see Figure 5-2). However, the PMMA unit cell is only present on the surface of the microchip (Figure 5-3). Therefore, if the volume of the microchip is decreased, more oxalyldihydrazide and proteins would be present within each capture cell. The higher concentration of crosslinker and proteins would result in higher capture within the microchannel. The lack of a volume consideration probably contributes to the underestimation of the model.

This particular protein has 104 amino acid residues. Of those, there are four proline residues, eighteen lysine residues, two arginine residues, and nine threonine residues, for a total of 33 possible carbonylation sites. A binding energy of - 4.51 kcal/mol per binding site is calculated from the weighted average of these residues. Because it is impossible to calculate which residue is reacting with the oxalyldihydrazide molecule at each point, it is important to consider a weighted average of the amino acid residues to get the best approximation. The total binding energy between cytochrome c and the oxalyldihydrazide-immobilized PMMA unit cell is 121.7 kcal/mol,

256.8 kcal/mol, 297.4 kcal/mol, and 297.4 kcal/mol, respectively, for the different

concentrations within the lower density channel. For the higher density channel, the total

binding energy for the different concentrations are 81.1 kcal/mol, 175.7 kcal/mol,

297.4 kcal/mol, and 297.4 kcal/mol, respectively. The results of this study are shown in

Figure 5-8.
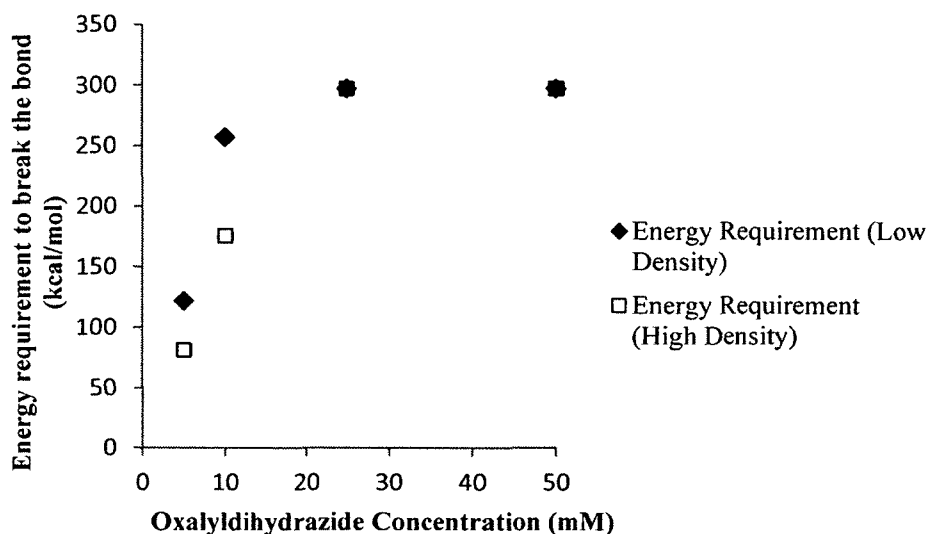
Figure 5-8: Energy requirements to break the bond between cytochrome c and
oxalyldihydrazide at the different oxalyldihydrazide concentrations

The presence of 33 possible binding sites on cytochrome c limits the model. The

model assumes that every oxalyldihydrazide molecule will bind with cytochrome c. At

full saturation (25 mM and 50 mM), there are 66 immobilized oxalyldihydrazide

molecules per cytochrome c surface area. If all possible binding sites on cytochrome c are

considered, then full saturation occurs at a concentration of oxalyldihydrazide that is

below 10 mM. However, steric hindrance would prevent additional protein capture

inside the microchip. It is important to consider this steric hindrance as it will alter the

binding energy between cytochrome c and the oxalyldihydrazide-immobilized PMMA

unit cell. This consideration changes the binding energies in the lower density channel to

121.6 kcal/mol at 5 mM and to 148.7 kcal/mol for the 10 mM, 25 mM, and 50 mM

concentrations. The higher density channel has a binding energy of 81.1 kcal/mol at

5 mM and 148.7 kcal/mol for the other concentrations. These results are compared to the

results that the model gave us in Figure 5-9.
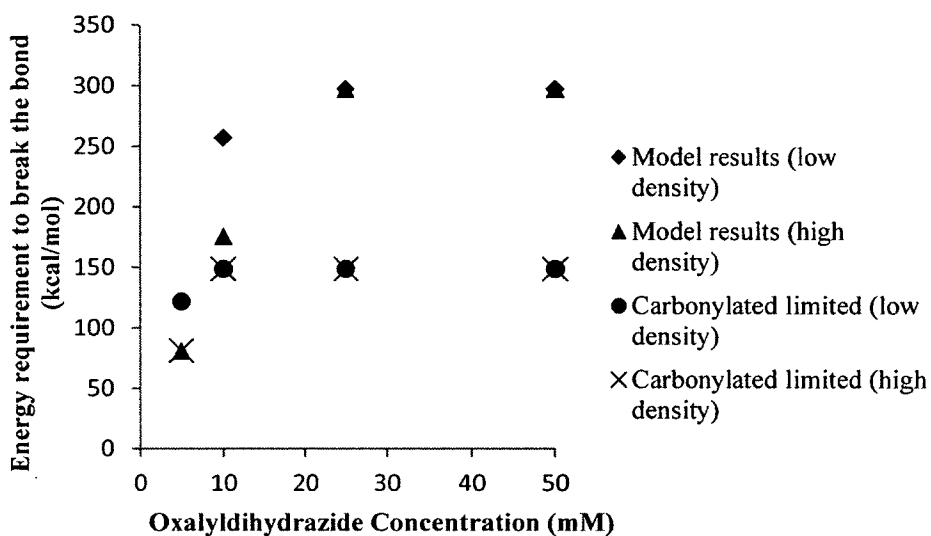
Figure 5-9: Comparison of the model's results and the site-limited results

The results here imply a significant change in capture efficiency based on protein

size. Cytochrome c is a small protein, around 12 kDa. Other proteins are much larger,

such as bovine serum albumin (BSA), at around 66 kDa. In addition, BSA contains over

600 amino acid residues, compared to cytochrome c's 104 residues. With increased size,

the amount of binding with immobilized oxalyldihydrazide molecules would increase.

Therefore, the binding energy would be higher for larger proteins as there would be more

amino acid binding residues. However, the tradeoff in this case would be the limited

space inside the microchip. Therefore, higher binding energy could be achieved in

exchange for fewer proteins captured within the microchannel.

5.3.4　Critical Velocity Calculations

Lastly, Stokes' Law was used to determine a critical velocity at which these bonds between oxalyldihydrazide and the amino acid residues would be broken. First, the critical force had to be determined for the oxalyldihydrazide and the cytochrome c binding site. This value was calculated to be 6.28×10^{-6} dynes. The calculation is included in this dissertation, beginning with Eq. 5-1:

$$f_c = 1.6 \times 10^{-5} \frac{E_0}{r_0}. \qquad \text{Eq. 5-1}$$

The E_0 value corresponding to a binding energy of 8.5 kcal/mole, the typical strength of an antibody-antigen interaction, is 0.37 eV. Because electron-volts are a linear unit, the weighted average binding strength of a binding site on cytochrome c (4.51 kcal/mol) correlates to an E_0 value of 0.19 eV. As given by Bell (1978), a good approximation of r_0 is 0.5 nm. Therefore, the calculation continues as follows:

$$f_c = 1.6 \times 10^{-5} \times \frac{0.19}{0.5}. \qquad \text{Eq. 5-2}$$

The calculation yields the result $f_c = 6.28 \times 10^{-6}$ dynes per bond. This value was applied to Stokes' Law to determine the critical velocity. Because the proteins will be delivered in a buffer solution, the viscosity chosen for the calculation is the kinematic viscosity of water at 20 °C (1.002 cP). Using the critical force, a critical velocity of 74.8 m/s at 5 mM and 91.5 m/s at all the other concentrations was obtained for the lower density channel. This velocity would be required in order to completely remove the protein from the oxalyldihydrazide molecules tethered to the lower density microchannel surface.

The calculation for the 5 mM concentration will be shown below for an example, starting with Stokes' Law (Eq. 5-3):

$$F = 6\pi\eta r v.$$ Eq. 5-3

First, the total critical force for removing the cytochrome c completely from the oxalyldihydrazide molecules immobilizing it is calculated. This value is found by multiplying the critical force for each bond by the number of bonds immobilizing the protein, shown in Eq. 5-4:

$$F_c = f_c N_r A_c.$$ Eq. 5-4

$N_r A_c$ is the number of oxalyldihydrazide molecules per cytochrome c surface area. For 5 mM, $N_r A_c = 27$, as calculated in an earlier section (see Figure 5-5). The product of the critical force, calculated from Eq. 5-2, and $N_r A_c$, yields a total critical force of $F_c = 1.70 \times 10^{-4}$ dynes.

Because all of the terms in Stokes' Law are independent of velocity, substituting the total critical force into Eq. 5-3 yields Eq. 5-5:

$$F_c = 6\pi\eta r v_c.$$ Eq. 5-5

Solving for the unknown value, v_c, the following calculation can be done:

$$v_c = \frac{(1.70 \times 10^{-4})(10^{-5})}{6\pi(1.002)(1.2 \times 10^{-9})}.$$ Eq. 5-6

This calculation gives a critical velocity of $v_c = 74.8 \ m/s$. For the higher density channel, the critical velocities are 49.9 m/s at the 5 mM concentration and 91.5 m/s at all the other concentrations. The values used for the calculations are shown in Table 5-4.

Table 5-4: Variables used in critical velocity calculations

Variable	Definition	Value
E_0	The free energy change on binding	0.19 eV
r_0	The range of the minimum work	0.5 nm
r	The radius of the binding target	1.2 nm
η	The viscosity of the flowing solution	1.002 cp

One of the assumptions of this model is that every binding site on the protein can

and does react with the immobilized oxalyldihydrazide molecules. However, because the

protein is spherical, it is highly likely that this assumption would not hold in reality.

Many of the binding sites probably are not in contact with the oxalyldihydrazide

molecule area. Therefore, the number of bonds per protein would be lower than the

33 bonds it is capable of forming. The fewer the bonds, the lower the critical velocity

would be to break the bonds. In addition, if more of the bonds are formed using proline

residues, the binding energy will be lower. Conversely, more bonds with threonine

residues will result in a higher binding energy. Figure 5-10 shows the range of binding

energy possible for cytochrome c based upon the number of bonds formed. Two ways to

increase the probability of forming more bonds between cytochrome c and the

oxalyldihydrazide molecules experimentally would be to reduce the disulfide bonds of

cystine, which would break some of the turns of the spherical protein, and denaturing the

protein using heat and/or extreme pH conditions. However, such an approach would

have a tradeoff as the denatured protein would consume a larger area. Therefore, higher

binding energy would be possible at the expense of fewer proteins being captured.
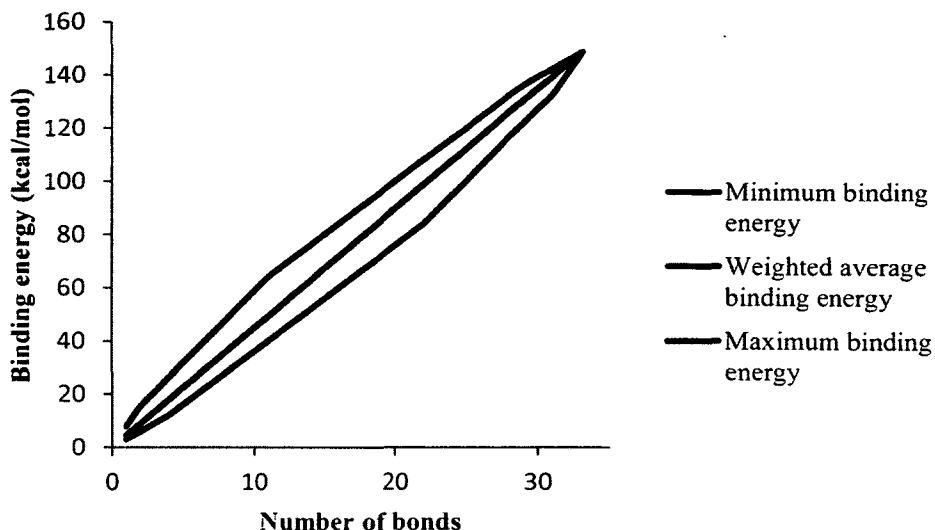
Figure 5-10: The maximum and minimum binding energies possible based on the number of bonds formed

Using the least favorable conditions for binding energy (1 proline residue bond formed), a critical velocity for breaking this bond would be 1.88 m/s, a 1000-fold higher than experimental loading conditions. In a microfluidic environment, the likelihood of the bonds breaking because they exceed the critical velocity is low. At the rates necessary to break the bonds, even at the least favorable condition, the pressure drop within the microchannel would be insurmountable. Therefore, microdevice failure is more likely to be caused by the breaking of a seal than by the breaking of the bonds breaking inside the channels.

5.4   Conclusions

In this chapter, a theoretical modeling approach geared toward optimizing enrichment of carbonylated proteins within a microfluidic device was presented. Two interior chip geometries were used. The model generated the binding energy between oxalyldihydrazide and PMMA, as well as the binding energy between oxalyldihydrazide

and select amino acid residues. A total binding energy of cytochrome c with the immobilized oxalyldihydrazide molecules was found. Lastly, Stokes' law was used to calculate the critical velocity that would result in the breaking of the chemical bonds. It was determined theoretically that flow conditions will not cause the microfluidic enrichment technique to fail, as the flow velocities needed to dissociate the bonds exceed feasible flow velocities within a microdevice.

The model provides guidance toward the optimization of the novel enrichment methodology. However, the model has a few limitations. The assumptions of the model represent an ideal environment. The model does not consider reactions that occur during protein loading. Lastly, when the number of proteins captured is converted to a mass quantity, it was found that the model underestimated the experimentally determined mass in Chapter 4 by over an order of magnitude. In the next chapter, suggestions for improving the model will be discussed.

CHAPTER 6

CONCLUSIONS AND FUTURE WORK

6.1   Conclusions

The development of a novel enrichment technology for carbonylated proteins has

been discussed. Advantages of using this system to the conventional technique of affinity

column chromatography include reduced sample consumption, reduced time, and

minimized sample preparation steps. These advantages are outlined in Table 6-1.

Because the process is done on a microfluidic platform, experiments can easily be run in

parallel in order to achieve high-throughput protein analysis. When proteins are eluted

from this system, they are readily available for additional analysis, such as mass

spectroscopy or electrophoresis. Because samples do not require derivatization prior to

loading into the microchip, no additional considerations, such as molecular weight shift,

need to be taken when the samples are analyzed further.

This microfluidic technique is used for positive enrichment of carbonylated

proteins. The technique could also be used for negative enrichment of carbonylated

proteins; in case these low abundance proteins are not desirable in a sample of interest.

In addition, because of the ease of modifying the surface of PMMA, the technique can be

modified for analyzing other protein modifications present in diseased state tissue. An

important feature of this process is its versatility. While oxalyldihydrazide was used in

this study for carbonylated protein enrichment, other crosslinkers can be used for other

post-translational modifications. Because of its versatility, the technique has potential for applications in both basic and clinical sciences.

The microfluidic enrichment technique provides a promising platform for carbonylated protein biomarker discovery in conditions where carbonylated proteins have been implicated. This device can provide a stepping stone in the development of novel diagnostic technologies making use of biomarkers. It has the ability to be at the forefront of quantitative biomarker discovery in conditions such as Alzheimer's Disease, ALS, and other neurodegenerative diseases. The technique is an attractive alternative to the conventionally used avidin affinity chromatography. Because it is microfluidic-based, it consumes little benchtop space. The technique can provide the building blocks for a clinically-translatable technology that can yield a quick result on the diagnosis of neurodegenerative diseases. The process is highly automated, therefore little training would be required on the part of a clinician to use it and get a result. In addition, because it is polymer-based, it is disposable and reduces the chance for cross-contamination between samples. The high versatility of the technique grants a wide range of applications in both basic and clinical sciences.

Table 6-1: Comparison between the enrichment technology in different phases and avidin affinity chromatography

Category	Phase 1 Enrichment	Phase 2 Enrichment	Avidin Affinity Chromatography
Time Requirement	20 hours	4.5 hours	18 hours
Sample Requirement	100 μg	40 μg	10 mg
Reagent Requirement	50 mM crosslinker for immobilization	25 mM crosslinker for immobilization	Already packaged, not determinable
Elution Volume	15 μL	15 μL	4 column volumes (> 12 mL)
Minimum sample size	> 1 μg	> 1 μg	> 4 mL
Need for Derivatization	No	No	Yes

6.2   Future Work

6.2.1   High–throughput Chip Design

The technique discussed in this dissertation produced a preconcentration factor of 2.65. This number depends on the concentration of proteins in a sample. In a clinical sample, where concentration is much lower than our experimental conditions, the preconcentration factor will be greatly enhanced. However, the chip design would need to be changed to allow for high-throughput analysis. Without such an adjustment, the time advantages offered by the technique would be sacrificed. A simple change to the design that would increase its high-throughput abilities would be to place numerous channels on a chip, allowing for a sample to be run in parallel.

6.2.2   Enrichment of Multiple Proteins on a Single Microfluidic Device

Since the capture process has been optimized, future directions involve studying

the enrichment behavior of the chip when multiple carbonylated proteins are present. In

all the studies discussed in this dissertation, only one carbonylated protein has been

present in a sample. However, as discussed in Chapter 5, the binding characteristics of

proteins vary greatly depending upon their size and amino acid sequence. Therefore, it

would be important to analyze the capture ability of the device when using multiple

carbonylated proteins within one sample. A good approach to this analysis would be the

use of protein standards of different sizes. The proteins could be labeled with different

fluorescent tags, and capture could be analyzed using the methods described in this

dissertation. However, a better approach may be to couple the microchip to a standard

benchtop analytical technique, such as capillary electrophoresis, to determine the

technique's ability to enrich multiple carbonylated proteins. While this approach lacks

the quantitative ability of the fluorescence approach used in this dissertation, the

experiment will be less costly because each protein in the sample could be derivatized

with the same fluorophore. To use the fluorescence technique described in this

dissertation, each protein in the sample would require the use of a unique fluorophore.

The fluorophores would need to have similar excitation wavelengths, but different

emission wavelengths. However, excitation and emission wavelengths tend to be

correlated for different fluorophores. For example, few fluorescence agents absorb at

488 nm and emit at a wavelength other than 514 nm. If each fluorescent tag were probed

at a different time point, valuable data could be lost and interpolation would be required,

reducing the reliability of the data. Therefore, coupling the microchip to a technique like electrophoresis will yield more reliable results, with a decreased quantitative ability.

6.2.3   Use of a Biological Sample on the Microdevice

In addition, biological samples need to be examined in future work. Such a sample would be the most complicated sample tested on the microchip. However, the true power of the technique will only be seen when a biological sample is used. As an example, brain tissue could be homogenized, redissolved in a buffer, and then introduced into the microdevice, to determine whether the carbonylated proteins are detected. For this study, the proteins would not be labeled with fluorescent agents. Post-elution, the sample would be passed to another analytical technique to identify and detect protein targets.

6.2.4   Coupling the Microdevice for Protein Identification

The microfluidic enrichment technique, as developed, was never intended to be a stand-alone device in its current form. Figure 6-1 shows the modular approach toward protein enrichment, detection, and identification. As can be seen, the microfluidic enrichment technique is only a first step in the process. The microdevice will need to be coupled with a technique for identification of targets. Good candidates for coupling include capillary electrophoresis (conventional or microfluidic) or mass spectroscopy. Capillary electrophoresis is more promising as a coupling technology than traditional gel electrophoresis because it possesses some quantitative aspects. Capillary electrophoresis is a technique used for separating analytes within a solution (Feng et al., 2008). If capillary electrophoresis is coupled to laser-induced fluorescence, detection of analytes can be done following a fluorescence derivatization. Samples are loaded into a capillary

via hydrodynamic pressure. A charge is applied through the sample and the entire bulk of the sample moves toward the charge. Molecules are separated based upon size to charge (m/z) ratio. Molecules that are similarly charged to the bulk move more rapidly, while molecules with an opposite charge of the bulk migrate more slowly. Neutral-charged molecules move at the same pace as the bulk. If two molecules have a similar charge, larger molecules migrate more quickly. Relative carbonylation can be quantified using wide peak analysis. A standard setup for capillary electrophoresis is shown in Figure 6-2.

Microfluidic capillary electrophoresis uses the same principles as standard capillary electrophoresis (Wang et al., 2012). Microfluidic capillary electrophoresis is more attractive as a coupling technique than standard capillary electrophoresis because the enrichment technique is also microfluidic-based. A typical setup for microfluidic capillary electrophoresis is shown in Figure 6-3. The small volume eluted from the microfluidic enrichment technique (15 µL) would be complementary to the sample requirements for microfluidic capillary electrophoresis, as opposed to the higher volumetric requirements for standard capillary electrophoresis (100 µL). The elution volume is within the acceptable range for mass spectroscopy, which would be used to identify the proteins that are eluted from the microdevice. With identification, carbonylated proteins can be associated with different pathways and progress can be made toward identifying potential carbonylated protein therapeutic targets. Also, in the future, it may be possible to do an on-line coupling of the device to one of the techniques mentioned above.
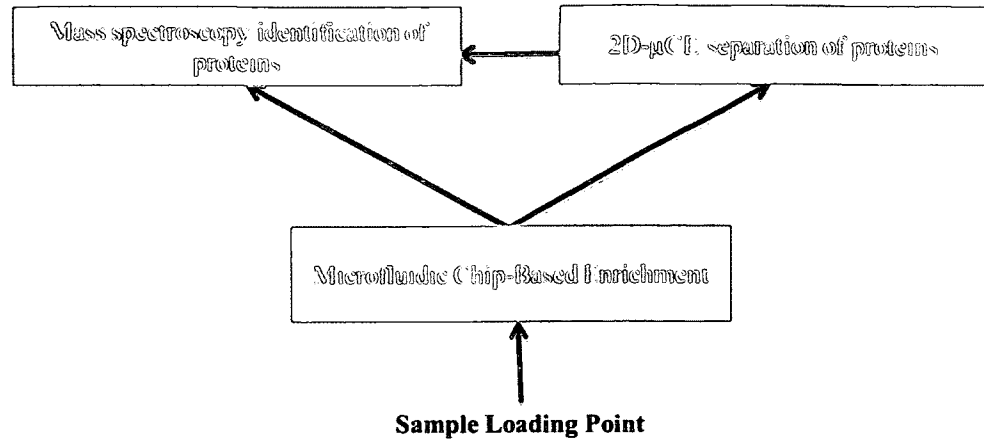
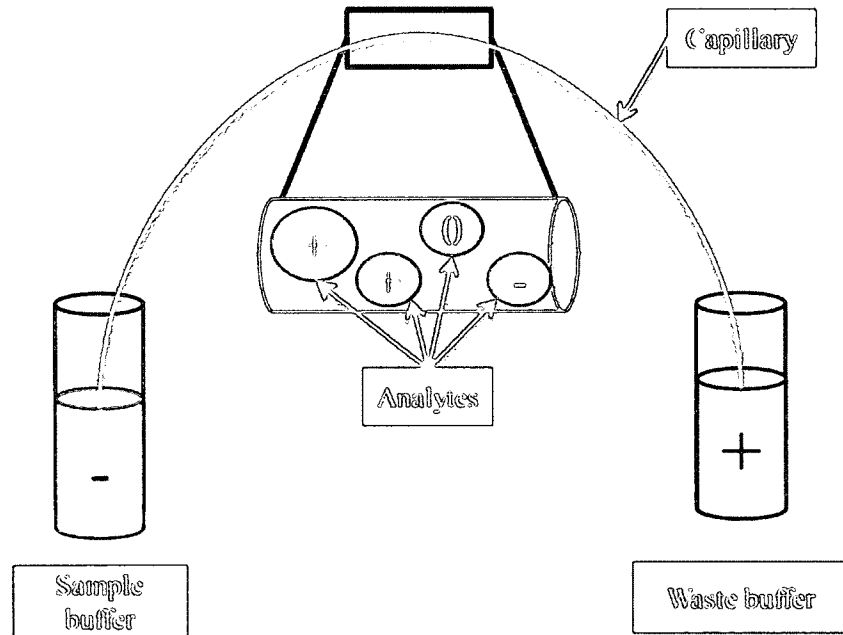Figure 6-1: Modular approach towards carbonylated protein biomarker discovery

Figure 6-2: Classic setup for capillary electrophoresis. After the sample is loaded into the capillary using hydrodynamic pressure, a charge is applied to the sample. Molecules migrate through the channel based upon size to charge (m/z) ratio. Neutral charged molecules move at the same pace as the bulk solution. Larger molecules with the opposite charge of the bulk solution migrate at a slower pace than smaller, oppositely charged molecules. Larger molecules with the same charge as the bulk solution migrate faster than smaller, similarly charged molecules.
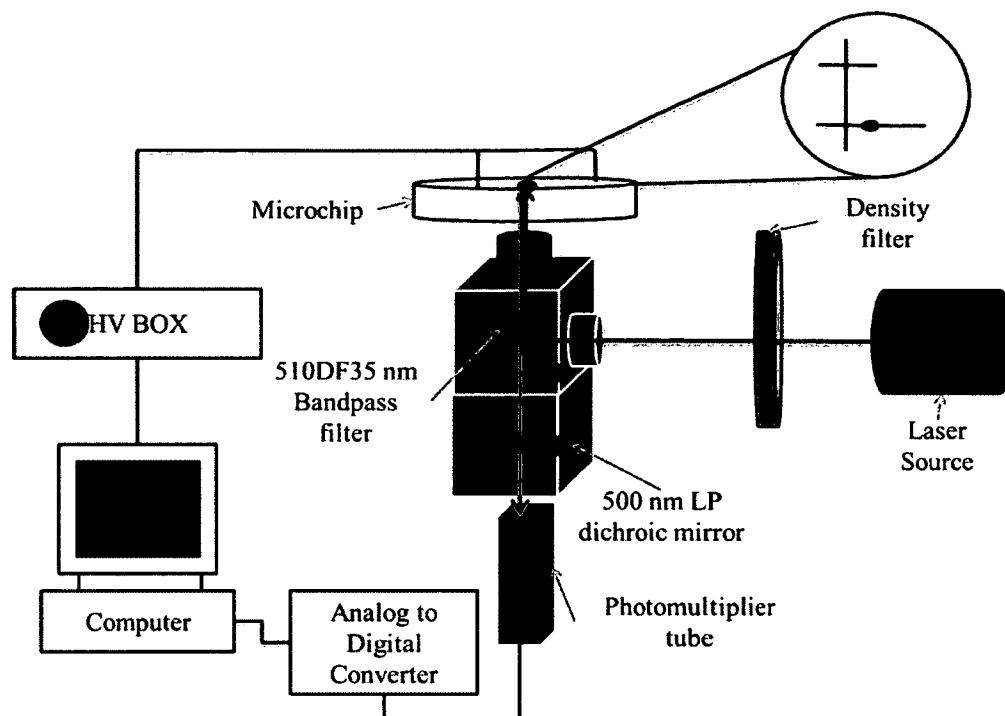
Figure 6-3: Instrumentation for microfluidic capillary electrophoresis

6.3   Method Improvements

6.3.1   Pulsed Flow vs. Continuous Flow

Biological samples, such as blood, cerebrospinal fluid, or plasma, are precious. Other biological samples, such as urine or saliva, are more available and require less invasive methods for obtaining them. Regardless of the availability of the sample or the invasiveness of the method to collect it, the most optimal method for protein capture (including both protein capture and time requirement) must be employed. In all the studies described in this dissertation, a continuous flow injection was used, followed by an incubation period. This procedure exposes the device to a large amount of proteins. Use of a pulsed flow may provide enhanced protein capture over a shorter time frame. A flow rate duty cycle will allow proteins increased contact time during the loading cycle.

As stated in Chapter 4, an increased contact time allows for more bonds to be formed. A 50 % duty cycle (five minutes on, five minutes off), may allow experiments completed in 40 minutes of continuous injections to be completed in two cycles. In the first cycle, 5 µg of proteins (assuming optimal conditions determined in Chapter 4) would be injected into the channel and then allowed to have contact time in a stationary flow field. The second cycle, also 5 µg, would be injected to fill any capture areas not already occupied by proteins from the first cycle. After 20 minutes, 10 µg of proteins would have been exposed to the device. This mass amount is the near the upper limit of proteins captured during the optimization process.

6.3.2   BioMEMS vs. BioNEMS

BioMEMS is an emerging technology for on-chip cell cultures. This technology is a great platform for cell studies because the dimensions are on the same scale as cells, as the average animal cell diameter is 10 µm. For protein work, however, the scale may be too large. As shown in Figure 5-3 and discussed in Chapter 5, much of the space within the microchip is not usable for protein enrichment. A viable alternative technology is Biological Nano-Electromechanical Systems, or BioNEMS. Nano-electromechanical systems (NEMS) incorporate mechanical and electrical components on the nanometer scale. BioNEMS is the use of NEMS for biological applications, such as the one discussed in this dissertation. These chips could be constructed using electron-beam lithography, or EBL, that can create structures on the order of sub-100 nm range (Hao et al., 2010), more in line with the size of proteins. EBL has been used on PMMA substrates to form complex nanostructures (Gautsch et al., 2010). Therefore, moving the enrichment technique from a microfluidic platform to a nanofluidic platform has merit.

One issue that would need to be considered in this leap from micro to nano would be overcoming the increased pressure drop. Pressure drop in microfluidic channels have been studied by numerous groups (Fuerstman et al., 2007; Akbari et al., 2009; Vanapalli et al., 2007). For a rectangular channel, the equation for pressure drop is given as:

$$\Delta P = \frac{a\mu Q L}{W H^3}.$$

<div align="right">Eq. 6-1</div>

For any rectangular channel where the aspect ratio (W/H) is below 1, and the Reynolds number is below 1000, Eq. 6-1 is accurate to within 0.26 %. The above equation demonstrates the challenge that comes with the transition from micro to nano. In order to have sufficient capture, the channel will either have to be longer than the current format (L increases), shorter in width (W decreases), or more shallow in depth (H decreases). Any one of these changes will increase the pressure drop. Therefore, a successful transition to BioNEMS would require a design change toward higher-throughput capability.

One group has suggested a method of microfluidic device design that would minimize pressure drop (Yeom et al., 2009). They propose a figure-of-merit (FOM) that optimizes surface area and volume of the device so that the functionality of the device is maximized while the pressure drop is minimized. The use of a FOM analysis on the nanofluidic device may assist in the development of a system that is not overcome by the pressure drop.

6.3.3   Modeling the Flux of Oxalyldihydrazide and Proteins

The current model ignores reactions during the injection flow. Knowledge of mass transport through the chip would be beneficial. As seen in Figure 5-3, there are many cells within the channel that are not capable of capturing oxalyldihydrazide or

proteins. However, it is assumed that the oxalyldihydrazide is dispersed evenly through the microchip, with an equal amount of oxalyldihydrazide and proteins in each cell of the chip. Because oxalyldihydrazide is only captured on the cells that contact the surface of the microchannel, the molecules traveling in the innermost cells must migrate toward the wall. The flux could be determined in three dimensions from a series of one-compartment models.

6.3.4   Modeling Concentration Changes throughout the Chip

In addition to flux changes, concentration changes throughout the chip can be modeled with fluid dynamics software, such as COMSOL. The software modeling can perform the flux calculations needed and generate a visual representation of the concentration changes inside the microchip. Figure 6-4 shows a representative example of the expected results from such modeling, showing the anticipated profiles at different locations along the x-axis. Figure 6-5 shows the expected concentration profiles along the x-axis.
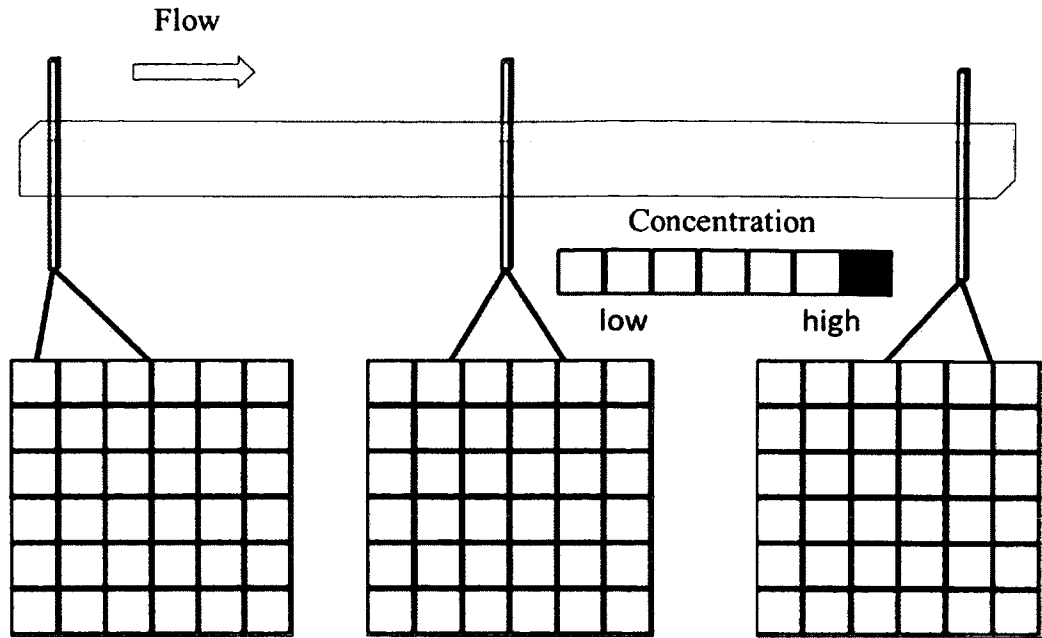
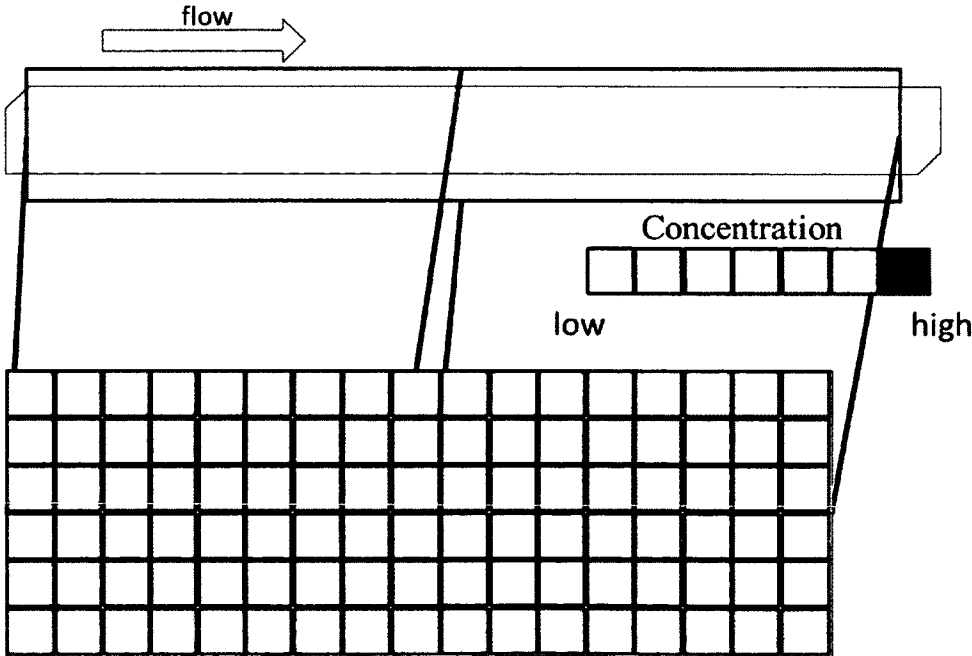Figure 6-4: Expected concentration profiles along the x-axis of the microfluidic device

Figure 6-5: Anticipated concentration profiles along the x-axis of the microfluidic device

6.3.5 Modeling Protein Capture under Flowing Conditions

The model was designed to predict protein capture. When the number of proteins captured was converted to a mass quantity, the mass was over an order of magnitude below the experimentally determined values in Chapter 4. This difference implies that the reactions that take place during the crosslinker loading and protein loading are not insignificant. In fact, binding kinetics should be considered in future experiments, as well as possible protein orientation inside the microchip.

APPENDIX

ADDITIONAL INFORMATION ON THE AMINO ACIDS

The structures, abbreviations, chemical properties, and possible oxidative modifications of the amino acids are given in this appendix. The pI and pK_a values were obtained from Carey (2011). The oxidative modifications that are possible are found in Madian and Regnier (2010).
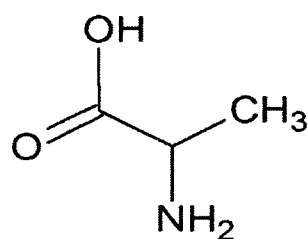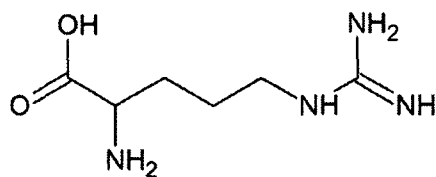
ALANINE (Ala, A)

-Group: Neutral, non-polar

-pI: 6.00

-pK_a: N/A
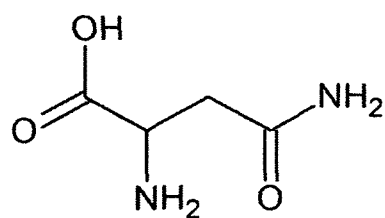
-Oxidation modification: None

ARGININE (Arg, R)

-Group: Basic, polar

-pI: 10.76

-pK_a: 12.48

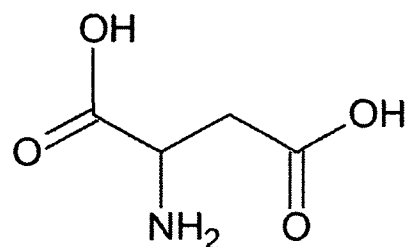-Oxidation modification: glutamic semialdehyde

ASPARAGINE (Asn, N)

-Group: Neutral, polar

-pI: 5.41

-pK$_a$: N/A

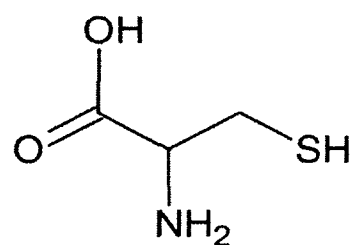-Oxidation modification:
hydroxylation

ASPARTIC ACID (Asp, D)

-Group: Acidic, polar

-pI: 2.77

-pK$_a$: 3.65
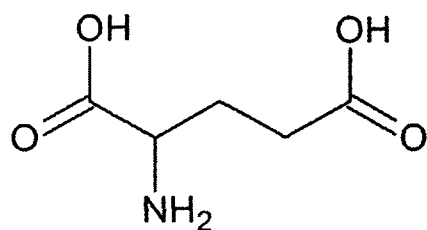
-Oxidation modifications:
hydroxylation

CYSTEINE (Cys, C)

-Group: Neutral, polar

-pI: 5.07

-pK$_a$: N/A

-Oxidation modifications:
cysteic acid, sulfinic acid,
sulfenic acid,
hydroxynonenal (HNE)
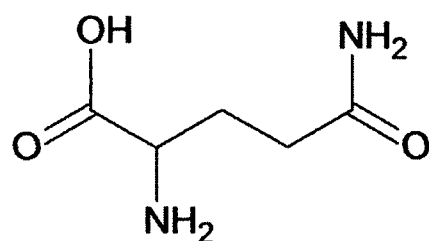Michael adduct

GLUTAMIC ACID (Glu, E)

-Group: Acidic, polar

-pI: 3.22

-pK$_a$: 4.25
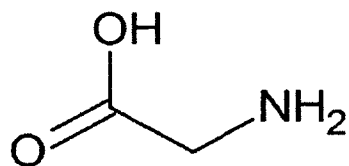
-Oxidation modification: None

GLUTAMINE (Gln, Q)

-Group: Neutral, polar

-pI: 5.65

-pK$_a$: N/A

-Oxidation modification: None

GLYCINE (Gly, G)

-Group: Neutral, non-polar

-pI: 5.97

-pK$_a$: N/A

-Oxidation modification: None

HISTIDINE (His, H)

-Group: Basic, polar

-pI: 7.59

-pK$_a$: 6.00

-Oxidation modifications: 4-hydroxy glutamate, asparagine, aspartate, 2-oxo-histidine, hydroxynonenal (HNE) Michael adduct

ISOLEUCINE (Ile, I)

-Group: Neutral, non-polar

-pI: 6.02

-pK$_a$: N/A

-Oxidation modification: None
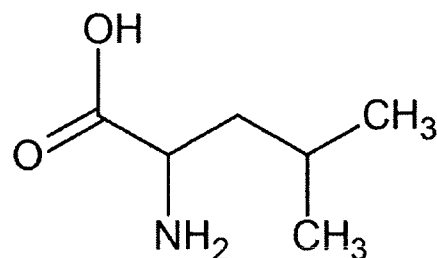
LEUCINE (Leu, L)

-Group: Neutral, non-polar
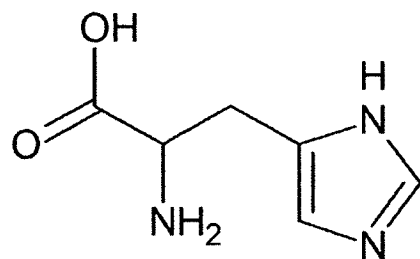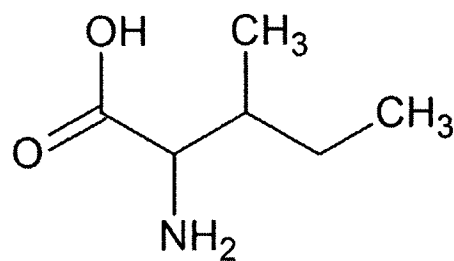
-pI: 5.98

-pK$_a$: N/A

-Oxidation modification: hydroxyleucine
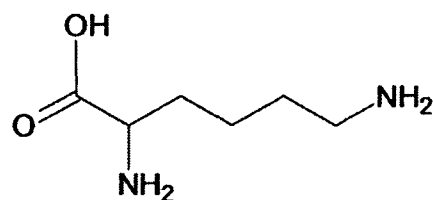
LYSINE (Lys, K)

-Group: Basic, polar

-pl: 9.74

-pK$_a$: 10.53

-Oxidation modifications: aminoadipic semialdehyde, Amadort adduct, 3-deoxyglucosone adduct, glyoxal adduct, methylglyoxal adduct, hydroxylation, hydroxynonenal (HNE) Michael adduct, malondialdehyde
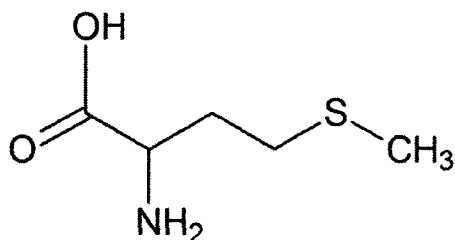
METHIONINE (Met, M)

-Group: Neutral, non-polar

-pl: 5.74

-pK$_a$: N/A

-Oxidation modifications: sulfoxide, sulfone
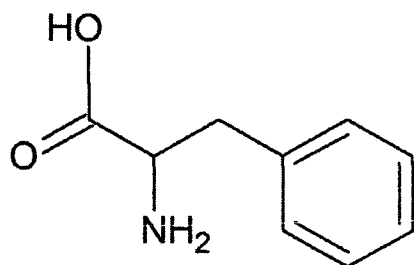
PHENYLALANINE (Phe, F)

-Group: Neutral, non-polar

-pl: 5.48

-pK$_a$: N/A

-Oxidation modifications: hydroxylation, dihydroxyphenylalanine
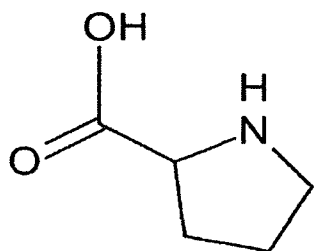
PROLINE (Pro, P)

-Group: Neutral, non-polar

-pI: 6.30

-pK$_a$: N/A

-Oxidation modifications: hydroxylation, glutamic semialdehyde, pyroglutamic acid, pyrrolidinone
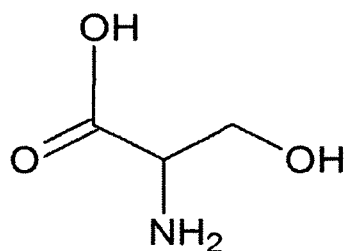
SERINE (Ser, S)

-Group: Neutral, polar

-pI: 5.68

-pK$_a$: N/A

-Oxidation modification: None
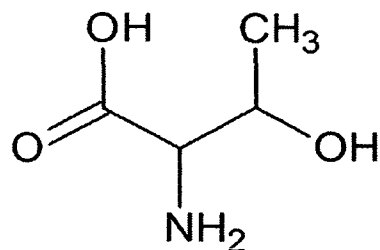
THREONINE (Thr, T)

-Group: Neutral, polar

-pI: 5.60

-pK$_a$: N/A

-Oxidation modification: 2-amino-3-oxo-butanoic acid

TRYPTOPHAN (Trp, W)

-Group: Neutral, polar

-pl: 5.89

-pK$_a$: N/A

-Oxidation modifications: formylkynurenin, kynurenin, 2,4,5,6,7 hydroxylation of trytophan, oxolactone

TYROSINE (Tyr, Y)

-Group: Neutral, polar

-pl: 5.66

-pK$_a$: N/A

-Oxidation modification: hydroxylation

VALINE (Val, V)

-Group: Neutral, non-polar
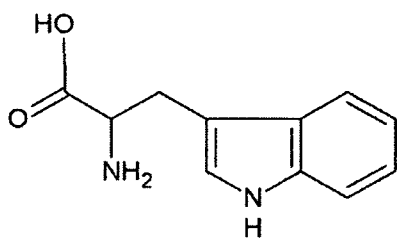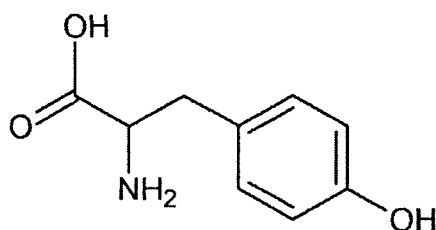
-pl: 5.96

-pK$_a$: N/A

-Oxidation modification: None
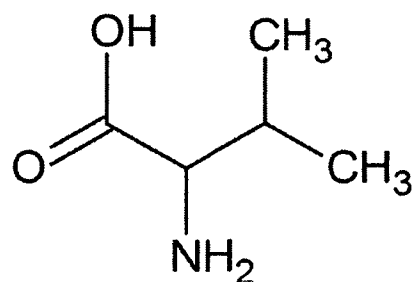
BIBLIOGRAPHY

Adams, A. A., Okagbare, P. I., Feng, J., Hupert, M. L., Patterson, D., Gottert, J., McCarley, R. L., Nikitopoulos, D., Murphy, M. C., and Soper, S. A., "Highly efficient circulating tumor cell isolation from whole blood and label-free enumeration using polymer-based microfluidics with an integrated conductivity sensor." *Journal of the American Chemical Society*, 2008, 130, 27, 8633-8641

Aggarwal, R. C. and Singh, B., "Synthesis and structural studies of oxalyldihydrazide complexes of Mn(II), Fe(II), Co(II), Ni(II), Cu(II), and Zn(II)."*ZAAC: Journal of Inorganic and General Chemistry*, 2004, 445, 1, 227-232

Ahn, C. H., Choi, J-W., Beaucage, G., Nevin, J. H., Lee, J-B., Puntambekar, A., and Lee, J. Y., "Disposable smart lab on a chip for point-of-care clinical diagnostics." *Proceedings of the IEEE*, 2004, 92, 1, 154-173

Akbari, M., Sinton, D., and Bahrami, M., "Pressure drop in rectangular microchannels as compared with theory based on arbitrary cross section." *Journal of Fluids Engineering*, 2009, 131, 041202

Alberghina L. and Colangelo, A.M., "The modular systems biology approach to investigate the control of apoptosis in Alzheimer's disease neurodegeneration." *BMC Neuroscience*, 2006, 7, Supplement1, S2

Amici, A., Levine, R. L., Tsai, L., and Stadtman, E. R., "Conversion of amino acid residues in proteins and amino acid homopolymers to carbonyl derivatives by metal-catalyzed oxidation reactions." *The Journal of Biological Chemistry* 1989, 264, 6, 3341-3346

Apelt J., Bigl M., Wunderlich, P., and Schliebs, R., "Aging-related increase in oxidative stress correlates with developmental pattern of beta-secretase activity and beta-amyloid plaque formation in transgenic Tg2576 mice with Alzheimer-like pathology." *International Journal of Developmental Neuroscience*, 2004, 22, 7, 475-484

Arnold, D. W., Bailey, C. G., Garguilo, M. G., Matzke, C. M., Wendt, J. R., Sweatt, W. C., Kravitz, S. H., Warren, M. E., and Rakestraw, D. J., "Microseparations in microfluidic studies." *Proceedings of the Micro-TAS '98*, 1998, 435-438

Aruna, S. T. and Patil, K. C., "Combustion synthesis and properties of nanostructured ceria-zirconia solid solutions." *Nanostructured Materials*, 1998, 10, 6, 955-964

Ayon, A. A., Bayt, R. L., and Breuer, K. S., "Deep reactive ion etching: a promising technology for micro- and nanosatellites." *Smart Materials and Structures*, 2001, 10, 1135-1144

Bai, Y., Koh, C. G., Boreman, M., Juang, Y-J., Tang, I-C., Lee, L. J., and Yang, S-T, "Surface modification for enhancing antibody binding on polymer-based microfluidic device for enzyme-linked immunosorbent assay." *Langmuir*, 2006, 22, 9458-9467

Balahan, R. S., Nemoto, S., and Finkel, T., "Mitochondria, oxidants, and aging." *Cell* 2005, 120, 4, 483-495

Barber, S. C. and Shaw, P. J., "Oxidative stress in ALS: Key role in motor neuron injury and therapeutic target." *Free Radicals Biology and Medicine* 2010, 48, 629-641

Barreiro, E., Gea, J., Di Falco, M., Kriazhev, L., James, S., and Hussain, S. N. A., "Protein carbonyl formation in the diaphragm." *American journal of respiratory cell and molecular biology*, 2005, 32, 1, 9-17

Beale, R. N. and Croft, D., "The microdetermination of biological copper with oxalyldihydrazide." *Journal of Clinical Pathology*, 1960, 17, 3, 260-263

Bealing, C. R., Baumgardner, W. J., Choi, J. J., Hanrath, T., and Hennig, R. G., "Predicting nanocrystal shape through consideration of surface-ligand interactions." *ACS Nano*, 2012, 6, 3, 2118-2127

Becker, H. and Lacascio, L. E., "Polymer microfluidic devices." *Talanta*, 2002, 56, 267-287

Becker, H. and Heim, U., "Hot embossing as a method for the fabrication of polymer high aspect ratio structures." *Sensors and Actuators A*, 2000, 83, 130-135

Bell, G. I., "Models for the specific adhesion of cells to cells." *Science*, 1978, 200, 618-627

Boedicker, J. Q., Li, L., Kline, T. R., and Ismagilov, R. F., "Detecting bacteria and determining their susceptibility to antibiotics by stochastic confinement in nanoliter droplets using plug-based microfluidics." *Lab on a Chip*, 2008, 8, 8, 1265-1272

Buss, H., Chan, T. P., Sluis, K. B., Domigan, N. M., and Winterbourn, C. C., "Protein carbonyl measurement by a sensitive ELISA method." *Free Radical Biology Medicine*, 1997, 23, 361-366

Carey, F. A., "Chapter 27: Amino Acids, Peptides and Proteins." *On-Line Learning Center for "Organic Chemistry"*, 2011, Accessed from http://www.mhhe.com/physsci/chemistry/carey5e/Ch27/ch27-1-4-2.html

Chang, T. C., Chou, W.Y., and Chang, G.G., "Protein oxidation and turnover." *Journal of Biomedical Science*, 2000, 7, 5, 357-363

Cheung, K. C. and Renaud, P., "BioMEMS for medicine: on-chip cell characterization and implantable microelectrodes." *Solid-State Electronics*, 2006, 50, 551-557

Choi, E. J. and Dimitriadis, E. K., "Cytochrome c adsorption to supported, anionic lipid bilayers studied via atomic force microscopy." *Biophysical Journal*, 2004, 87, 5, 3234-3241

Christel, L., Peterson, K., McMillan, W., and Northrup, M. A., "Nucleic acid concentration and PCR for diagnostic applications." *Proceedings of the Micro-TAS '98*, 1998, 277-280

Chun, M-S., Shim, M. S., and Choi, N. W., "Fabrication and validation of a multi-channel type microfluidic chip for electrokinetic streaming potential devices." *Lab on a Chip*, 2006, 6, 302-309

Colak, E., "New markers of oxidative damage to macromolecules." *Journal of Molecular Biology* 2008, 1

Czapski, G., Samuni, A., and Goldstein, S., "Superoxide dismutase mimics: antioxidative and adverse effects." *Methods in Enzymology*, 2002,349, 234-242

Dalle-Donne, I., Giustarini, D., Colombo, R., Rossi, R., and Milzani, A., "Protein carbonylation in human diseases." *TRENDS in Molecular Medicine*, 2003, 9, 4, 169-176

Dalle-Donne, I., Rossi, R., Giustarini, D., Milzani, A., and Colombo, R., "Protein carbonyl groups as biomarkers of oxidative stress." *Clinica Chimica Acta* 2003, 329, 23-28

Davis, K. J. A., Delsignore, M. E., and Lin, S. W., "Protein Damage and Degradation by Oxygen Radicals." *The Journal of Biological Chemistry*, 1987, 262, 20, 9902-9907

Dharmasiri, U., Witek, M. A., Adams, A. A., Osiri, J. K., Hupert, M. L., Bianchi, T. S., Roelke, D. L., and Soper, S. A., "Enrichment and detection of *Escherichia coli* O157:H7 from water samples using an antibody modified microfluidic chip." *Analytical Chemistry*, 2010, 82, 2844-2849

Dharmasiri, U., Balamurugan, S., Adams, A. A., Okagbare, P. I., Obubuafo, A., and Soper, S. A., "Highly efficient capture and enumeration of low abundance prostate cancer cells using prostate-specific membrane antigen aptamers immobilized to a polymeric microfluidic device." *Electrophoresis*, 2009, 30, 18, 3289-3300

Diercks, A. H., Ozinsky, A., Hansen, C. L., Spotts, J. M., Rodriguez, D. J., and Aderem, A., "A microfluidic device for multiplexed protein detection in nano-liter volumes." *Analytical Biochemistry*, 2009, 386, 1, 30-35

Duquet, A., Polesskaya, A., Cuvellier, S., Sylvain, A., Ait-Si-Ali, S., Patrick, H., Pritchard, L. L., Matthieu, G., and Harel-Bellan, A., "Acetylation is important for MyoD function in adult mice." *EMBO reports* 2006, 7, 11, 1140-1146

Eckert, A., Schulz, K. L., Rhein, V., and Gotz, J., "Convergence of Amyloid-β and tau pathologies on mitochondria *in vivo.*" *Molecular Neurobiology*, 2010, 41, 107-114

Feng, J. and Arriaga, E. A., "Quantification of carbonylated proteins in rat skeletal muscle mitochondria using capillary sieving electrophoresis with laser-induced fluorescence detection." *Electrophoresis*, 2008, 29, 2, 475-482

Feng, J., Navratil, M., Thompson, L. V., and Arriaga, E. A., "Principal component analysis reveals age-related and muscle-type-related differences in protein carbonyl profiles of muscle mitochondria." *Journal of Gerontology Series A: Biological Sciences and Medical Sciences*, 2008, 63, 12, 1277-1288

Finkel, T. and Holbrook, N.J., "Oxidants, oxidative stress and the biology of ageing." *Nature*, 2000, 408, 6809, 239-247

Fischer, L. R., Li, Y., Asress, S. A., Jones, D. P., and Glass, J. D., "Absence of SOD1 leads to oxidative stress in peripheral nerve and causes a progressive distal motor axonopathy." *Experimental Neurology* 2012, 233, 163-171

Frederick, K. and Ibba, M., "How the sequence of a gene can tune its translation." *Cell*, 2010, 141, 227-229

Fuerstman, M. J., Lai, A., Thurlow, M. E., Shevkoplyas, S. S., Stone, H. A., and Whitesides, G. M., "The pressure drop along rectangular microchannels containing bubbles." *Lab on a Chip*, 2007, 7, 1479-1489

Gautsch, S., Studer, M., and de Rooij, N. F., "Complex nanostructures in PMMA made by a single process step using e-beam lithography." *Microelectronic Engineering*, 2010, 87, 1139-1142

Ghosal, S., "Microfluidics". Accessed from http://www.mech.northwestern.edu/fac/ghosal/ghosal_encycl_microfluidics.pdf. Accessed May 17, 2012

Grayson, A. C. R., Shawgo, R. S., Johnson, A. M., Flynn, N. T., Li, Y., Cima, M. J., and Langer, R., "A BioMEMS review: MEMS technology for physiologically integrated devices." *Proceedings of the IEEE*, 2004, 92, 1, 6-21

Hao, Q., Zeng, Y., Wang, X., Zhao, Y., Wang, B., Chiang, I-K., Werner, D. H., Crespi, V., and Huang, T. J., "Characterization of complementary patterned metallic membranes produced simultaneously by a dual fabrication process." *Applied Physics Letters*, 2010, 97, 193101

Harman, D., "Aging: a theory based on free radical and radiation chemistry." *Journal of Gerontology*, 1956, 298-300

Harman, D., "Free radical theory of aging: an update: increasing the functional life span." *Annals of the New York Academy of Sciences*, 2006, 1067, 10-21

Harman, D., "Origin and evolution of the free radical theory of aging: a brief personal history, 1954-2009." *Biogerontology*, 2009, 10, 773-781

Hollins, B. C., Soper, S. A., and Feng, J., "Enriching carbonylated proteins inside a microchip through the use of oxalyldihydrazide as a crosslinker." *Lab on a Chip*, 2012, 12, 2526-2532

Iliescu, C., Tay, F. E. H., and Miao, J., "Strategies in deep wet etching of pyrex glass." *Sensors and Actuators A: Physical*, 2007, 133, 2, 395-400

Kameoka, J., Craighead, H. G., Zhang, H., Henion, J., "A polymeric microfluidic chip for CE/MS determination of small molecules." *Analytical Chemistry*, 2001, 73, 1935-1941

Kang, L., Chung, B. G., Langer, R., and Khademhosseini, A., "Microfluidics for drug discovery and development: from target selection to product lifecycle management." *Drug Discovery Today*, 2008, 13, 1, 1-13

Kekki, M. and Siltanen, P., "Microdetermination of protein by determining the protein bound copper of the biuret complex with oxalyldihydrazide." *Scandinavian Journal of Clinical and Laboratory Investigation*, 1960, 12, 2, 235-238

Keller, R. J., Halmes, N. C., Hinson, J. A., and Pumford, N. R., "Immunochemical detection of oxidized proteins." *Chemical Research in Toxicology*, 1993, 6, 430-433

Kim, P., Kwon, K. W., Park, M. C., Lee, S. H., Kim, S. M., and Suh, K. Y., "Soft lithography for microfluidics: a review." *Biochip Journal*, 2008, 2, 1, 1-11

Klatt, P. and Lamas, S., "Regulation of protein function by S-glutathiolation in response to oxidative and nitrosative stress." *The European Journal of Biochemistry*, 2000, 267, 4928-4944

Kovacic, P. and Jacintho, J. D., "Systemic lupus erythematosus and other autoimmune diseases from endogenous and exogenous agents: unifying theme of oxidative stress." *Mini Reviews in Medicinal Chemistry*, 2003, 3, 568-575

Krause, D. L. and Muller, N., "Neuroinflammation, microglia and implications for anti-inflammatory treatment in Alzheimer's disease." *International Journal of Alzheimer's Disease*, 2010, doi:10.4061/2010/732806

Kunjumon, A., "Role of ammonia in the activation of methanol dehydrogenase/cytochrome cL enzyme." *Dissertations/Louisiana Tech University*, 2011, 119 pages

Lee, G-B., Lin, C-H., Lee, K-H., and Lin, Y-F., "On the surface modification of microchannels for microcapillary electrophoresis chips." *Electrophoresis*, 2005, 26, 4616-4624

Lenz, A., Costabel, U., Shaltiel, S., and Levine, R. L., "Determination of carbonyl groups in oxidatively modified proteins by reduction with tritiated sodium borohydride." *Analytical Biochemistry*, 1989, 177, 419-425

Levine, R. L., Garland, D., Oliver, C. N., Amici, A., Climent, I., Lenz, A. G., Ahn, B. A., Shaltiel, S., and Stadtman, E. R., "Determination of carbonyl content in oxidatively modified proteins." *Methods in enzymology*, 1990, 186, 464-478

Li, D., Wang, Y., and Han, K., "Recent density functional theory model calculations of drug metabolism by cytochrome P450."*Coordination Chemistry Reviews*, 2012, 256, 1137-1150

Li, P., Gao, Y., and Pappas, D., "Negative enrichment of target cells by microfluidic affinity chromatography." *Analytical Chemistry*, 2011, 83, 7863-7869

Llopis, S. L., Osiri, J., and Soper, S. A., "Surface modification of poly (methyl methacrylate) microfluidic devices for high-resolution separations of single-stranded DNA." *Electrophoresis*, 2007, 28, 984-993

Lusk, G., "The fate of the amino acids in the organism." *Journal of the American Chemical Society*, 1910, 671-680

Madian, A. G. and Regnier, F.E., "Proteomic identification of carbonylated proteins and their oxidation sites." *Journal of Proteome Research*, 2010, 9, 8, 3766-3780

Madian, A. G., Myracle, A. D., Diaz-Maldonado, N., Rochelle, N. S., Janle, E. M., and Regnier, F. E., "Differential carbonylation of proteins as a function of *in vivo* oxidative stress." *Journal of Proteome Research*, 2011, 10, 3959-3972

Marcus, K., Schmidt, O., Schaefer, H., Hamacher, M., van Hall, A., and Meyer, H. E., "Proteomics-application to the brain." *International Review of Neurobiology*, 2004, 61, 285-311

Maehly, A. C. and Chance, B., "The assay of catalases and peroxidases." *Methods of Biochemical Analysis*, 1954, 1, 357-424

Mirzaei, H. and Regnier, F., "Affinity chromatographic selection of carbonylated proteins followed by identification of oxidation sites using tandem mass spectrometry." *Analytical Chemistry*, 2005, 77, 8, 2386-2392

Nagrath, S., Sequist, L. V., Maheswaran, S., Bell, D. W., Irimia, D., Ulkus, L., Smith, M. R., Kwak, E. L., Digumarthy. S., Muzikansky, A., Ryan, P., Balis, U. J., Tompkins, R. G., Haber, D. A., and Toner, M., "Isolation of rare circulating tumour cells in cancer patients by microchip technology." *Nature* 2007, 450, 7173, 1235-1239

Nakamura, A. and Goto, S., "Analysis of protein carbonyls with 2,4-dinitrophenylhydrazine and its antibodies by immunoblot in two-dimensional gel electrophoresis." *Journal of Biochemistry*, 1996, 119, 768-774

Nunomura, A., Castellani, R. J., Zhu, X., Moreira, P. I., Perry, G., and Smith, M. A., "Involvement of oxidative stress in Alzheimer disease." *Journal of Neuropathology and Experimental Neurology* 2006, 65, 7, 631-641

Okayama, Y., "Oxidative stress in allergic and inflammatory skin diseases." *Current Drug Targets – Inflammation and Allergy*, 2005, 4, 517-519

Osiri, J. K., Shadpour, H., Park, S., Snowden, B. C., Chen, Z. Y., and Soper, S. A., "Generating high peak capacity 2-D maps of complex proteomes using PMMA microchip electrophoresis." *Electrophoresis*, 2008, 29, 24, 4984-4992

Phillips, J. A., Xu, Y., Xia, Z., Fan, Z. H., and Tan, W., "Enrichment of cancer cells using aptamers immobilized on a microfluidic channel." *Analytical Chemistry*, 2009, 81, 1033-1039

Pinto, D., Arriaga, E. A. Arriaga, Schoenherr, R. M., Chou, S. S., and Dovichi, N. J., "Kinetics and apparent activation energy of the reaction of the fluorogenic reagent 5-furoylquinoline-3-carboxaldehyde with ovalbumin." *Journal of Chromatography: Analytical Technology for Biomedical Life Sciences,* 2003, 793, 107-114

Reed, M. C., Thomas, R. L., Pavisic, J., James, S. J., Ulrich, C. M., and Nijhout, H. F., "A mathematical model of glutathione metabolism." *Theoretical Biology and Medical Modeling*, 2008, 5, 8

Robberecht, W., "Oxidative stress in amyotrophic lateral sclerosis." *Journal of Neurology* 2000, 247, supplement 1, I/1-I/6

Robinson, C. E., Kashavarzian, A., Pasco, D. S., Frommel, T. O., Winshop, D. H., and Holmes, E. W., "Determination of protein carbonyl groups by immunoblotting." *Analytical Biochemistry*, 1999, 266, 48-57

Roe, M. R., Xie, H., Bandhakavi, S., and Griffin, T. J., "Proteomic mapping of 4-hydroxynonenal protein modification sites by solid-phase hydrazide chemistry and mass spectroscopy." *Analytical Chemistry*, 2007, 79, 3747-3756

Salem, F. B., "Spectrophotometric determination of phosphate in waters of Egypt." *Water, Air, and Soil Pollution*, 1991, 60, 27-33

Saliba, A-E., Saias, L., Psychari, E., Minc, N., Simon, D., Bidard, F-C., Mathiot, C., Pierga, J-Y., Fraisier, V., Salamero, J., Saada, V., Farace, F., Vielh, P., Malaquin, L., and Viovy, J-L., "Microfluidic sorting and multimodal typing of cancer cells in self-assembled magnetic arrays." *PNAS*, 2010, 107, 33, 14524-14529

Sane, S. B., Cagin, T., Knauss, W. G., and Goddard, W.A., "Molecular dynamics simulations to compute the bulk response of amorphous PMMA." *Journal of Computer-Aided Materials Design*, 2002, 8, 2-3, 87-106

Schulz, J. B., Lindenau, J., Seyfried, J., and Dichgans, J., "Glutathione, oxidative stress, and neurodegeneration." *European Journal of Biochemistry* 2000 267, 4904-4911

Schulenborg, T., Schmidt, O., van Hall, A., Meyer, H. E., Hamacher, M., and Marcus, K., "Proteomics in neurodegeneration-disease driven approaches." *Journal of Neural Transmission*, 2006, 113, 8, 1055-1073

Shacter, E., "Quantification and significance of protein oxidation in biological samples." *Drug Metabolism Reviews* 2000, 32, 307-326

Shadpour, H., Hupert, M. L., Patterson, D., Liu, C., Galloway, M., Stryjewski, W., Goetter, J., and Soper, S. A., "Multichannel microchip electrophoresis device fabricated in polycarbonate with an integrated contact conductivity sensor array." *Analytical Chemistry*, 2007, 79, 3, 870-878

Shadpour, H. and Soper, S. A., "Two-dimensional electrophoretic separation of proteins using poly (methyl methacrylate) microchips." *Analytical Chemistry*, 2006, 78, 11, 3519-3527

Shigi, N., "Post-translational modification of cellular proteins by a ubiquitin-like protein in bacteria." *The Journal of Biological Chemistry*, 2012, in press, Manuscript M112.359844

Simpson, P. C., Roach, D., Woolley, A. T., Thorsen, T., Johnston, R., Sensabaugh, G. F., and Mathies, R. A., "High throughput genetic analysis using microfabricated 96-sample capillary array electrophoresis microplates." *Proceedings of the National Academy of Sciences, USA*, 1998, 2256-2261

Singh, D. P., Kumar, R., and Singh, J., "Synthesis and spectroscopic studies of biologically active compounds derived from oxalyldihydrazide and benzil, and their Cr(III), Fe(III), and Mn(III) complexes." *European Journal of Medicinal Chemistry*, 2009, 44, 4, 1731-1736

Smith, M. A., Sayre, L. M., Anderson, V. E., Harris, P. L. R., Beal, M. F., Kowall, N., and Perry, G., "Cytochemical demonstration of oxidative damage in Alzheimer disease by immunochemical enhancement of the carbonyl reaction with 2,4-dinitrophenylhydrazine." *Journal of Histochemistry and Cytochemistry*, 1998, 46, 731-735

Smout, M. J., Kotze, A. C., McCarthy, J. S., and Loukas, A., "A novel high throughput assay for anthelmintic drug screening and resistance diagnosis by real-time monitoring of parasite motility." *PLoS Neglected Tropical Diseases*, 2010, 4, 11, e885

Stachowiak, T. B., Rohr, T., Hilder, E. F., Peterson, D. S., Yi, M., Svec, F., and Frechet, J. M., "Fabrication of porous polymer monoliths covalently attached to the walls of channels in plastic microdevices." *Electrophoresis*, 2003, 24, 3689-3693

Stadtman, E. R. and Oliver, C. N., "Metal-catalyzed oxidation of proteins." *Journal of Biological Chemistry*, 1991, 266, 4, 2005-2008

Stark, G. R. and Dawson, C. R., "Spectrophotometric microdetermination of copper in copper oxidases using oxalyldihydrazide." *Analytical Chemistry*, 1958, 30, 2, 191-194

Sultana, R., Perluigi, M., Newman, S. F., Pierce, W. M., Cini, C., Coccia, R., and Butterfield, D. A., "Redox proteomic analysis of carbonylated brain proteins in mild cognitive impairment and early Alzheimer's disease." *Antioxidants and Redox Signaling*, 2010, 12, 327-336

Suzuki, Y. J., Carini, M., and Butterfield, D.A., "Protein carbonylation." *Antioxidants and Redox Signaling*, 2010, 12, 3, 323-325

Tolan, N. V., Genes, L. I., and Spence, D. M., "Merging microfluidics with micro-titre technology for more efficient drug discovery." *JALA Charlottesville Virginia*, 2008, 13, 5, 275-279

Uddin, K. M., Warburton, P. L., and Poirier, R. A., "Comparisons of Computational and Experimental Thermochemical Properties of α-amino acids." *The Journal of Physical Chemistry B*, 8, 2012, 116, 3220-3234

Vanapalli, S., ter Brake, H. J. M., Jansen, H. V., Burger, J. F., Holland, H. J., Veenstra, T. T., and Elwenspoek, M. C., "Pressure drop of laminar gas flows in a microchannel containing various pillar matrices." *Journal of Micromechanics and Microengineering*, 2007, 17, 1381-1386

Vogel, C., "Translation's coming of age." *Molecular Systems Biology*, 2011, 7:498 doi:10.1038/msb.2011.33

Wang, Q., Zhao, X., He, S., Liu, Y., An, M., and Ji, J., "Differential proteomics analysis of specific carbonylated proteins in the temporal cortex of aged rats: the deterioration of the antioxidant system." *Neurochemical Research* 2010, 35, 13-21

Wang, S., Njoroge, S. K., Battle, K., Zhang, C., Hollins, B. C., Soper, S. A., and Feng, J., "Two-dimensional nitrosylated protein fingerprinting via poly (methyl methacrylate) microchips." *Lab on a Chip*, 2012, accepted for publication

Wei, S., Vaidya, B., Patel, A. B., Soper, S. A. and McCarley, R. L., "Photochemically patterned poly (methyl methacrylate) microanalytical devices." *Journal of Physical Chemistry B "*. 2005, 109, 35, 16988-16996

Weigl, B., Domingo, G., LaBarre, P., and Gerlach, J., "Towards non- and minimally-instrumented, microfluidics-based diagnostic devices." *Lab on a Chip*, 2008, 8, 12, 1999-2014

White, C. R., Brock, T. A., Chang, L., Crapo, J., Briscoe, P., Ku, D., Bradley, W. A., Gianturco, S. H., Gore, J., Freeman, B. A., and Tarpey, M. M., "Superoxide and peroxynitrite in atherosclerosis." *Proceedings of the National Academy of Sciences USA*, 1994, 91, 1044-1048

Wong, C. M., Marcocci, L., Liu, L., and Suzuki, Y. J., "Cell signaling by protein carbonylation and decarbonylation." *Antioxidants and Redox Signaling*, 2010, 12, 3, 393-404

Xia, H., Murray, K., Soper, S., and Feng, J., "Ultra sensitive affinity chromatography on avidin-functionalized PMMA microchip for low abundant post-translational modified protein enrichment." *Biomedical Microdevices*, 2012, 14, 67-81

Yan, L. J. and Sohal, R. S., "Gel electrophoretic quantitation of protein carbonyls derivatized with tritiated sodium borohydride." *Analytical Biochemistry*, 1998, 265, 176-182

Yan, L. J., Orr, W. C., and Sohal, R. S., "Identification of oxidized proteins based on sodium dodecyl sulfate-polyacrylamide gel electrophoresis, immunochemical detection, isoelectric focusing, and microsequencing." *Analytical Biochemistry*, 1998, 263, 67-71

Yang, J., Huang, J., Dasgupta, M., Sears, N., Miyagi, M., Wang, B., Chance, M. R., Chen, X., Du, Y., Wang, Y., An, L., Wang, Q., Lu, T., Zhang, X., Wang, Z., and Stark, G. R., "Reversible methylation of promoter-bound STAT3 by histone-modifying enzymes." *Proceedings of the National Academy of Sciences*, 2010, 107, 50, 21499-21504

Yeom, J., Agonafer, D. D., Han, J-H., and Shannon, M. A., "Low Reynolds number flow across an array of cylindrical microposts in a microchannel and figure-of-merit analysis of microposts-filled microreactors." *Journal of Micromechanics and Microengineering,* 2009, doi:10.1088/0960-1317/19/6/065025

Yoo, B. S. and Regnier, F. E., "Proteomic analysis of carbonylated proteins in two-dimensional gel electrophoresis using avidin-fluorescein affinity staining." *Electrophoresis,* 2004, 25, 9, 1334-1341

Young, E. W. K. and Beebe, D. J., "Fundamentals of microfluidic cell culture in controlled microenvironments." *Chemical Society Reviews,* 2010, 39, 3, 1036-1048

Zhao, Y. and Jensen, O.N., "Modification-specific proteomics: strategies for characterization of post-translational modifications using enrichment techniques." *Proteomics,* 2009.9, 20, 4632-4641

Zhou, L., Aon, M. A., Almas, T., Cortassa, S., Winslow, R.L., and O'Rourke, B., "A reaction-diffusion model of ROS-induced ROS release in a mitochondrial network." *PLoS Computational Biology,* 2010, 6, 1, e1000657